530
620.5
3
SS-1
X-1

A UNITED STATES DEPARTMENT OF COMMERCE PUBLICATION

SECTION C

JOURNAL OF RESEARCH

of the NATIONAL BUREAU OF STANDARDS

Volume 74C Nos. 3&4, July-Dec. 1970

Engineering and Instrumentation

U.S. DEPARTMENT OF COMMERCE
National Bureau of Standards

Journal of Research

of the

National Bureau of Standards

C. Engineering and Instrumentation

July–Dec. • 1970

VOLUME • 74C

NUMBERS • 3 and 4

Editor: Martin Greenspan

Associate Editors: G. F. Montgomery, R. V. Smith, A. F. Schmidt

Publication dates:
Feb. 15, May 15, Aug. 15, Nov. 15, 1970

J. Res. Nat. Bur. Stand. (U.S.), C
CODEN: JNBCA 74C (3 & 4) 63–150 (1970)

JOURNAL OF RESEARCH

The National Bureau of Standards Journal of Research reports research and development in the fields of activity shown at right. Also included from time to time are survey articles on topics closely related to the Bureau's scientific and technical program.

The Journal is published in three separate sections as follows:

A. Physics and Chemistry

Contains papers of interest primarily to scientists working in these fields. Issued six times a year. Annual subscription: domestic, $9.50; foreign, $11.75. Single copy, varies.

B. Mathematical Sciences

Presents studies and compilations designed mainly for the mathematician and the theoretical physicist. Issued quarterly. Annual subscription: domestic, $5.00; foreign, $6.25. Single copy, $1.25.

C. Engineering and Instrumentation

Reports research and development results of interest chiefly to the engineer and the applied scientist. Issued quarterly. Annual subscription: domestic, $5.00; foreign, $6.25. Single copy, $1.25.

U.S. DEPARTMENT OF COMMERCE
Maurice H. Stans, Secretary
NATIONAL BUREAU OF STANDARDS
Lewis M. Branscomb, Director

Order all publications from the Superintendent of Documents
U.S. Government Printing Office, Washington, D.C. 20402.

Use of funds for printing this publication approved by the Director of the Bureau of the Budget (June 22, 1966).

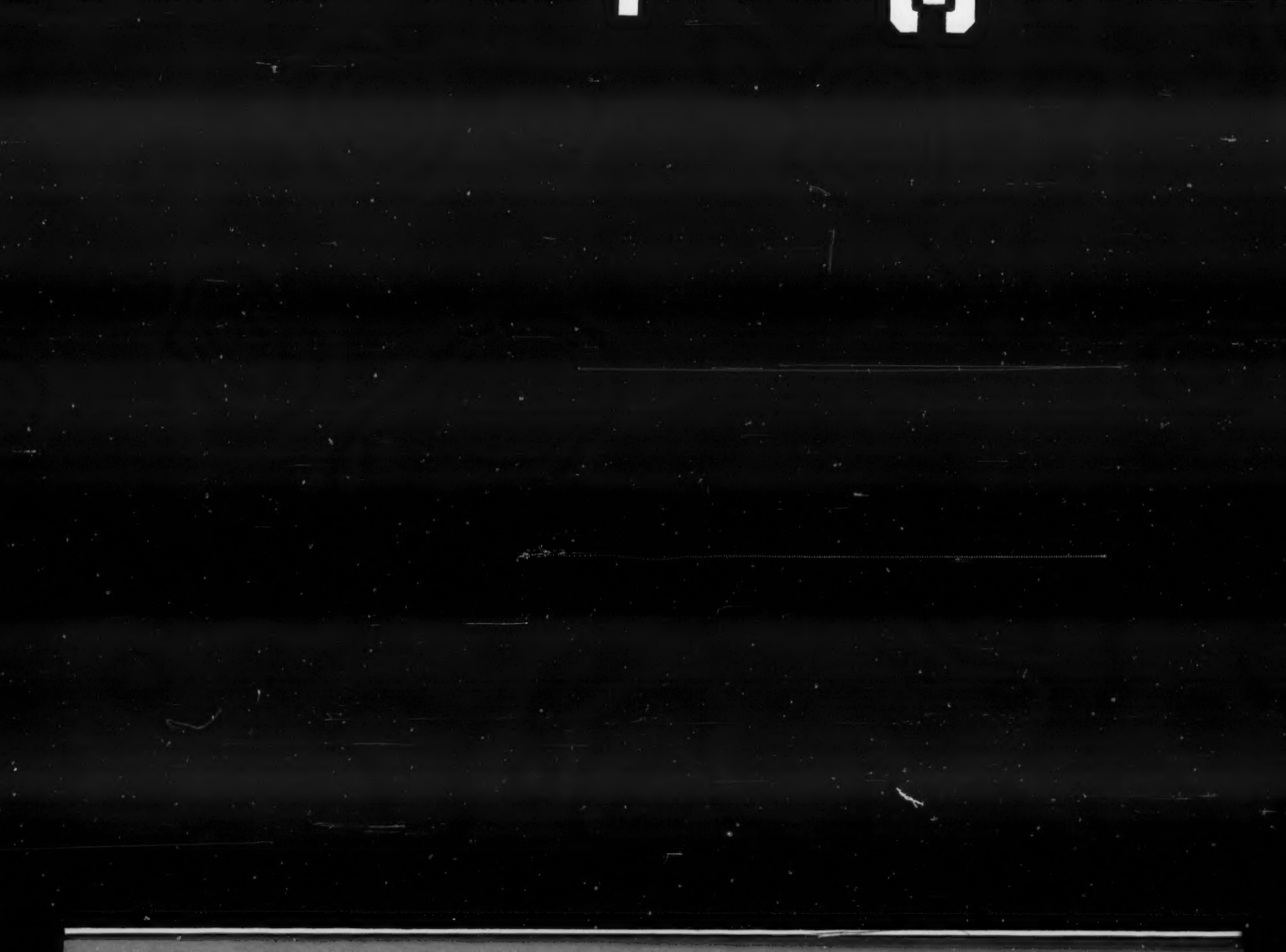

JOURNAL OF RESEARCH of the National Bureau of Standards—C. Engineering and Instrumentation
Vol. 74C, Nos. 3 and 4, July–December 1970

Techniques for Comparing Four-Terminal-Pair Admittance Standards

R. D. Cutkosky

Institute for Basic Standards, National Bureau of Standards, Washington, D.C. 20234

(June 26, 1970)

Some of the advantages of four-pair admittance standards and some of the special problems encountered in their measurement are pointed out. Detailed descriptions of three distinct types of four-pair bridges and some of their limitations are presented. These three bridges form a vital part of a very precise absolute measurement of resistance based on a calculable capacitor being undertaken at the National Bureau of Standards, but are believed to be of more general usefulness.

Key words: AC direct-reading ratio set; ac measurements; bridge; coaxial chokes; defining transformers; equal power bridge; four-pair standards; frequency-dependent bridge; quadrature bridge.

1. Introduction

The quest for improved accuracy in the measurement of audiofrequency admittances has led from the now universally accepted practice of utilizing two pair standards, such as so-called three-terminal capacitors for high-impedance devices and such as mutual inductors for low-impedance devices, to a composite system combining the advantages of both techniques. A theoretical justification of this composite system in which the standards are provided with four pairs of terminals was published in 1964 [1][1], but with the exception of a paper by Homan [2] which was limited to measurements on fairly small impedances, no systematic investigation of four-pair admittance measurements has yet been described. The process of converting to four-pair measurement systems has been underway at the National Bureau of Standards for several years, during which time many of the special problems involved in their use have been investigated. This paper is an attempt to describe some of the techniques which have evolved, and to indicate the order of precision that may be obtained.

The techniques described in this paper are of general applicability but were developed for the specific purpose of comparing the reactances of capacitors having nominal values of 10 pF with the resistance of a special 1000-Ω resistor having a negligible frequency dependence [3]. The three basic types of bridges used for making this comparison are described here in some detail. It is intended to calibrate the 10-pF capacitors by means of a calculable capacitor now under construction at NBS. A dc comparison of the 1000-Ω resistor with the bank of 1-Ω resistors presently maintaining the NBS unit of resistance will then complete an absolute measurement of the ohm.

Because of the large number of intervening steps between the calculable capacitor and the bank of 1-Ω resistors, very elaborate precautions are necessary to maintain a high level of accuracy. Using the techniques outlined here, it is expected that the principal uncertainties in the measurement sequence will be due to mechanical imperfections in the calculable capacitor.

Although a rather complex sequence of auxiliary balances is required with the bridges described in this paper, they are not prohibitively time-consuming for the limited number of comparisons needed in an absolute ohm determination. These techniques would be considerably less attractive for a bridge in constant use, but this would be less of a drawback in a computer-operated system. It is considered that techniques similar to those described in this paper are essential if uncertainties must be kept smaller than 1 part in 10^8 over a large range of impedances at audiofrequencies.

The equivalent circuit of a four-pair admittance standard is shown in figure 1a, taken from the paper cited above [1], and in an abbreviated form, in figure 1b. The standard may be viewed as a device in which the ratio of current in pair 3 to the open circuit voltage at pair 2, subject to the condition that both the voltage and current at pair 4 are zero, is the parameter of interest. This parameter has the dimensions of admittance and may be written

$$P_{32}^{14}=\frac{i_3}{e_2}\bigg|i_2=i_4=0,\quad e_4=0. \tag{1}$$

It may be shown using figure 1a that

$$P_{32}^{14}=Y_t(1+Y_2Z_2)(1+Y_3Z_3). \tag{2}$$

[1] Figures in brackets indicate the literature references at the end of this paper.

An interesting reciprocity theorem also exists, which shows that $P_{32}^{14} = P_{23}^{41}$ for any four-pair network.

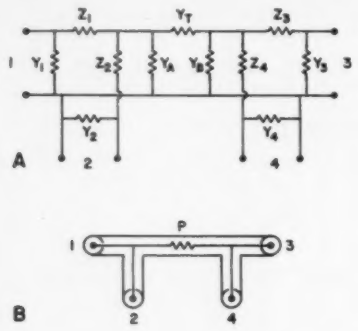

FIGURE 1. *Four-pair admittance standards:* (a) *Complete circuit.* (b) *Pictorial representation.*

Some properties of four-pair admittance standards which make them particularly useful are their relative insensitivities to variations in series impedances and shunt admittances in the leads as is implicit in (2), and the fact that standards of either very small or very large admittance may be constructed in such a way that their four-pair admittances are nearly identical with their ordinary two-pair admittances obtained by either open circuiting or short circuiting the two extra terminal pairs. These properties are discussed in the reference cited above [1].

Ordinarily the relationship between the four-pair admittance of a standard and its admittance when treated as a two-pair standard is of interest only when the standard is some kind of absolute or calculable instrument, and it is necessary to determine the difference between the calculated admittance at some internal and inaccessible location, and the effective four-pair admittance at the external connection points. Examples of this type of standard are calculable capacitors, calculable inductors, and resistors having calculable phase angles or ac-dc differences. Such devices are outside the scope of this paper, which is restricted to the problem of comparing four-pair admittance standards with each other.

Implicit in the adoption of either a four-pair or a two-pair approach is the requirement that the connections are indeed treated as pairs, and that there is no net current from one terminal pair to another. Many advantages result from grouping the terminals of a standard in pairs. Consider the simple case of a three-terminal capacitor provided with two coaxial connectors and with a permanent connection between the shields of these connectors. Conceptually the measurement of the capacitor consists of applying a voltage, e, to one connector pair and measuring the short circuit current i at the other connector pair. The transfer admittance of the device is then given by

$$Y = j\omega C + G = \frac{i}{e}.$$

The transfer admittance defined in this way is a function of the impedance in the connection between the shields of the coaxial connectors, but there is no ambiguity in the definition as there would be if a single ground connection of unspecified placement were used for both the input and output.

One of the principal reasons for defining the standards in terms of isolated coaxial connector pairs as sketched above is that under these conditions there is exactly the same current but with reversed sign in the inner wire of each cable as there is in the surrounding coaxial shield, and therefore the magnetic field exterior to both cables is zero. This eliminates possible mutual inductive couplings between the cables used to interconnect a number of components together to form a bridge. Likewise, even if stray magnetic fields were present in the vicinity of the coaxial cables, no induced voltages would be produced by these fields to affect the measurement. Although these arguments pertain only to the connecting leads of the devices, the devices themselves can be quite easily isolated from each other by providing them with individual mu-metal shields when this is needed.

Four-pair admittance standards are constructed with four coaxial connectors, and the advantages gained by preventing net currents from flowing between the four connector pairs are very great, as this eliminates external magnetic fields and their effects on the measurement. In this respect, the practice of dealing with five terminal standards having a single, common ground connection cannot be recommended.

It is necessary to maintain the conditions of zero net currents in the cables of components defined as outlined above when they are interconnected to form a bridge circuit. Coaxial chokes were developed for dealing with this problem [4], and are effective in attenuating the net currents in the cables by a factor of several hundred. Unfortunately the net currents are not completely suppressed by coaxial chokes. A method for estimating the errors caused by incomplete suppression of net currents by coaxial chokes is described later in this paper.

Most of the bridge circuits appearing in this paper show explicitly the coaxial nature of the components. This was done to emphasize the importance of considering the return currents in the shields. After some practice in dealing with circuits drawn in this way, they are much easier to relate to the physical bridge setup than are the conventional textbook bridge circuits. Some difficulty may be experienced at first in translating the still useful and important body of classical bridge theory to the coaxial form of presentation. It may be an aid in understanding some of the circuits in this paper to redraw them with a common ground point. If this is done, the similarities between many of the auxiliary balance systems used here and common classical techniques, such as yoke and lead balancing in Kelvin double bridges, and the use of Wagner and conjugate Wagner arms in ac bridges, can be readily seen. Redrawing the circuits in this way must be thought of purely as an aid to understand-

ing, because any attempt actually to construct a circuit without proper attention to the details of the shield return circuits would result in large and erratic errors dependent upon the accidental arrangement of the leads.

A final but important introductory point about comparisons of four-pair admittances, or indeed any other kind of admittances, is that even though the standards are defined subject to certain constraints on the currents and voltages, it is not necessary when comparing two such standards to satisfy *any* of the defining conditions; it is merely required that the same result be obtained for the ratio of the four-pair admittances being compared as would have been obtained *if* the conditions had all been satisfied. This observation opens up a very wide range of possibilities in the design of bridge circuits, and is related to the techniques described by Thompson for dealing with bridges involving multiple balances [4]. The Kelvin bridge for comparing four-terminal dc resistors also makes use of this principle, since currents exist in the potential leads of the resistors, but cause no errors.

2. Basic Comparison Circuits

Figure 2 shows four four-pair admittances connected in a bridge circuit involving six generators and six detectors. The balance procedure consists (for example) of arbitrarily fixing one generator, and then adjusting the other five generators and one of the four

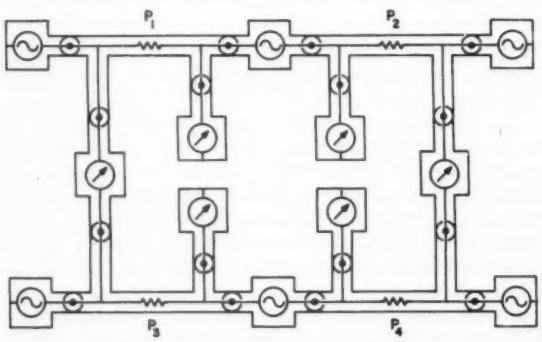

FIGURE 2. *Elementary four-pair bridge.*

four-pair admittances until all six detectors are balanced. The balance condition is $P_1P_4=P_2P_3$. If all generators and detectors are interchanged, the bridge network retains its form, and it may be shown, using the reciprocity theorem for four-pair networks, that the balance condition is unchanged.

The scheme of figure 2 contains a number of drawbacks, chief among which is the difficulty in simultaneously nulling six detectors, all of which are affected in various ways by the six adjustable parameters. This problem is solved in principle by mixing the various null detector responses in a suitable combining network to obtain six new null detector responses, each of which is a weighted average of the six original null detector inputs. The combining network parameters are chosen so that the matrix relating the new detector responses to the adjustable parameters is diagonal [4,5]. In this case, only the detector which responds to the adjustable four-pair admittance, called the main detector, is of interest, and the others need to be balanced only if the non-diagonal elements of the matrix are not exactly zero.

A more fundamental problem encountered in realizing figure 2 has to do with shunt admittances to ground associated with the detectors which compare the open circuit voltage of one standard with that of another, and with shunt admittances to ground associated with the generators between the current leads of two adjacent standards. By the reciprocity theorem the effects of these sets of leads are similar, and any solution found for one problem may be immediately applied to the other. The nature of the problem and the order of magnitude of the possible errors likely to occur may be seen from (2), which shows that the effect of admittance to ground in the potential lead is to load the leads joining the internal junction points of the standard with the point at which the open circuit potential is to be measured. The effect of admittance to ground at the current lead is to shunt some of the current to ground before it enters the adjacent standard.

The lead effects described above are unlikely to exceed a few parts in 10^7 at audiofrequencies, unless interconnecting cables longer than several meters are used. Even with very long cables, no errors result provided that these cables are treated as part of the standard, so that their effects are the same when the standard is calibrated as when it is used for calibrating another standard. However, the stabilities of the series impedances and shunt admittances of the cables must be considered.

The network used to interconnect the ends of the two cables and the null detector or generator is in principle a three-pair network, since the interaction of the null detector or generator terminal pair must be included in the matrix description of the network. This network must be carefully constructed so that the admittances shunting the cables from the standards are small, equal, and measurable; and so that the interaction of the null detector or generator with the other two terminal pairs is simple to analyze. An ideal three-pair circuit for accomplishing the desired objectives would provide a direct, completely reproducible connection between the two coaxial cables, except for an infinitesimal gap between their inner conductors, and with provision for connecting a null detector or generator across this gap. A network electrically equivalent to the above is employed at NBS which we call a defining transformer, shown pictorially in figure 3. A particular advantage of this network is that one side of the detector or generator terminal pair is at ground potential.

When used in the potential leads of the bridge shown in figure 2, the potential leads from the two standards are connected to terminals A and B of the defining transformer. The direct internal connection between the inner conductors, in connection with the

return through the outer shield, provides a one-turn loop around the high-permeability core shown shaded. A detector is connected to a 100-turn winding on this core via the coaxial connector C, and indicates a null

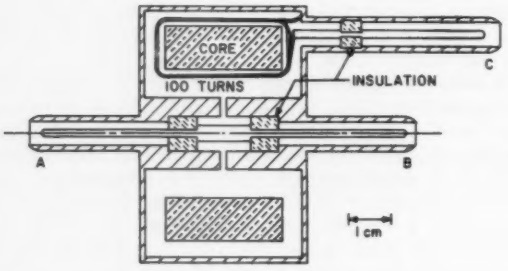

FIGURE 3. *"Defining transformer" for terminating current and potential leads of four-pair standards.*

if the potentials at A and B are equal. Capacitance between the 100-turn winding and the connection between the inner connectors of A and B could cause substantial errors. An internal shield with a thin air gap as shown eliminates this problem. Incomplete shielding can be detected by interchanging A and B.

When using defining transformers in a bridge, the potential leads are considered to terminate at the center of the device, in the region of the insulated gap in the inner shield. A number of nearly identical defining transformers have been built such that they may be used interchangeably to terminate the potential leads of the standards without changing the loads on the leads. These devices are used in the current leads also, in which case a generator may be substituted for the null detector.

Some objection may be made to the use of these devices, in that the standard is no longer an entity in itself, but has a definition dependent upon a termination; which might more properly be considered as part of the measuring instrument. Precedents do exist for this type of procedure, an example being the use of a precision coaxial connector on a two-terminal capacitor, for which a correct measurement requires a mating precision connector. In practice a very substantial simplification of our measurements was found to result from the introduction of defining transformers.

The technique which we use for measuring the effects of net currents between one terminal pair and another in a bridge containing coaxial chokes is rather cumbersome, but provides a reliable measure of the errors caused by non-ideal coaxial chokes. It is first assumed that every ground loop in the system to be investigated contains a coaxial choke, and that the minimum possible number of chokes to accomplish this purpose is used. This does not imply that one cannot add as many ground loops as may be desired, but simply that in the final circuit all ground loops are interrupted with a minimum number of coaxial chokes. Singling out a particular choke for investigation, a single turn of wire is wrapped around the core of the choke and connected to an auxiliary detector. The deflection of this detector is a measure of the voltage tending to drive current through the choke.

A quantitative measure of this voltage may be obtained using the voltage insertion transformer shown in figure 4. This device consists of a high permeability

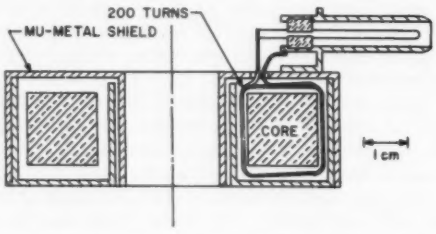

FIGURE 4. *Voltage insertion transformer for investigating errors caused by net currents in coaxial cables.*

toroidal core wrapped with 200 turns of wire connected to a coaxial connector. A toroidal mu-metal shield surrounds the core and winding, so that negligible magnetic fields exist outside of the shield when the 200-turn winding is excited. In use, the cable leading to the choke selected for testing is passed through the hole in the shield of this device, forming a 200:1 transformer. A voltage source derived from the same oscillator supplying the bridge, and adjustable in both real and imaginary components, is connected to the 200-turn winding. We find that an operational amplifier circuit described in an earlier paper [6] is convenient for this purpose.

The voltage source is adjusted until the auxiliary detector monitoring the voltage across the coaxial choke registers a null. The real and imaginary parts of the adjustable voltage required to obtain this null are recorded. The next step is to remove the auxiliary detector and to change the adjustable voltage by an amount large enough to yield sufficient sensitivity but not large enough to drive the choke into a nonlinear region. The real and imaginary parts of the change in balance point of the bridge caused by this change in applied voltage are recorded. A straightforward manipulation of the various complex quantities obtained by this scheme allows one to calculate the real and imaginary parts of the error caused by incomplete suppression of net current by the coaxial choke.

All of the coaxial chokes in the system are evaluated in this way. An algebraic addition of the individual errors then gives the total error, which is applied as a correction to the raw results of the measurement.

The technique sketched above could be generalized for a system with M chokes by providing each of the M chokes with voltage insertion transformers, and by bringing all of the choke voltages simultaneously to a null as indicated by M auxiliary detectors. In this case no net currents with their attendant errors would exist, and there would be no corrections to apply to the bridge balance. The complete system applied in the circuit of figure 2 could then be viewed as one with

$M+6$ adjustable parameters and with $M+6$ null detectors. One could conceivably construct a combining network to diagonalize the matrix relating these two vector quantities to make the effects of net choke currents less important. This has not yet been required for our purposes, since the residual errors due to net currents through the chokes are small enough to be measured with adequate precision using the extrapolation technique sketched above.

It is very important that one uses the minimum number of chokes necessary to break all ground loops when the normal loop voltages are measured by balancing them out as indicated above. If two chokes of equal impedance were in series in a particular loop, the method described would assign the total loop voltage to each choke, when in reality each choke would have across it only half of the total voltage. A simple test for multiply choked loops is to measure the voltages at each choke produced by exciting each loop in turn with a voltage insertion transformer. If the nondiagonal terms of the resultant matrix are much smaller than the diagonal terms, no multiply choked loops exist.

It is found in measuring the effects of the chokes in a given system that they can often be placed in categories according to the amount of voltage driving the loop, and according to the effect of a loop voltage on the bridge balance. The measurement error caused by a coaxial choke having insufficient impedance is large only if the loop voltage driving a choke is large *and* if a voltage in this loop has a strong effect on the bridge balance. It is usually possible to arrange a bridge in such a way that no choke has both undesirable characteristics. This usually requires the addition of extra ground connections with an extra choke for each added connection. The procedure for accomplishing this is at this time largely empirical.

Coaxial chokes do not provide the only means for suppressing net currents in coaxial cables. Isolation transformers are used in some cases, and net currents can then result from unbalanced interwinding capacitances. If the interwinding capacitances are very poorly balanced, the effective ground loop voltage can be quite high, and the accurate measurement of the errors due to the resultant ground loop current is rather difficult. In such cases it is usually best to measure the current directly, for example by converting the voltage insertion transformer to a current sensor by connecting a phase-sensitive voltmeter in parallel with a low impedance load to the 200-turn winding.

About the only other errors likely to occur in a four-pair bridge are those caused by stray couplings between the various components. These effects can usually be made negligible with electrostatic and electromagnetic shields, and tests for the effectiveness of these shields are not difficult to perform. Eccentric coaxial cables usually cause no serious problems, but must be considered. In some cases acoustic couplings can be troublesome, particularly if the generator and detector circuits both contain partially magnetized transformers. The 100:1 bridge described in section 5 suffered from this effect initially, but after the cores were carefully demagnetized and after the addition of some acoustic insulation, the errors due to acoustic coupling were reduced to a few parts in 10^{10}. The mechanism responsible for the acoustic coupling involves magnetostriction in the core of the transformer in the generator circuit. If the core is partially magnetized, the acoustic output of the core will contain a component at the same frequency as the generator in addition to the expected but less troublesome components at the even harmonics of the generator frequency. The resultant mechanical excitation of the transformer in the detector circuit causes no trouble unless the detector transformer is also partially magnetized, in which case a fundamental frequency component of current can be generated.

Some care must be taken when adjusting the meters of the null detector to zero deflection in the absence of a signal. It had been the practice at NBS to disconnect the admittance standards of a bridge from the voltage transformer to which they were normally connected and to zero the meters with the voltage transformer excited. This technique eliminates most of the errors due to magnetic coupling from the oscillator and voltage transformer to the detector, and also eliminates some of the errors caused by imperfect coaxial chokes. When the choke errors are measured independently as sketched above, this procedure could result in a double correction for some of the choke errors.

3. Quadrature Bridge

As the first example of an actual four-pair bridge, we will use a type of frequency-dependent bridge of which two-pair versions have been in existence for some time [4, 7, 8, 9]. The circuit is basically the same as that described by Thompson [4] and uses the twin-tee detector coupling network proposed by him. The NBS bridge contains two 10^5-Ω four-pair resistors and two 1-nF four-pair capacitors, and operates at an angular frequency of 10^4 rad/s, which corresponds to a frequency of about 1592 Hz. Figure 5 shows a partial schematic of the NBS four-pair quadrature bridge, in which D_1 through D_8 are null detectors, T_5 through T_9 are defining transformers, and P_1 through P_4 are the four-pair admittance standards. Seven of the eight complex adjustments required to balance the eight null detectors are indicated by either admittances or generators with arrows through their symbols. These seven adjustments are required only for realizing the defining conditions for the four-pair admittances, and may be uncalibrated. The eighth complex adjustment required to balance the bridge is made through the use of two seven-dial inductive voltage dividers T_2 and T_3, which drive small fixed capacitors labeled Y_5 and Y_6. This complex pair of adjustments serves to indicate the relationship between P_1, P_2, P_3, and P_4. Using the notation indicated on figure 5, we have when all detectors are balanced

$$i_1 = e_a P_1 + e_d Y_5 \approx -e_c P_2$$

and

$$i_2 = e_b P_4 + e_f Y_6 \approx -e_c P_3.$$

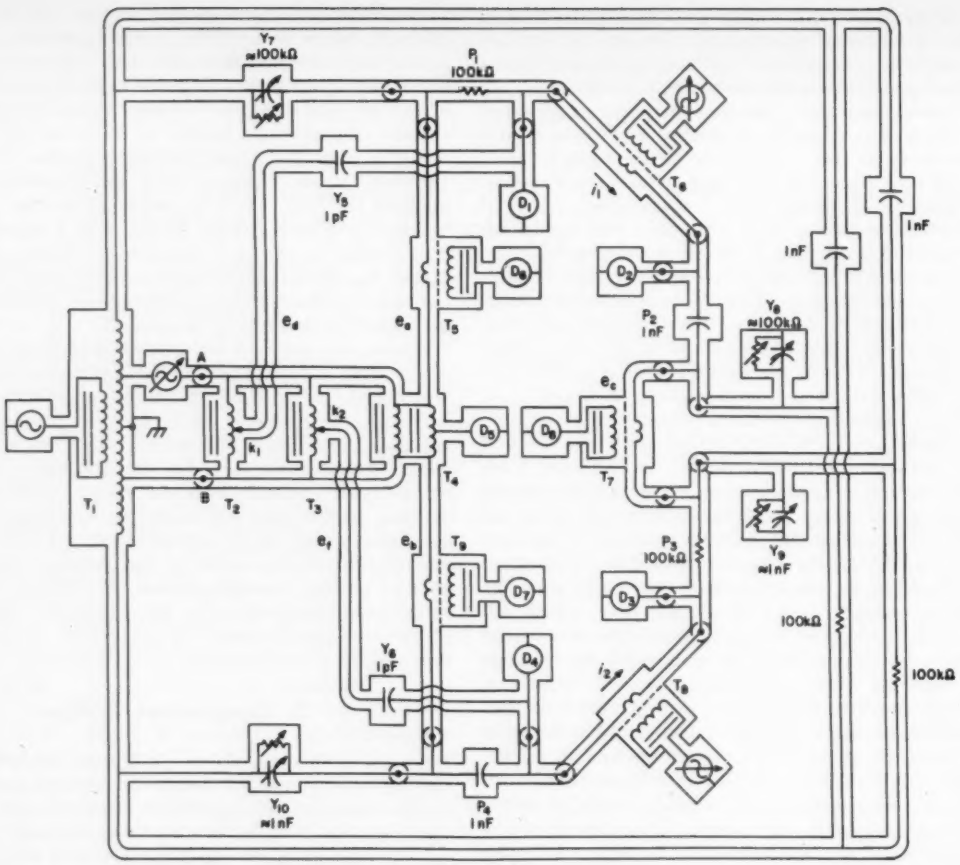

FIGURE 5. *Four-pair quadrature bridge with detector combining network deleted.*

If we represent the ratio of T_4 by $e_b = -e_a(1+\delta)$ with δ complex and $|\delta| \ll 1$, and since $e_d \approx e_a(2k_1-1)$ and $e_f \approx -e_b(2k_2-1)$, we have the balance condition

$$P_3[P_1+Y_5(2k_1-1)] \approx -P_2(1+\delta)[P_4-Y_6(2k_2-1)]. \tag{3}$$

A repeat measurement is made with the connections interchanged at points A and B, and with the connections between T_4 and the defining transformers T_5 and T_9 interchanged. This reverses the sign of δ to first order, and also reverses T_2 and T_3, so that

$$e_d' \approx e_a(1-2k_1') \qquad \text{and} \qquad e_f' \approx -e_b(1-2k_2').$$

The resultant balance condition is

$$P_3[P_1+Y_5(1-2k_1')] \approx -P_2(1-\delta)[P_4-Y_6(1-2k_2')]. \tag{4}$$

Averaging (3) and (4) we have

$$P_3[P_1+Y_5(k_1-k_1')] \approx -P_2[P_4-Y_6(k_2-k_2')]. \tag{5}$$

If we let $P_n = G_n + j\omega C_n$, $Y_5 = j\omega C_5$ and $Y_6 = j\omega C_6$ and assume that $G_1 \approx G_3 \approx \omega C_2 \approx \omega C_4$ and that $\omega C_1 \ll G_1$, $\omega C_3 \ll G_3$, $G_2 \ll \omega C_2$ and $G_4 \ll \omega C_4$, we may separate real and imaginary parts of (5) to obtain

$$\frac{G_3 G_1}{\omega^2 C_2 C_4} \approx 1 + \frac{C_6}{C_4}(k_2 - k_2') \tag{6}$$

which relates the main components of the four-pair admittances, and

$$\frac{\omega C_1}{G_1} + \frac{\omega C_3}{G_3} + \frac{G_2}{\omega C_2} + \frac{G_4}{\omega C_4} \approx \frac{G_5}{C_2}(k_1' - k_1) \tag{7}$$

which relates the phase angles of the four-pair admittances.

The approximations made in deriving (6) and (7) cause no errors exceeding 2 parts in 10^{10} for the NBS four-pair quadrature bridge. Under less ideal conditions, the second-order correction terms might be required.

The nominally 1 : 1 transformer T_4 in figure 5 is of two-stage construction [6, 10], with a mu-metal shield between the first and second stages, and with another mu-metal shield surrounding the entire transformer. It can be seen that when the null detectors D_6 and D_7 are balanced, the output terminal pairs of T_4 are subject to open circuit conditions as defined at the central reference planes of the defining transformers T_5 and T_9. The voltages e_a and e_b in the equations above are referred to these reference planes in a manner analogous to the definitions of the open circuit voltages of the four pair standards. Reversal of T_4 is accomplished by reconnecting the cables at the points of entry to T_5 and T_9, which has a negligible effect on the open circuit ratio.

Three of the eight null detectors shown in figure 5 are not operated on by the combining network used with the bridge. The detectors labeled D_6, D_7, and D_8 connected to T_5, T_7, and T_9 are brought to a null one at a time by adjusting Y_7, Y_{10}, and either Y_8 or Y_9, after which these detector terminals are shorted to reduce the effect on the main detector of a slight error in these auxiliary balances. This technique works very well for adjusting Y_7 and Y_{10}, but some convergence problems exist with the balance of Y_8 or Y_9. Ideally, one would like to null the detector D_8 connected to T_7 by adjusting $Y_8 - Y_9$ while keeping $Y_8 + Y_9$ fixed. One of the other balance conditions turns out to involve $Y_8 + Y_9$ but not $Y_8 - Y_9$. In practice, we have been able to achieve fast convergences of these two auxiliary balances without the elaboration of ganged switches by manually tracking Y_8 with Y_9.

The guiding principle behind the combining network used with the bridge (see fig. 6) is to combine the various detector terminal pairs two at a time and further to combine the new detector terminals so formed until only one detector terminal pair remains. We begin by combining the detector terminals D_1 and D_2 of P_1 and P_2 to form a single detector terminal D_9 which does not respond to excitation of T_6, and by similarly combining the detector terminals D_3 and D_4 of P_3 and P_4, to form a single detector terminal D_{10} which does not respond to excitation of T_8. The initial combining network linking the detector terminals D_1 and D_2 can be understood by letting $e_a = e_c = 0$ in figure 5 and observing that the circuit between T_6 and D_9 in figure 6 is a Schering bridge, for which a complex balance may be obtained by adjusting the two variable capacitors C_{11} and C_{12}. The circuit is adjusted by actually connecting the bridge generator to the input lead of T_6 rather than to the input of T_1. After C_{11} and C_{12} are adjusted, the input terminal of T_6 is shorted. The result is that although the voltage at neither D_1 nor D_2 is exactly nulled, these voltages are very small; and since changing the excitation on T_6 does not change the voltage at D_9, no error results from failure to adjust this excitation to obtain individual nulls on the detector pairs D_1 and D_2. The combining network between the detector terminals of D_3 and D_4 is identical with that described above, and is adjusted by varying C_{13} and C_{14}. The relative sizes of the admittances are chosen to produce a minimal effect on the bridge sensitivity and on the operation of the twin-tee combining network linking D_9 and D_{10}.

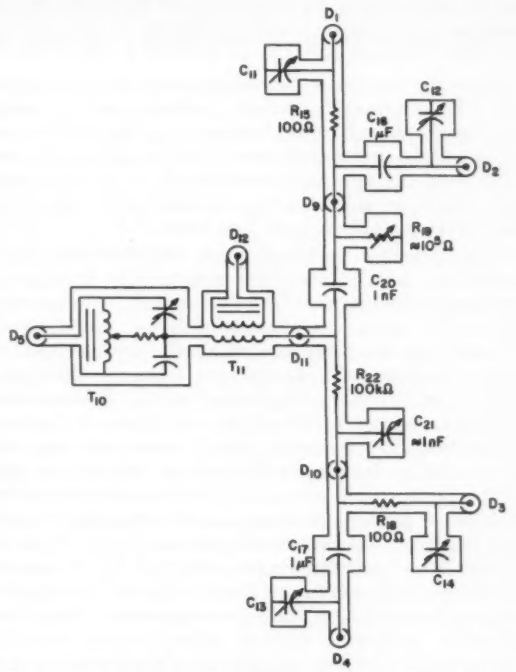

FIGURE 6. *Detector combining network for quadrature bridge.*

The network linking D_9 and D_{10} may be understood by letting all generators in figure 5 be zero and by assuming that a generator is inserted to make $e_c \neq 0$. The network can be recognized as a twin-tee circuit in which a null can be produced at D_{11} by adjusting R_{19} and C_{21}. After making this balance, the voltage at D_{11} is independent of the auxiliary adjustment $Y_8 + Y_9$. In practice the twin-tee is adjusted so that changing $Y_8 + Y_9$ produced no change in the detector voltage at D_{11} and $Y_8 + Y_9$ is adjusted so that changing the twin-tee setting produces no change in the detector voltage at D_{11}.

Although a twin-tee combining network is convenient for a quadrature bridge, a detailed noise calculation shows that it rather greatly augments the thermal agitation noise already present in P_1 and P_3. With 4 mW dissipated in P_1 and P_3, one has difficulty in detecting an unbalance smaller than one or two parts in 10^9. A substantial improvement could be made by maintaining the combining network at low temperature, or by separately amplifying the voltages at D_9 and D_{10} before coupling them together.

The final combining network links D_{11} and D_5 with D_{12}. It is adjusted by means of the decade inductive voltage divider T_{10} and the associated phase-shifting network so that inserting a 5-Ω resistor in one of the cables joining T_1 with T_2, T_3, and T_4 to simulate the generator shown in figure 5 does not change the detector voltage at D_{12}. After making this adjustment the 5-Ω resistor is removed.

The sequence of adjustments outlined above is easier to perform than to describe. The entire bridge can be adjusted in 10 minutes, and the auxiliary adjustments have been found to drift in a week by less than that required to yield an error of 1 part in 10^9.

The complete quadrature bridge consisting of figures 5 and 6 contains 25 coaxial chokes, each of which was checked using the techniques described in section 2. The largest individual error was found to be 1 part in 10^{10}, and the total error resulting from the existence of net currents in all chokes, the algebraic sum of the individual errors, was about 2 parts in 10^{11}.

Some special problems are encountered in a quadrature bridge simply because the balance is frequency-dependent. One especially important problem is caused by intermodulation distortion in the bridge detector between adjacent harmonics of the bridge fundamental frequency. These distortion products may have components at the fundamental frequency, which would cause a substantial error. The individual harmonic components entering the detector of a frequency-dependent bridge are not nulled with the fundamental as they are in a frequency-independent bridge, and may be of rather high amplitude. We use a special filter between T_{11} of figure 6 and the detector amplifier to reject all harmonics of the bridge fundamental frequency before the signals reach any strongly nonlinear elements. The filter contains a bridge network to obtain a zero transfer admittance for the second and third harmonics of the fundamental frequency, and a doubly tuned circuit to attenuate all higher harmonics. The circuit is similar to that used in an earlier quad bridge [7] but has been modified to yield a smaller noise figure.

The need for a good filter is indicated by the fact that removing the filter results in an apparent change in the bridge balance of several parts in 10^8. With the filter in, tests indicate that the error due to intermodulation distortion is less than 1 part in 10^9. A convenient check on the effectiveness of the filter is to augment each of the harmonics present at the detector terminal D_{12} by injecting an additional current into D_{12} with a small capacitor connected to an auxiliary oscillator tuned to the appropriate harmonic. Other tests using two auxiliary oscillators confirm that the effect is indeed due to intermodulation distortion. The technique is very sensitive, and can be used to detect distortion products resulting from nonlinear mixing of frequencies up to at least the 15th harmonic. The technique gives only an upper bound to the error and would probably not be reliable for determining corrections.

If a frequency-dependent bridge is balanced at an angular frequency $\omega=\omega_0$, then for $\omega \approx \omega_0$, the detector input voltage will be given by $e_d=k_1(\omega-\omega_0)e_g$ where k_1 is a complex constant and e_g is the bridge generator voltage. If the detector contains a sharply tuned single section filter (6 dB/octave) having a bandwidth $2\omega_d$, then for frequencies near ω_0 the detector output voltage will be of the form

$$e_0=\frac{k_2(\omega-\omega_0)e_g}{1+\frac{j(\omega-\omega_0)}{\omega_d}}. \tag{8}$$

The power transfer function between the bridge input terminals and the detector is then given by

$$TF_1 \propto \frac{(\omega-\omega_0)^2}{1+\left(\frac{\omega-\omega_0}{\omega_d}\right)^2}=\frac{\Delta\omega^2}{1+\left(\frac{\Delta\omega}{\omega_d}\right)^2}. \tag{9}$$

If a two section filter were used (12 dB/octave), the power transfer function would be

$$TF_2 \propto \left(\frac{\Delta\omega}{1+\left(\frac{\Delta\omega}{\omega_d}\right)^2}\right)^2. \tag{10}$$

TF_1 and TF_2 are plotted in figures 7 and 8 for several values of ω_d. In both cases, oscillator noise components with frequencies very near ω_0 are strongly attenuated, and those at the edge of the filter pass band are the least attenuated.

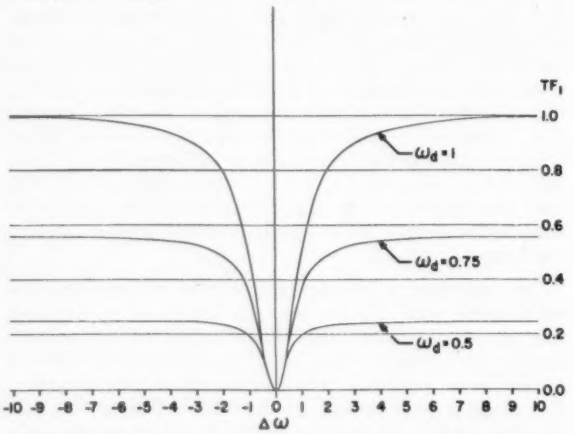

FIGURE 7. *Power transfer functions for a frequency-dependent bridge followed by a single section filter.*

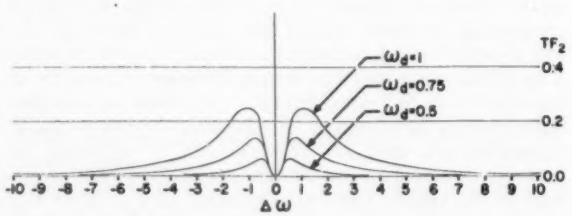

FIGURE 8. *Power transfer functions for a frequency-dependent bridge followed by a double section filter.*

The total noise power reaching the detector depends upon the noise spectrum of the oscillator. This is not known a priori, but in general is highest near ω_0. We will assume arbitrarily that the noise spectrum is of constant amplitude, in order to simplify the calcula-

tions. In this case, the total noise power with a single section filter would be of the form

$$W_1 \propto \int_0^\infty \frac{(\omega-\omega_0)^2}{1+\left(\frac{\omega-\omega_0}{\omega_d}\right)^2} d\omega \rightarrow \infty \qquad (11)$$

and for a two-section filter,

$$W_2 \propto \int_0^\infty \left[\frac{\omega-\omega_0}{1+\left(\frac{\omega-\omega_0}{\omega_d}\right)^2}\right]^2 d\omega \rightarrow \frac{\pi\omega_d^3}{2}. \qquad (12)$$

The expression (11) for W_1 is not realistic because (9) is correct only for $\omega \approx \omega_0$. In general TF_1 would decrease when $\Delta\omega$ is very large and would not remain constant, so that W_1 would be very large but finite.

The advantage of using a two-section filter is obvious from figures 7 and 8 and from (11) and (12), and in addition the very strong dependence of W_2 on the filter bandwidth can be seen. If the oscillator noise spectrum had a peak at $\omega=\omega_0$, the exponent of ω_d in (12) would be reduced, but in practice the observed detector noise due to oscillator noise decreases faster than that due to ordinary thermal agitation noise in the bridge components when the detector bandwidth is decreased. We find with the NBS quadrature bridge connected to a reasonably clean oscillator that the use of two cascaded filters with time constants of 0.3 s makes the portion of the detector noise due to oscillator noise about equal to that due to thermal agitation noise in the bridge components. Filters with 3-s time constants are normally employed, in which case the effect of oscillator noise is negligible.

The above discussion deals with noise power and makes no distinction between the different effects of FM and AM noise. If a frequency-dependent bridge is connected to a two-phase phase sensitive detector adjusted so that the first channel responds only to the "real" part of the bridge balance and the second channel responds only to the "phase" part of the bridge balance, then the effect of FM noise on the oscillator is to give noise only on the first or real channel of the phase-sensitive detector, as might be expected. It can also be shown that the effect of AM noise on the oscillator is to give noise only on the second or "phase" channel of the detector. The latter effect is not usually anticipated. One consequence of this effect is that when the power level of the bridge is being changed, the phase channel of the detector is thrown off balance, usually by enough to saturate the detector and to require a short wait before the detector recovers. The separation of FM and AM noise with a frequency-dependent bridge can be helpful in the study of oscillator noise.

The main components, P_1, P_2, P_3, and P_4 of the NBS quadrature bridge are maintained at 25 ± 0.001 °C in an oil bath. The precision of the bridge is limited by the temperature variations in the bath and by the load coefficients of P_1 and P_3. The sum of all other errors, including that due to thermal agitation noise, is believed to be less than 1 part in 10^9.

4. Four-Pair Direct-Reading Ratio Set (DRRS)

The bridge to be described next was actually the first four-pair admittance bridge to be completed at NBS, and is in some ways not as well conceived as the more recent quadrature bridge described above. It is nevertheless a highly accurate and wide range instrument, and has received much use in the last few years. The bridge has a number of rather complex features, making it difficult to understand without prior experience with four-pair bridges. It is for this reason that its description follows that of the quadrature bridge.

The four-pair direct-reading ratio set was intended to provide a means of comparing two four-pair admittances whose ratio is nominally 10:1. It was designed so that it could also be used to compare ordinary two-pair standards. Fewer auxiliary balances are required with the two-pair configuration, so this usage will be described first.

An elementary schematic of the bridge is shown in figure 9. The two admittances to be compared are labeled Y_1 and Y_2, and are connected to three star connectors as indicated. The star connectors are constructed in accordance with a design first described by

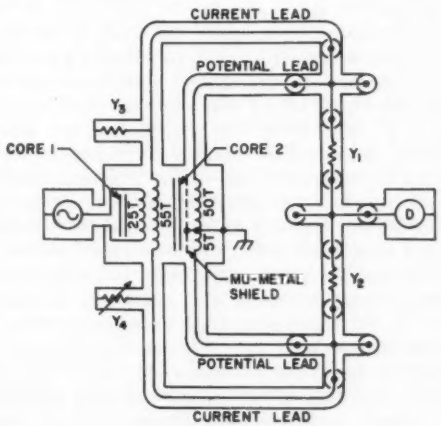

FIGURE 9. *Elementary 10:1 bridge using a two-stage transformer.*

Hamon [11] for dc junctions, but are provided with ground potential shields to allow their use with alternating current. The equivalent circuit of an ideal four-pair star connector consists of five impedances linking the five terminals to an inaccessable internal junction point. The impedance to ground is typically much larger than the other four. With this system, the admittances under test are considered to terminate at the internal junction points of the star connectors, rather than at the ends of the coaxial cables leading to the standards. The discrepancy between the two

definitions of a standard is small if its admittance is small, but could be accounted for to first order.

The transformer in figure 9 is a two-stage device in which the 25-turn primary and the 55-turn current winding are wound around core 1 only. The 50-turn and 5-turn potential windings are wound around both cores and are isolated from the inner windings and the two cores by a mu-metal shield.

If there were no capacitance between windings or to ground, there would be very little current in the potential leads to Y_1 and Y_2, and a detector connected to the star connector between Y_1 and Y_2 would register a null when Y_1/Y_2 equalled the open circuit ratio of the potential windings. Because of loading effects, both in the potential winding circuit and in Y_1 and Y_2 and the associated cables, two auxiliary balances are required to obtain zero current in both potential leads. The first auxiliary balance can be conveniently obtained by means of an adjustable admittance to ground Y_4 so that Y_3 and Y_4 serve as a conventional Wagner circuit, and the second balance can be obtained by means of an auxiliary winding around core 2 only (not shown), whose excitation is adjustable and derived from a high impedance source. It may be noted here that one anticipates that only a very small excitation will be required on core 2, to drive current through the interwinding capacitance of the transformer potential windings, and that very little voltage will appear across the auxiliary winding on core 2 because of the two-stage construction. Ideally, an adjustable current source could be used to drive core 2.

The balance procedure for the system of figure 9 would be first to adjust Y_1 or Y_2 to achieve a null on the detector; second, to disconnect both potential leads between the transformer and the star connectors and to adjust Y_4 to restore the null (a balance which is completely independent of the excitation of core 2); and third, to reconnect one of the potential leads and to restore the null by adjusting the core 2 excitation. The process is repeated until the adjustment of Y_1/Y_2 converges to a fixed ratio, which is equal to the open circuit ratio of the transformer potential windings.

A fast convergence of this series of balances is obtained if the equivalent impedences in series with the potential windings are very small with respect to the impedences of the second core excitation circuit and of the Wagner circuit. A technique for eliminating the impedance in series with the high-voltage secondary winding of a three-winding transformer at the expense of slightly increasing the impedence in series with the low-voltage secondary winding has been described [6]. This technique is illustrated by the equivalent circuits based on ideal transformers shown in figures 10a and 10b. The circuit of figure 10a is equivalent to the circuit of figure 10b, with $z_1' = z_1 - 9z_3$ and $z_2' = z_2 + 0.9z_3$ for a transformer with a 10:1 ratio. The unlabeled impedences and turns ratio are not precisely equal in the two figures, but this is not important. The significant result is that z_3 can be adjusted to make $z_1' = 0$.

A technique for making the effective impedance in series with the low potential winding also equal to zero is shown in figure 11. If there is no current in the low potential winding, there will be no voltage across transformer T_2, and hence no current through the

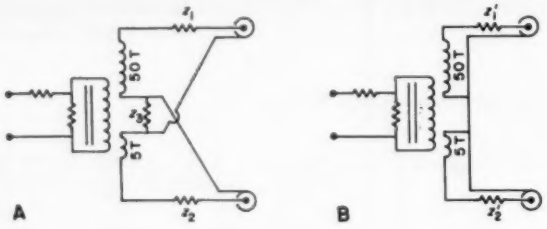

FIGURE 10. *Equivalent circuits for showing the effect of* z_3 *on* z_1' *(see text).*

auxiliary admittance Y_2'. However, if there is a current in the potential winding, T_2 will be excited, producing a compensating current in Y_2'. In the worst case, suppose the potential lead of Y_2 is shorted. Then if $z_2'' = z_2'$, the voltage on the 100-turn winding of T_2 will be $e_1/2$, and the voltage applied to Y_2' will be equal to e_1. The drastic measure of shorting the potential lead of Y_2 would then cause no deflection of the null detector provided $Y_2' = Y_2$. An argument based on the circuit linearity indicates that smaller currents in the low potential lead would likewise cause no deflection of the null detector.

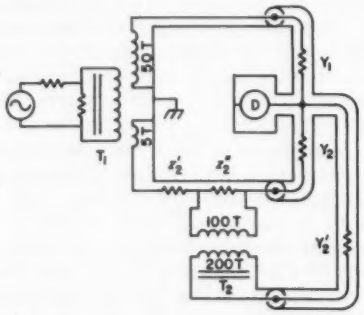

FIGURE 11. *Compensation scheme for eliminating the effect of* z_2'.

Applying the concepts of figures 10 and 11 to the basic circuit of figure 9 we have a system in which the currents in both potential leads can be adjusted to zero, but in which the bridge balance condition is not strongly dependent upon either auxiliary balance. In order to make the potential lead impedances definite so that z_3 and z_2'' need only be adjusted once during construction of the bridge, we have elected to plug the star connectors directly into the potential terminals on top of the bridge. The adjustments of z_3 and z_2'' then serve to make the effective impedances from the internal junction points of the star connectors to the equivalent voltage generators of the transformer potential windings equal to zero, using an auxiliary admittance $Y_2' = Y_2$. It is to be noted that when this

bridge was designed, the special defining transformers described in section 2 had not yet been invented and the potential leads were open circuited by simply unplugging them. This technique is adequate in this particular case since the potential lead equivalent series impedances are very small. When the junctions between the current and potential leads are located remotely from the bridge, as is the case when measuring four-pair admittances, the lead impedances are not small, and the Wagner and second core excitation adjustments are very critical. The shunt capacitance uncertainties caused by unplugging the coaxial connector could then cause substantial errors.

In order to make a direct reading ratio set out of the circuit of figure 9, a means must be provided for adjusting the ratio of the potential winding in accurately divided steps. The adjustment of the magnitude of the ratio is straightforward, and can be accomplished in principle by means of a step-down transformer T_4 and a six-decade inductive voltage divider T_3 magnetically coupled to the potential windings of T_1 as shown in figure 12. Although T_3 and T_4 are represented as being ordinary single-stage transformers, they are actually both two-stage devices. The first stage of T_3 is coupled to the first stage of T_1 only, and is used to excite the first stage of T_4. The switching of the first and second stages of T_3 are ganged, which improves the accuracy of the voltage division, and results in a negligible interaction with the core 2 excitation adjustment for T_1.

Constructing an accurate quadrature adjustment for a direct-reading ratio set is much more difficult than constructing an equally accurate magnitude adjustment. At the heart of the problem is the requirement for a 90° phase-shifting circuit. The conflicting requirements of small output impedance, relatively large output voltage, and reasonably small power dissipation tend to limit the accuracy and range of most passive quadrature balance circuits.

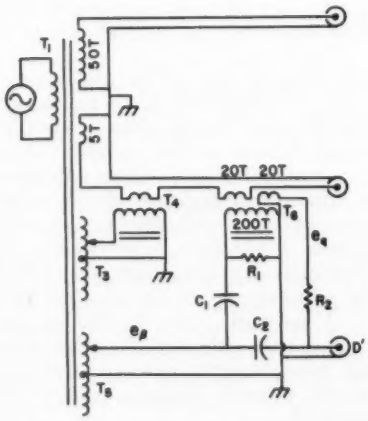

FIGURE 12. *Circuitry for adjusting the real and quadrature components of a transformer ratio.*

In the quadrature balance system shown in figure 12, the output of a phase shifting circuit consisting of a 0.01-μF capacitor C_1 and a 10-Ω resistor R_1 is connected to the primary of the three-winding transformer T_6. One secondary of T_6 is in series with the low potential winding of T_1. R_1 is small compared to the input impedance of T_6, and since $\omega R_1 C_1 \ll 1$, the voltage e_q added to T_1 by T_6 is nearly orthogonal to the voltage across T_5 and nearly of the desired magnitude. A test of the voltage added to T_1 by T_6 can be made by setting up a bridge using a precision 1-nF capacitor C_2 and a precision 10-Ω resistor R_2. A detector connected to terminal D' will register a null when $e_\beta j\omega C_2 = e_q/R_2$. A small complex adjustment of the excitation to the primary of T_6 may be made to give a null at D', so that $e_q = e_\beta j\omega C_2 R_2$. Divider T_5 is a six-decade, two-stage device similar to T_3, and in fact has separate windings on ganged switches to separate the coarse output tap connected to C_1 from the precision output tap connected to C_2. Resistor R_2 may at this stage be considered to include the equivalent series impedance of the winding on T_6 to which it is connected, but in the final design an extra winding was put on T_6 to provide a four-terminal connection for R_2.

When the circuits of figures 9, 10, 11, and 12 are combined, the result is a system with two sets of detector terminals. The advantages of combining the two to give a single detector whose response is essentially independent of the excitation of T_6 is by now quite apparent. The NBS bridge has been designed so that connecting an auxiliary admittance $Y_2'' = Y_2$ from D' to the main null detector D indicated in figure 9 achieves the desired effect. Rather than using two equal auxiliary admittances Y_2' and Y_2'', a single admittance is used for both purposes by connecting the 200-turn output winding of T_2 in figure 11 between terminal D' in figure 12 and the auxiliary admittance. This serves to add the compensating voltage produced in the quadrature balance circuit of figure 12 to that produced in the load compensation circuit of figure 11.

The complete four-pair direct-reading ratio set contains all of the features described above, and some special compensation circuits for obtaining a quadrature adjustment which is precisely proportional to frequency. The only critical impedances required in the bridge are the capacitor C_2 and the resistor R_2 involved in the quadrature adjustment circuit.

The bridge was a test bed for a number of previously untried ideas, and as such it grew in a rather haphazard manner. It is felt that the bridge could be greatly improved if it were rebuilt, and while this is not contemplated at this time, a complete circuit of the existing bridge would be more exposing than revealing, and therefore no such circuit appears in this paper. It is perhaps useful to point out that the key to achieving highly accurate and stable ratios in critical transformers and inductive dividers is to make generous use of multi-stage transformers with magnetic shielding between stages. The principal errors in such transformers are due to capacitive loading effects working on their output impedances. Both the interwinding

capacitances and the output impedances are minimized by minimizing the number of turns on the transformer. The optimum number of turns on a shielded two-stage transformer designed for audiofrequencies is believed to be less than 100 turns, which is much smaller than the number normally employed in a single-stage design.

The calibration of the bridge was in some ways even more formidable than its construction. The first step was to check the linearity of the bridge dials at several frequencies by an external calibration technique in which a fixed admittance was repeatedly added in parallel with one side of the bridge for various settings of an auxiliary admittance in parallel with the other side. Both magnitude and quadrature balance linearities of all dials were checked in this way. A resolution of 1 part in 10^{10} was obtained at 1592 Hz, and of 1 part in 10^9 at all other frequencies.

The second step was to determine the actual bridge settings which would produce an exact 10:1 ratio. A modification of the permutation method described in an earlier paper [12] was used for this purpose.

The last step in the calibration was to determine the actual magnitudes and phase angles corresponding to changes of the real and quadrature dials of the bridge over their entire ranges. A quadrature bridge and a system for comparing admittances in a 1000:1 ratio are needed for this step. Three step-ups using the 10:1 ratio of the bridge under test provided the 1000:1 ratio with ample accuracy.

The bridge accuracy is optimum at 1592 Hz, at which frequency the ratio is adjustable over a range of ± 5 parts in 10^4 in steps of 1 part in 10^9 for both real and quadrature components. A complete calibration using the procedure outlined above disclosed that the bridge readings are linear at 1592 Hz over the entire range of the dials within an estimated uncertainty of 3 parts in 10^{10}. The actual changes in both real and imaginary parts of the bridge ratio produced by changing the dials over their entire ranges differ slightly from the values indicated on the dials. The discrepancies are never greater than 5 parts in 10^9, even when the bridge dials are at the limits of their ranges. Corrections for linear errors of this form are relatively easy to apply.

At 159.2 Hz, the range of the bridge quadrature balance control decreases to ± 5 parts in 10^5, and at 15920 Hz it increases to ± 5 parts in 10^3. The first decade of the quadrature balance control is somewhat nonlinear above 10 kHz, but if the bridge is not used for comparing admittances for which the quadrature component of their ratio exceeds ± 5 parts in 10^4, no errors exceeding 5 parts in 10^9 exist from 159.2 Hz to 15920 Hz.

The additional circuitry needed when using the bridge for comparing four-pair standards, P_1 and P_2, is shown in figure 13. The critical leads to the standards P_1 and P_2 are terminated at the reference planes of the defining transformers T_7, T_8, and T_9, and the leads between these transformers and the standards are treated as part of the standards. The combining network involving T_{10} and the associated phase-shifting network, which joins the detector terminals D_1 and D_2 of the two standards, is adjusted to obtain a null on D_6 when an oscillator is connected to the 100-turn input winding of the defining transformer T_8. Then the input winding of T_8 is shorted and the oscillator is reconnected normally. Alternatively, this adjustment can be made by leaving the oscillator connected normally, and adjusting the network so that D_6 does not respond when the short on T_8 is removed.

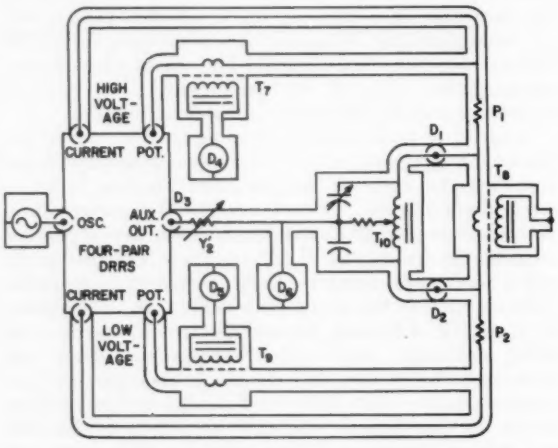

FIGURE 13. *Comparison of four-pair admittances with the four-pair DRRS.*

The Wagner balance and second core excitation of the four-pair bridge are adjusted to obtain nulls on detectors connected to points D_4 and D_5 of defining transformers T_7 and T_9 rather than by disconnecting the potential leads to the bridge. With this system the bridge ratio is defined at the reference planes in T_7 and T_9, and differs from the ratio defined at the potential terminals of the bridge. Techniques for comparing the ratios defined in these two ways can be easily developed, or alternatively the permutation method for measuring the bridge ratio [12] can be modified to give the ratio at the reference planes of T_7 and T_9 directly. A standard pair of cables for connecting T_7 and T_9 to the potential terminals of the bridge is obviously required.

The circuit of figure 13 is not easy to operate directly, partly because the deflections of the auxiliary detectors connected to D_4 and D_5 both change when either the bridge Wagner Balance or the second core excitation is changed, and partly because these balances are both much more critical than they are when comparing two-pair admittances. The criticalness is caused by the extra equivalent impedances in series with the bridge potential terminals resulting from the added cables between these terminals and the internal junctions of P_1 and P_2. A network with the double purpose of combining the output of D_5 with the main detector and of providing two auxiliary detector outputs, one of which responds to each bridge auxiliary balance, is shown in figure 14.

The 100-turn windings of both T_7 and T_9 are terminated with 50-Ω resistors, which when referred to the

1-turn input windings yields a very small impedance. The voltages across the 100-turn windings are thus proportional to the currents in T_7 and T_9. The output voltage at terminal D_8 is proportional to the sum of these two currents, and responds to changes in the

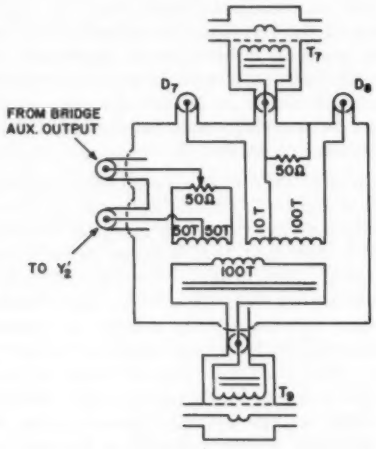

FIGURE 14. *Combining network for assuring fast convergence of DRRS auxiliary balances.*

Wagner balance but not to changes in the second core excitation. The output voltage at terminal D_7 is proportional to the current in T_7 minus 1/10 of the current in T_9. It responds to changes in the second core excitation, but not to changes in the Wagner balance. A very rapid convergence of the auxiliary balances can thus be obtained.

A complete combining network for joining the two auxiliary detector points D_7 and D_8 with the main detector D_6 would require two complex adjustments for a total of four adjustable parameters. The simple combining network of figure 14 contains only one adjustable resistor and does not give perfect compensation. It is adequate at 1592 Hz and below because the reactances of the bridge cables are much smaller than their resistances at this frequency, because the impeddance of the high-voltage potential lead is only one-tenth as important as the impedance of the low-voltage potential lead, and because a factor of 10 reduction in the criticalness of the auxiliary balances was found to be sufficient.

A detailed calculation to verify the above conclusions is not appropriate to this paper. The analysis can be carried out with the aid of the equivalent circuit for the bridge potential circuit shown in figure 15, in which i_1 represents the second core excitation, i_2 represents the effect of changing the Wagner balance, i_3 and i_4 are the currents in the potential leads, i_d is the short circuit current at the main detector, and Y_1 and Y_2 are the admittances under test. The voltage generator in the current leads of the bridge is represented by e_1, and can be set equal to zero when analyzing the behavior of the auxiliary balances.

The use of an auxiliary admittance Y_2' as indicated in figure 13 for combining several null detectors causes no appreciable reduction in bridge sensitivity when the admittances under test are capacitors, but when one is measuring ac resistors this technique substantially increases the thermal agitation noise appearing at the detector. The alternative combining network shown in figure 16 avoids this problem, and works well when the smaller of the resistors under test is $10^4\ \Omega$ or less. The alternative combining network has been

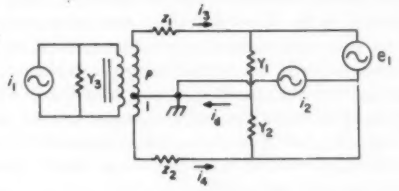

FIGURE 15. *Equivalent circuit representing the DRRS auxiliary balances and their effects.*

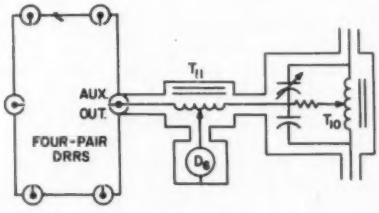

FIGURE 16. *Alternative combining network for use when* $|Y_2| \geq 10^{-4}$ *siemen.*

found to be more convenient than the circuit of figure 13 for the measurement of all admittances for which $|Y_2| \geq 10^{-4}$ siemens. The circuit of figure 13 is usually easier to adjust when $|Y_2| \leq 10^{-5}$ siemens, because it is not as strongly affected by admittances to ground at the junction of Y_1 and Y_2 and in the combining network involving T_{10}. The circuit of figure 14 works equally well with either combining network.

Although no coaxial chokes are shown in any of the circuits for this bridge, they are obviosuly essential for proper operation. They are inserted where needed to break ground loops, and tested in accordance with the principles laid out in section 2.

5. Equal-Power 100 : 1 Resistance Bridge

The comparison of two resistors whose ratio substantially differs from unity is usually made either by connecting them directly in series and comparing their voltages, or by applying equal voltages to them and comparing their currents. As a result, the powers dissipated in the two resistors differ greatly, and if the load coefficients of the two resistors are about equal, the excitation of the bridge is limited by the load coefficient of the resistor which dissipates the most power. In this case, the bridge sensitivity is much less

than would be obtained with a unity ratio bridge containing resistors of comparable load coefficients.

Using a voltage transformer bridge such as the direct-reading ratio set described above, the larger resistor dissipates ten times as much power as the smaller resistor. Using a current transformer bridge such as the conjugate bridge obtained by interchanging generators and null detectors, the smaller resistor dissipates ten times as much power as the larger resistor.

If a bridge contains a voltage transformer of ratio N_1 *and* a current transformer of ratio N_2, then the balance condition is $R_1 = N_1 N_2 R_2$; and the powers dissipated in the two resistors are equal if $N_1 = N_2$. The bridge sensitivity in this case is equal to that of a unity ratio bridge for comparing equal resistors. The technique is only applicable for resistors whose ratio is a perfect square, but this is not a fundamental limitation since a rational number can be found that is arbitrarily close to any irrational number.

For the very important case in which the two resistors to be compared have a ratio of 100, each transformer must have a ratio of 10. The bridge described in section 4 above contains all of the components required of the voltage transformer in such a system, and in principle another bridge exactly like it but with a subtractive rather than an additive ratio could be used for the current transformer. Fortunately the current transformer part of the bridge need not be provided with an adjustable ratio, and is therefore much easier to build. A quite different approach to an equal-power, four-terminal (but not four-pair) impedance bridge has been developed by Henry Hall of the General Radio Company.[2] Both two-pair and four-pair equal-power bridges have been described in the literature [12], but the operation of the four-pair version is not clear unless two-stage transformers are employed.

[2] A paper describing this work was presented at the 1970 Conference on Precision Electromagnetic Measurements at Boulder, Colorado. The text of this paper will be published in an issue of the IEEE Transactions on Instrumentation and Measurement.

The 100:1 bridge used at NBS for comparing a 10^3-Ω four-pair resistor with a 10^5-Ω four-pair resistor at 1592 Hz is shown in figure 17. It is convenient for the purpose of analyzing the behavior of this circuit mentally to interchange all generators and detectors and to work with the conjugate bridge. Although the circuit could of course be described directly without making use of the fictitious interchange, and although this would seem a more natural approach to people familiar with current comparators, the interchange is helpful here because it allows the use of the same terminology as was developed for describing the direct reading ratio set of section 4.

If we consider then that a generator is connected to terminal B in figure 17, it can be seen that the second core excitation circuitry is identical with that described in section 4, but that the Wagner circuitry is much more complex. The Wagner circuit combines a 10:1 voltage transformer T_{15} with a 10:1 current transformer T_{16} to obtain simultaneously nearly the correct 10:1 voltage ratio and 10:1 current ratio in the two resistors under test. Note that the ratio of currents in the two windings of T_{16} is nominally equal to the turns ratio, so that very little voltage appears across either winding. The two auxiliary adjustments then provide only the small corrections necessary to meet exactly the required conditions of zero current in the defining transformers T_{12} and T_{13}.

Although a much simpler Wagner balance system involving resistors could have been used, the circuit chosen is superior because it leads to a negligible augmentation of the thermal agitation noise appearing at a detector connected at point B. This consideration is of no importance in the Wagner circuit of the voltage transformer part of the bridge, and the use of R_3 to extend the limited range of the internal Wagner adjustment of the direct-reading ratio set is perfectly satisfactory.

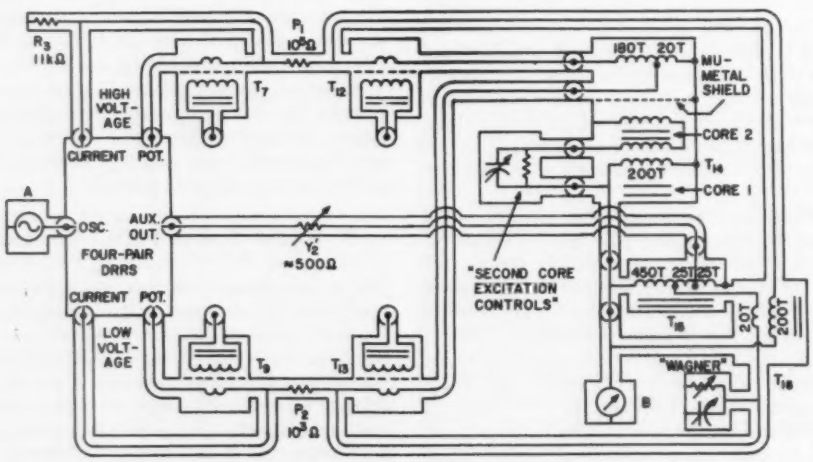

FIGURE 17. *A 100:1 equal power bridge making use of the four-pair DRRS.*

The auxiliary resistor required for proper operation of the quadrature balance controls of the direct-reading ratio set would most conveniently consist of a 10^4-Ω resistor connected between the auxiliary output terminal of the bridge and the detector point B. This would produce an unacceptably large thermal agitation noise. The use of a 500-Ω auxiliary resistor for Y_2' which is connected to a tap on T_{15} eliminates this problem. This does not interfere with the use of the circuit of figure 14 to reduce the criticalness of the direct-reading ratio set auxiliary balances.

A circuit similar to that of figure 14 and connected to defining transformers T_{12} and T_{13} is used to reduce the criticalness of the current transformer auxiliary balances and to provide a means of quickly making the current transformer auxiliary balances. This circuit is shown in figure 18. An auxiliary admittance Y_3 (not shown) is connected between this circuit and the generator terminal A on the direct-reading ratio set.

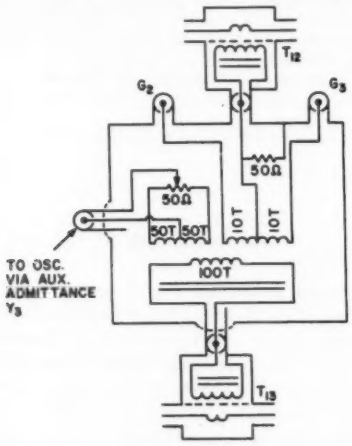

FIGURE 18. *Combining network for assuring fast convergence of current transformer auxiliary balances.*

The circuit of figure 18 is complimentary to the circuit of figure 14. In use, the current transformer auxiliary balances are adjusted so that temporarily connecting a generator to either G_2 or G_3 produces no change in the detector connected to terminal B in figure 17. The adjustable 50-Ω resistor in figure 18 or the auxiliary admittance Y_3 is set so that these auxiliary balances are not critical.

It was necessary to compromise in choosing the number of turns for transformer T_{14} in figure 17 in order to achieve a reasonably stable ratio without unduly augmenting the thermal agitation noise due to excessive shunt conductance in the transformer. With 200 turns on T_{14}, the shunt conductance measured at point B with P_1 and P_2 removed was found to be 1.8×10^{-5} siemens which is only slightly less than the 2×10^{-5} siemens conductance contributed by the resistors under test. With 4×10^{-3} W dissipated in each resistor (20 V on P_1), the sensitivity is sufficient to resolve 1 part in 10^9 using a phase-sensitive detector followed by a recorder, which is considered to be adequate.

The easiest way to measure the ratio of the current transformer T_{14} is to interchange the connections with respect to the direct-reading ratio set so that a balance is obtained when P_1 is nominally equal to P_2. Interchanging P_1 and P_2 and rebalancing allows the current transformer ratio to be determined from the known ratio of the direct-reading ratio set. A slight change in the Wagner circuit of the current transformer is also required. This consists of interchanging the windings of T_{16}. Resistors cannot be used for P_1 and P_2 because of their large load coefficients, so a pair of 1-nF capacitors is used instead. The voltages on the two capacitors change from 20 V to 200 V in the course of the measurement, so their voltage dependencies must be accurately known. Techniques for measuring the voltage dependencies of capacitors to the required accuracy have been described by Shields [14].

6. Conclusions

The series of bridges described above were built to provide the admittance comparisons necessary for an absolute ohm determination, as sketched in the introduction. It has been found that all of the comparisons necessary for this work can be made with an overall uncertainty of a few parts in 10^9 using these bridges. In practice, the largest source of uncertainty results from instabilities in the admittance standards used in the measurements. This problem can be handled only be carefully controlling the temperature of the standards.

7. References

[1] Cutkosky, R. D., Four-terminal-pair networks as precision admittance and impedance standards, commun. and Electronics **70,** 19–22 (Jan. 1964).

[2] Homan, D. N., Some techniques for measuring small mutual inductances, J. Res. Nat. Bur. Stand. (U.S.), **70C** (Eng. and Instr.), No. 4, 221–226 (Oct.–Dec. 1966).

[3] Haddad, R. J., A resistor calculable from DC to $\omega = 10^5$ rad/s, Master's thesis, School of Engineering and Applied Science, The George Washington University, Washington, D.C., 1–57 (Apr. 1969).

[4] Thompson, A. M., AC bridge methods for the measurement of three-terminal admittances, IEEE Trans. Instr. Meas. **IM–13,** No. 4, 189–197 (Dec. 1964).

[5] Kavanagh, R. J., Noninteracting controls in linear systems, Trans. AIEE **76,** part 2, 95–100 (May 1957).

[6] Cutkosky, R. D., Active and passive direct reading ratio sets for the comparison of audio-frequency admittances, J. Res. Nat. Bur. Stand. (U.S.), **68C** (Eng. and Instr.), No. 4, 227–236 (Oct.–Dec. 1964).

[7] Cutkosky, R. D., Evaluation of the NBS unit of resistance based on a computable capacitor, J. Res. Nat. Bur. Stand. (U.S.), **65A** (Phys. and Chem.), No. 3, 147–158 (May–June 1961).

[8] Thompson, A. M., An absolute determination of resistance based on a calculable standard of capacitance, Metrologia **4,** No. 1, 1–7 (Jan. 1968).

[9] Millea, A., and Ilie, P., A class of double-balance quadrature bridges for the intercomparison of three-terminal resistance, inductance and capacitance standards, Metrologia **5,** No. 1, 14–20 (Jan. 1969).

[10] Brooks, H. B., and Holtz, F. C., The two-stage current transformer, AIEE Trans. **41,** 382–393 (1922).

[11] Hamon, B. V., A 1–100 Ω build-up resistor for the calibration of standard resistors, J. Sci. Instr. **31,** 450–453 (1954).
[12] Cutkosky, R. D., and Shields, J. Q., The precision measurement of transformer ratios, IRE Trans. Instr. **I–9,** No. 2, 243–250 (1960).
[13] Clark, H. A. M., and Vanderlyn, P. B., Double-ratio AC bridges with inductively-coupled ratio arms, Proc. IEE **96,** Pt. 3, 189–202 (1949).
[14] Shields, J. Q., Voltage dependence of precision air capacitors, J. Res. Nat. Bur. Stand. (U.S.), **69C** (Eng. and Instr.), No. 4, 265–274 (Oct.–Dec. 1965).

(Paper No. 74C3&4–299)

JOURNAL OF RESEARCH of the National Bureau of Standards—C. Engineering and Instrumentation
Vol. 74C, Nos. 3 and 4, July–December 1970

Some Applications for Series Impedance Elements in Radio Frequency Immittance Measurements

Leslie E. Huntley*

Institute for Basic Standards, National Bureau of Standards, Boulder, Colorado 80302

(January 29, 1970)

A series impedance element equipped with coaxial connectors may be evaluated as a two-port network. Precision connectors greatly reduce the uncertainties associated with the series connection, making practical several measurement techniques which involve series impedances. This paper discusses techniques for extending the range of immittance bridges to high values of admittance or impedance, for measuring very small admittances with incremental standards of ordinary range, and for using a bridge to measure its own reference open-circuit admittance or short-circuit impedance.

Key words: Immittance measurement; radio frequency; series elements; two-port standards.

1. Introduction

A number of measuring techniques which are commonly used at audio frequencies, have long been considered impractical for use at radio frequencies. Among these are the techniques which require connecting one component in series with another. The use of precision coaxial connectors (1, 2), greatly reduces uncertainties in series and shunt immittances associated with the connection, making it practical to use series connected components for precision measurements at radio frequencies.

When a circuit element is equipped with precision connectors, the elements of its equivalent circuit are fixed by the shielding afforded by the coaxial construction and by the precisely repeatable connection. A shielded series element may be treated as a two-port network and represented by an equivalent pi or tee at a given frequency, and if it is equipped with precision connectors, the elements of the equivalent pi or tee may be accurately evaluated by open- and short-circuit measurements. This paper discusses the use of series immittances in the form of precision two-port standards in extending the range of immittance measuring instruments to large immittances, in measuring low-valued admittances in terms of relatively large incremental standards, and in measuring the impedance of the reference short-circuit of an impedance bridge, or the admittance of the reference open-circuit of an admittance bridge.

2. Method for Evaluating Two-Port Immittances

A two-port immittance may be represented by an equivalent pi network such as that of figure 1, at any single frequency [3]. The procedure for measuring the elements of the pi is well known, but is reviewed here for the sake of convenience.

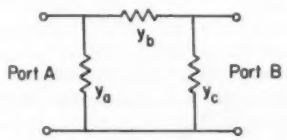

FIGURE 1. *Pi equivalent of two-port network.*

With port A of the two-port connected to an admittance bridge, and port B shorted, the input admittance measured by the bridge is

$$Y_1 = Y_a + Y_b. \tag{1}$$

When the short is removed, port B is open circuited, and the bridge measures the input admittance

$$Y_2 = Y_a + \frac{Y_b Y_c}{Y_b + Y_c}. \tag{2}$$

With port B connected to the bridge and port A shorted, the input admittance is given by

$$Y_3 = Y_b + Y_c. \tag{3}$$

*Electromagnetics Division, Circuit Standards Section, National Bureau of Standards, Boulder Laboratories, Boulder, Colo. 80302.

403-833 O - 70 - 2

When the short is removed, port A is open, and the input admittance is

$$Y_4 = Y_c + \frac{Y_a Y_b}{Y_a + Y_b}. \tag{4}$$

Note that the two-port must be equipped with nominally identical connectors for this series of measurements to be possible. Equations (1), (2), and (3) are solved simultaneously for Y_a, Y_b, and Y_c, yielding

$$Y_b = [(Y_1 - Y_2)Y_3]^{1/2}, \tag{5}$$

$$Y_a = Y_1 - Y_b, \tag{6}$$

and

$$Y_c = Y_3 - Y_b. \tag{7}$$

So far it has been assumed that the open circuit actually represents zero admittance across the open port, and that the short circuit actually represents zero impedance. This assumption is not accurate. The short may have an impedance consisting of about 0.5 mΩ (milliohm) resistance and 5×10^{-12} henry inductance, and the open may have an admittance consisting of a fringing capacitance of the order of 0.2 pF [4]. The conductance of an open circuit can usually be neglected, as can the error caused by a non-zero short where all admittances are of the order of 0.1 mho or smaller. When the fringing capacitance at the open end of the two-port is taken into account, (2) becomes

$$Y_2 = Y_a + \frac{Y_b(Y_c + Y_{f1})}{Y_b + Y_c + Y_{f1}}, \tag{8}$$

and (4) becomes

$$Y_4 = Y_c + \frac{Y_b(Y_a + Y_{f2})}{Y_a + Y_b + Y_{f2}}, \tag{9}$$

where Y_{f1} is the "fringe admittance" at one open end of the two-port, and Y_{f2} is the fringe admittance at the other. Fringe admittance is used instead of fringe capacitance because the equations than apply to the more general case of a lossy open circuit. If the two-port is equipped with precision connectors, the two fringe admittances will be very nearly equal.

The fringe admittance at the bridge terminal, Y_{f3}, is removed when connection is made to the bridge terminal. Each of the measurements (1) through (4) is therefore in error by the amount Y_{f3}, and this admittance must be added to the measured admittance in order to obtain the correct values for $Y_a + Y_b$, etc.

Note that Y_{f3} will be different from Y_{f1} and Y_{f2} unless the connectors are sexless. Even when precision connectors, which are sexless by definition, are used, Y_{f3} may be different from Y_{f1} and Y_{f2} because of differences in the configuration of conductors near the open circuit. For example, the fringe capacitance of a connector mounted flush with a large ground plane will differ considerably from that of an identical connector at the end of a two-port several inches above the ground plane. The three fringe admittances for precision connectors can be made virtually identical by using a shielding cap instead of an open terminal to provide the reference open circuit admittance. When the corrections for the fringe admittances are made, (1) through (4) must be rewritten

$$Y_1 + Y_{f3} = Y_a + Y_b, \tag{10}$$

$$Y_2 + Y_{f3} = Y_a + \frac{Y_b(Y_c + Y_{f1})}{Y_b + Y_c + Y_{f1}}. \tag{11}$$

$$Y_3 + Y_{f3} = Y_b + Y_c \tag{12}$$

and

$$Y_4 + Y_{f3} = Y_c + \frac{Y_b(Y_a + Y_{f2})}{Y_a + Y_b + Y_{f2}}. \tag{13}$$

where Y_1, Y_2, etc., still refer to the admittances measured at the bridge terminal. The first three equations of this set may be solved as before, yielding

$$Y_b \equiv G_b + jwC_b = [(Y_1 - Y_2)(Y_3 + Y_{f1} + Y_{f3})]^{1/2}, \tag{14}$$

$$Y_a = Y_1 + Y_{f3} - Y_b, \tag{15}$$

and

$$Y_c = Y_3 + Y_{f3} - Y_b. \tag{16}$$

Section 3.3 of this paper describes a technique for measuring the reference, or "fringe," admittance of an admittance bridge and of a two-port admittance.

A two-port immittance may also be represented by the equivalent tee of figure 2, and the elements

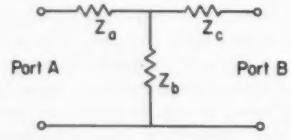

FIGURE 2. *Tee Equivalent of two-port network.*

evaluated by measurements with an impedance bridge. With port A connected to the bridge and B open, the bridge measures

$$Z_1 + Z_{s3} = Z_a + Z_b, \tag{17}$$

where Z_{s3} is the impedance of the reference short circuit which is removed when the two-port is connected to the bridge, and the effect of fringing capacitance is considered negligible. When port B is shorted, the bridge measures

$$Z_2 + Z_{s3} = Z_a + \frac{Z_b(Z_c + Z_{s1})}{Z_b + Z_c + Z_{s1}}, \tag{18}$$

where Z_{s1} is the impedance of the short on port B, and is not necessarily equal to Z_{s3}. With port B connected to the bridge and port A open, the bridge measures

$$Z_3 + Z_{s3} = Z_b + Z_c. \tag{19}$$

With port A shorted, the bridge measures

$$Z_4+Z_{s3}=Z_c+\frac{Z_b(Z_a+Z_{s2})}{Z_a+Z_b+Z_{s2}}. \tag{20}$$

The first three equations of this set may be solved for Z_a, Z_b, and Z_c, yielding

$$Z_b=[(Z_1-Z_2)(Z_3+Z_{s1}+Z_{s3})]^{1/2}, \tag{21}$$

$$Z_a=Z_1+Z_{s3}-Z_b, \tag{22}$$

and

$$Z_c=Z_3+Z_{s3}-Z_b. \tag{23}$$

Section 3.3 presents a technique for measuring the short-circuit impedances.

Solving (14) for Y_b involves taking the square root of a complex number. The solutions are

$$G_b^2=\frac{A\pm\sqrt{A^2+B^2}}{2}, \tag{24}$$

and

$$C_b^2=\frac{-A\pm\sqrt{A^2+B^2}}{2\omega^2}, \tag{25}$$

where

$$A=(G_1-G_2)G_3-\omega^2(C_1-C_2)(C_3+C_{f1}+C_{f3}), \tag{26}$$

and

$$B=\omega[(G_1-G_2)(C_3+C_{f1}+C_{f3})+G_3(C_1-C_2)]. \tag{27}$$

Thus, G_b and C_b are obtainable in terms of measured conductances and capacitances.

The effect of measurement errors on a measurement of this type may be evaluated by the technique of taking the total differential of the quantity measured [5]. The approximate error in G_b, denoted by δG_b, is given by

$$\delta G_b\simeq\frac{\partial G_b}{\partial A}\,\delta A+\frac{\partial G_b}{\partial B}\,\delta B, \tag{28}$$

where δA and δB are small errors in A and B given by

$$\delta A\simeq\frac{\partial A}{\partial G_1}\,\delta G_1+\frac{\partial A}{\partial G_2}\,\delta G_2+\ldots+\frac{\partial A}{\partial C_{f1}}\,\delta C_{f1}+\frac{\partial A}{\partial C_{f3}}\,\delta C_{f3} \tag{29}$$

and

$$\delta B\simeq\frac{\partial B}{\partial G_1}\,\delta G_1+\ldots+\frac{\partial B}{\partial C_{f3}}\,\delta C_{f3}. \tag{30}$$

While there is little to be gained by pursuing the algebra further, it is instructive to take a simple example to illustrate the order of magnitude of the errors to be expected in measurements of this type. If a conductance with sufficiently high q[2] ($q\simeq 200$ for error of 1 in 10^4) is measured, the expression for G_b^2 reduces to $G_b^2\simeq A$. Furthermore, for a high-q conductance

$$\omega^2(C_1-C_2)(C_3+C_{f1}+C_{f3})\ll(G_1-G_2)G_3, \tag{31}$$

and

$$\delta G_b\simeq\frac{1}{2G_b}[G_3(\delta G_1-\delta G_2)+(G_1-G_2)\delta G_3]. \tag{32}$$

For the case described, $G_1\simeq G_3\gg G_2$, and

$$\delta G_b\simeq(1/2G_b)(2G_b\delta G_1)=\delta G_1,$$

and the error in measuring a pure series conductance by this technique is approximately the same as the error in measuring a two-terminal conductance with the same bridge.

3. Applications

3.1. Range Extension to Very Large Immittances

Hartshorn [6] shows that capacitors too large for direct measurement may be measured by connecting them in series with smaller known capacitors. The capacitance of the series combination is smaller than that of either capacitor and this capacitance may be made to fall within the range of direct measurement. The same principle may be used in measuring any admittance too large for direct measurement with available instruments. The measurement is accomplished by evaluating the elements of the equivalent pi (fig. 1) then connecting the unknown admittance to the two-port and measuring the input admittance of the combination. The value of the unknown admittance is then calculated from the computed elements of the pi and the measured input admittance of the combination.

If the unknown admittance, Y_x, is connected to port B and port A is connected to the bridge, the measured input admittance is given by

$$Y_5=Y_a+\frac{Y_b(Y_c+Y_x)}{Y_b+Y_c+Y_x}-Y_{f3}, \tag{33}$$

from which is obtained

$$Y_x=\frac{Y_b(Y_5+Y_{f3}-Y_a)}{Y_a+Y_b-Y_5-Y_{f3}}-Y_c. \tag{34}$$

[2] The Quality Factor of an immittance element, denoted by "q," is defined to be the ratio of the major immittance component to the minor immittance component. Thus, $q_1=\frac{\omega L}{R}$, $q_c=\frac{\omega C}{G}$, $q_r=\frac{R}{\omega L}$, and $q_g=\frac{G}{\omega C}$.

In some cases, the elements of the pi are of no particular interest, and it is desirable to calculate Y_x directly from the measured values Y_1, Y_2, and Y_3. In this case an expression for Y_x is obtained by substituting (14), (15), and (16) into (33):

$$Y_x = \frac{(Y_5 - Y_2)(Y_3 + Y_{f3}) + (Y_1 - Y_2)Y_{f1}}{Y_1 - Y_5}. \quad (35)$$

After expanding (34) or (35) and separating variables, the error in measuring G_x and C_x may be evaluated, as before, by taking the total differential of the quantity. The operation is straightforward, if somewhat laborious, and will not be pursued further. An idea of the magnitude of errors to be expected in measurements of this sort may be obtained by considering the case of a pure capacitor measured in series with a pure capacitor—that is, all conductances are zero. For this idealized case, (35) becomes

$$C_x = \frac{(C_5 - C_2)(C_3 + C_{f3}) + (C_1 - C_2)C_{f1}}{C_1 - C_5}, \quad (36)$$

and the error in measuring C_x is

$$\delta C_x = \frac{1}{C_1 - C_5}[(C_{f1} - C_x)\delta C_1 - (C_3 + C_{f1} + C_{f3})\delta C_2 + (C_5 - C_2)\delta C_3 + (C_3 + C_x + C_{f3})\delta C_5 + (C_5 - C_2)\delta C_{f3} + (C_1 - C_2)\delta C_{f1}]. \quad (37)$$

The errors in C_1, C_2, C_3, and C_5 are composed of two components; a calibration error and a random error due to imprecision of the measuring capacitor. If C_1 and C_3 are approximately equal, the calibration error will be the same for both, and it is proper to consider the sign of the error term in combining the errors. Since C_2 and C_5 may be greatly different from C_1 and C_3, there is no assurance the calibration errors are in the same direction; and their signs should not be considered in combining the error terms. Figure 3 shows the accuracy which may be expected in series measurement of capacitors between 10 pF and 0.01 μF assuming the error in measuring C_1, C_2, C_3, and C_5 to be $\pm(0.05\% + 0.05$ pF), the error in C_{f1} and C_{f3} to be about 0.001 pF, and

$$C_1 \simeq C_3 \simeq 1000 \text{ pF}$$
$$C_2 \simeq 5 \text{ pF}$$
$$C_{f1} \simeq C_{f3} \simeq 0.2 \text{ pF},$$

and rms addition of the random errors. The accuracy obtainable by direct measurement under the same conditions is shown for comparison.

The range of admittances which can be measured with a given instrument by this method lies between zero (two-port open) and infinity (two-port shorted). Because the accuracy is not as good as that obtained for direct measurement, only values outside the range of available instruments will ordinarily be measured in this way. The technique was tested by measuring a number of capacitors directly, and in series with a two-port capacitor. The results appear in table 1. The good agreement between the two methods shows there are no serious errors inherent in the technique.

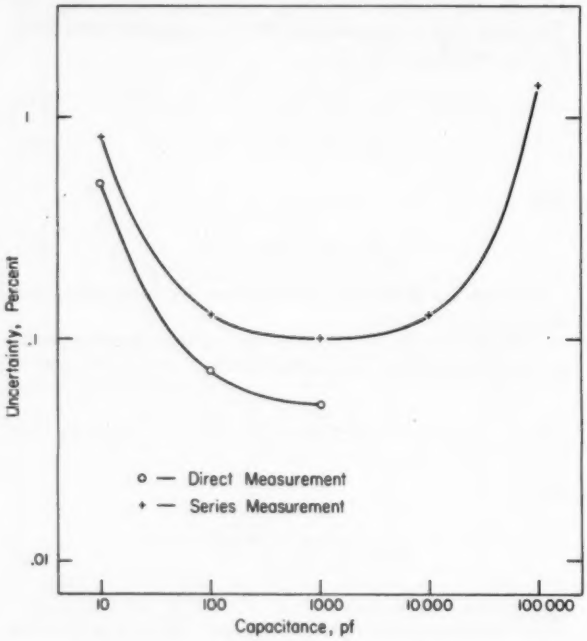

FIGURE 3. *Accuracy obtainable in measurement of capacitance by direct measurement, and by series measurement.*

TABLE 1. *Capacitance measured at 3 MHz by direct measurement and by measurement in series with a 100-pF capacitor*

Nominal capacitance	Direct measurement pF	Series measurement pF	Difference (percent)
1000 pF (A)	1006.77	1006.62	0.014
1000 pF (B)	1002.76	1002.63	.013
500 pF	501.78	501.71	.014
200 pF	200.66	200.71	−.025
100 pF	101.06	101.09	−.03

The usable range of an impedance bridge may be similarly extended by connecting an unknown large impedance in parallel with a smaller impedance whose value is within the range of the bridge. In this case, the two-port is more conveniently represented by the equivalent tee of figure 2. In practice, the two-port may be formed by connecting the smaller impedance to one port of a coaxial tee junction and using the other two as active ports (fig. 4). In this case, the elements of the tee are obtained by impedance measurements, and the unknown impedance, Z_x, is given by

$$Z_x = \frac{(Z_5 - Z_2)(Z_3 + Z_{S3}) + (Z_1 - Z_2)Z_{S1}}{Z_1 - Z_5}. \quad (38)$$

Here again, the range of the bridge is extended to cover impedances between zero (two-port shorted) to infinity (two-port open).

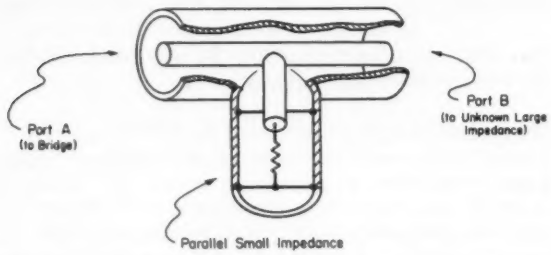

FIGURE 4. *Tee arrangement for measuring large impedance in parallel with smaller impedance.*

3.2. Range Extension to Very Small Admittances

Hartshorn [6] also discusses the measurement of very small capacitors using an incremental capacitor of ordinary range. As he puts it: "Condensers of very low value may also be measured by a series method. A condenser of low value c is placed in series with a variable standard of ordinary range C. The capacitance of the combination being $cC/(C+c)$, a small change ΔC in the standard produces a change in the combination of approximately $\Delta Cc^2/(C+c)^2$, which is for example, 100 times smaller than ΔC if $C/c=9$. Thus, if the small condenser to be measured is added in parallel with such a combination, and the standard condenser if then diminished until the resultant capacitance is restored to its original value, the capacitance added is equal to the change in the reading of the standard divided by 100. This method is convenient when no standard of low range is available; but when a standard of the micrometer type is available the substitution method should be employed, as there is always some uncertainty in any estimation of the effect of the connecting lead in a series combination—however small the lead may be."

The same principle applies to measuring any small admittance, and the use of precision connectors eliminates much of the "uncertainty in any estimation of the effect of the connecting lead." The series admittance may be represented by an equivalent pi, and evaluated by measurements with an admittance bridge. When the incremental admittance is connected to the two-port, the circuit of figure 5 results.

The input admittance of this network, Y_i, is

$$Y_i = Y_a + \frac{Y_b(Y_1+Y_c)}{Y_1+Y_b+Y_c}, \tag{39}$$

and the change in input admittance with change in Y_1 is given by

$$\Delta Y_i = \frac{(Y_1'-Y_1)Y_b^2}{(Y_1+Y_b+Y_c)(Y_1'+Y_b+Y_c)}, \tag{40}$$

where Y_1 is the initial value, and Y_1' is the final value. When all the elements of the network are of like kind and are sufficiently pure (q greater than about 200 for

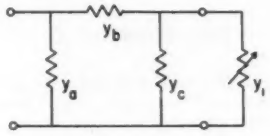

FIGURE 5. *Equivalent circuit of incremental admittance standard connected to two-port standard for measurement of very small admittances.*

1 in 10^4 error) the minor component may be neglected in calculating the change in effective value for the major component.

For sufficiently pure capacitors

$$\Delta C_i \simeq \frac{\Delta C_1 C_b^2}{(C_1+C_b+C_c)(C_1'+C_b+C_c)}, \tag{41}$$

and for nearly pure conductances

$$\Delta G_i \simeq \frac{\Delta G_1 G_b^2}{(G_1+G_b+G_c)(G_1'+G_b+G_c)}. \tag{42}$$

Again, some insight into the magnitude of errors to be expected in measurements of this type may be obtained by considering the measurement of a capacitor by an incremental capacitor in series with a two-port capacitor where all capacitors are lossless. The relative error in a measurement of this type, obtained by taking the total differential of (41) and dividing by ΔC_i, is

$$\frac{\delta(\Delta C_i)}{\Delta C_i} = \frac{\delta C_1' - \delta C_1}{C_1'-C_1} - \frac{\delta C_1' + \delta C_b + \delta C_c}{C_1'+C_b+C_c}$$

$$- \frac{\delta C_1 + \delta C_b + \delta C_c}{C_1+C_b+C_c} + \frac{2\delta C_b}{C_b}. \tag{43}$$

Perhaps the most useful application of this technique lies in checking the calibration of incremental capacitors against low-valued standards such as those provided by short sections of precision coaxial line. The Field and Sinclair technique [7] may be used for finding corrections proportional to C^2 in incremental capacitors; and it is easy to show that there are no significant errors proportional to C^2 or higher-order terms by measuring capacitors of appropriate value over different ranges of the incremental capacitor. None of these techniques are capable of detecting errors proportional to C, however, and another technique is needed for a complete calibration of these instruments.

If the error in measuring the small capacitor is given by

$$\delta C_b = kC_b \pm \epsilon \text{pF}$$

$$\delta C_c = kC_c \pm \epsilon \text{pF}$$

$$\delta C_1 = kC_1 \pm \epsilon \text{pF}$$

$$\delta C_1' = kC_1' \pm \epsilon \text{pF},$$

the maximum error in ΔC_1 may be written as

$$\frac{\delta(\Delta C_1)}{\Delta C_1} = (k) + \epsilon\left[\frac{2}{C_b} + \frac{3}{C_1' + C_b + C_c} + \frac{3}{C_1 + C_b + C_c} + \frac{2}{C_1' - C_1}\right]. \quad (44)$$

The term involving ϵ may be large enough to prevent a good determination of k with a single measurement; but this term is random in nature and may be reduced considerably by repeated measurements.

This technique was tested by measuring accurately-known (to within 0.01%) capacitors with nominal values of 5, 13, and 15 pF, in terms of a 1000 pF incremental capacitor connected in series with a nominally 100 pF capacitor and a nominally 82 pF capacitor. The results of the measurements, which appear in table 2, indicate a linear correction of the order of -0.01 to -0.03 percent in this particular capacitor.

TABLE 2. *Measurement of coaxial line capacitance standards at 3 MHz using a 1000-pF incremental capacitor with 82-pF and 100-pF series capacitors*

Nominal capacitance	Calculated capacitance	Series measurement		Difference (%)	
		82 pF	100 pF	82 pF	100 pF
5 pF	5.0753	5.0761	5.0757	0.016	0.008
12 pF	11.864	11.861	11.860	−.027	−.036
15 pF	15.240	15.235	15.233	−.033	−.064

3.3. Measurement of Reference Open-Circuit Admittance or Short-Circuit Impedance

Measurements of admittance or impedance will be in error by the uncertainty in the reference open-circuit admittance, or short-circuit impedance. Since this might be the principal source of error in measuring small immittances, it is desirable to measure these reference immittances accurately.

The measurement described in section 3.1. can be rearranged to allow an admittance bridge to measure the admittance of its reference open circuit or an impedance bridge to measure the impedance or its reference short circuit. Equation (35) may be rearranged to read

$$Y_x(Y_1 - Y_5) = (Y_5 - Y_2)(Y_3 + Y_{f3}) + (Y_1 - Y_2)Y_{f1}. \quad (45)$$

When Y_x is measured directly with the bridge, the quantity observed, Y_m, is Y_x less the admittance removed when Y_x is connected to the bridge terminal:

$$Y_m = Y_x - Y_{f3}. \quad (46)$$

Two different admittances may be measured, yielding the two equations

$$(Y_{m1} + Y_{f3})(Y_1 - Y_5) = (Y_5 - Y_2)(Y_3 + Y_{f3}) + (Y_1 - Y_2)Y_{f1}, \quad (47)$$

and

$$(Y_{m2} + Y_{f3})(Y_1 - Y_5') = (Y_5' - Y_2)(Y_3 + Y_{f3}) + (Y_1 - Y_2)Y_{f1}, \quad (48)$$

where it is now assumed that the two fringe admittances of the two-port are equal to Y_{f1}. Subtracting (48) from (47) and rearranging yields

$$Y_{f3} = \frac{Y_{m2}(Y_1 - Y_5') - Y_{m1}(Y_1 - Y_5)}{2(Y_5' - Y_5)} - \frac{Y_3}{2}, \quad (49)$$

and Y_{f3} may be obtained. Y_{f1} may be obtained by substituting Y_{f3} into one of the original equations.

When $Y_{f1} = Y_{f2} = Y_{f3} = Y_f$, as is the case when the terminals of the two-port and the bridge terminal are identical and have identical environments in the open-circuit condition, Y_f may be obtained from the equation

$$Y_f = \frac{Y_m(Y_1 - Y_5)}{2(Y_5 - Y_2)} - \frac{Y_3}{2}. \quad (50)$$

An exactly analagous situation exists for the measurement of the impedance of the short used as the reference for an impedance bridge. In this case, the equations are

$$Z_s = \frac{Z_m(Z_1 - Z_5)}{2(Z_5 - Z_2)} - \frac{Z_3}{2} \quad (51)$$

for $Z_{s1} = Z_{s2} = Z_{s3} = Z_s$ and

$$Z_{s3} = \frac{Z_{m2}(Z_1 - Z_5') - Z_{m1}(Z_1 - Z_5)}{2(Z_5' - Z_5)} - \frac{Z_3}{2} \quad (52)$$

for $Z_{s1} = Z_{s2} \neq Z_{s3}$.

This technique was used to measure the fringe capacitance of the NBS 0.750 in, 50-Ω coaxial connector at 1 kHz, with a 1-in long closed cap as the reference condition. The value obtained for the fringe capacitance, assuming $C_{f1} = C_{f2} = C_{f3}$, was 0.2078 pF with an estimated standard deviation of 0.0004 pF. This value agrees well with the 0.2070 pF obtained by a measurement involving a calculable line section.

An attempt to measure the impedance of the shorted NBS connector at 100 kHz, using an impedance bridge, yielded inconsistent values. The inconsistencies are attributed to the fact that the impedance of the short is

smaller than that which the bridge is capable of resolving. The resistance of the short was then measured at dc using a Wheatstone resistance bridge. The average of the measured values, attributed primarily to contact resistance, was 0.00016 Ω, with the values obtained ranging from 0.00004 to 0.00030 Ω.

4. Conclusions

The application of precision coaxial connectors to radio frequency immittance measurements makes practical the use of measurement techniques which are usually considered useful only at audio frequencies. In particular, series impedances equipped with precision connectors may be treated as two-port devices and accurately evaluated at a given frequency. Using these two-ports as series impedance transformers makes possible a significant range extension for admittance and impedance measuring instruments. These impedance transformers also make it practical to measure very small admittances in terms of large admittance increments—a technique which has been inverted and used to compare 1000 pF incremental capacitors to low-valued, coaxial line standards of capacitance. In addition, it is possible to use an admittance bridge to measure its own fringe capacitance and an impedance bridge to measure the impedance of its reference short-circuit by proper application of series impedance transformers.

5. References

[1] Fossum, D. E., Progress Report of IEEE Instrumentation and Measurement Group Technical Subcommittee on Precision Coaxial Connectors, IEEE Trans. Instr. Meas. **IM-13,** No. 4, 285 (Dec. 1964).

[2] Woods, D., A Coaxial connector system for precision R. F. measurement instrument and standards, Proc. IEE **108-B,** Paper No. 3499E, pp. 205–213, (March 1961).

[3] Tang, K. Y., Alternating Current Circuits (International Textbook Co., Scranton, Pa.), pp. 194–202 (1951).

[4] Jones, R. N., and Huntley, L. E., Precision coaxial connectors in lumped parameter immittance measurement, IEEE Trans. Instr. Meas. **IM-15,** No. 4, 375–380, (Dec. 1966).

[5] Topping, J., Errors of Observation and Their Treatment, London Institute of Physics (1955).

[6] Hartshorn, L., Radio Frequency Measurements by Bridge and Resonance Methods, pp. 219–220 (Wiley, New York, N.Y. Feb. 1940).

[7] Field, R. F., and Sinclair, D. B., A method for determining the residual inductance and resistance of a variable air condenser at radio frequencies, Proc. IRE **24,** No. 2, 255–274 (Feb. 1936).

(Paper 74C3&4–300)

JOURNAL OF RESEARCH of the National Bureau of Standards—C. Engineering and Instrumentation
Vol. 74C, Nos. 3 and 4, July–December 1970

A Pulse Heating Method for the Measurement of Melting Point of Electrical Conductors (Thin Wires) Above 2000 K*

A. Cezairliyan

Institute for Materials Research, National Bureau of Standards, Washington, D.C. 20234

(June 30, 1970)

A pulse heating method is described for the measurement of melting point of electrical conductors at high temperatures (above 2000 K) which are in the form of thin wires. The technique is checked by measuring the melting point of platinum. The results give 2044 ± 5 K on IPTS–1968.

Key words: High-speed measurements; high temperatures; melting point; platinum.

In general, melting points of substances are determided using quasi steady-state techniques, where the specimen is either heated or cooled very slowly until a phase change is detected. These methods present difficulties at high temperatures (above 2000 K) due to increased heat transfer, chemical reactions, evaporation, loss of mechanical strength, etc.

In order to overcome most of these difficulties experiments may be performed in short times by heating the specimen rapidly to its melting point. A technique utilizing this approach was described in the literature [1].[1] The specimen was of tubular form (100 mm long, 6.4 mm outside diameter, 0.5 mm wall thickness) with a small hole in the wall at the middle of the specimen. The cylindrical specimen approximated blackbody conditions for optical (pyrometric) temperature measurements. The specimen was heated from room temperature to its melting point in less than one second by the passage of a high current (2000 A) through it. The maximum temperature attained was the melting point. The melting point obtained by this method was reproducible within 1 K (standard deviation of the mean). The tubular specimen had to be destroyed during each determination. The cost and difficulty of fabricating specimens used in the above study make it unsuitable for general use.

The objective of this note is to describe a high-speed method of measuring melting point of electrical conductors (with melting points above 2000 K) where the specimens are in the form of thin wires. The method is based on detecting melting of a specimen which is wound around a tube as the latter is heated rapidly in vacuum. The limitation of the measurements to temperatures above approximately 2000 K is imposed by the optimization in the operation of the high-speed pyrometer.

The basic circuitry of the measurement system, shown in figure 1, was similar to that described in the literature [2]. The specimen was a high-purity (99.999 percent) platinum wire (diameter = 0.001 in, 0.025 mm),

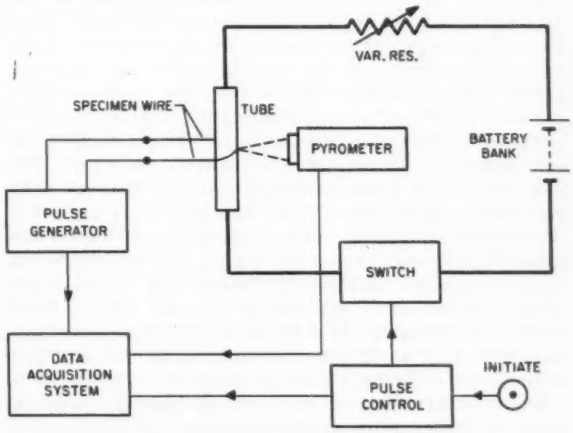

FIGURE 1. *Functional diagram of a high-speed system for the measurement of melting point of electrical conductors in the form of thin wires at high temperatures.*

which was wound (half turn) around a thin-wall molybdenum tube. The tube was electrically in series with the main power pulsing circuit. Two pulleys supported the wire. A 0.5-g weight was attached to each end of the wire to assure good contact between the wire and the tube. A schematic drawing showing the specimen and the tube assembly is presented in figure 2. The ends of the platinum wire were connected to a special electronic circuit which indicated the time of the open-

*This work was supported in part by the Propulsion Division of the U.S. Air Force Office of Scientific Research under contract ISSA–69–0001.

[1] Figures in brackets indicate the literature references at the end of this paper.

ing of the circuit resulting from the melting of platinum.

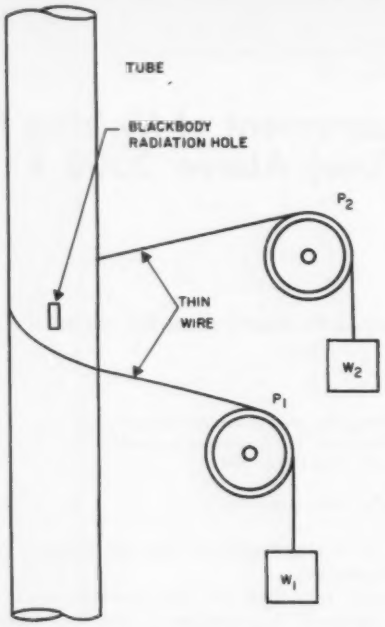

FIGURE 2. *Schematic diagram of the specimen and tube assembly.*

The break in the circuit took place at a point of contact with the tube as the latter was pulse heated. Duration of an experiment (heating of the specimen from room temperature to its melting point) was approximately 0.8 s. Heating rate of the tube at the melting point of platinum was approximately 2 K ms^{-1}. Temperature of the tube was measured with a high-speed photoelectric pyrometer [3], which permits 1200 evaluations of tube temperature per second. The pyrometer target was a small rectangular hole (1 mm × 0.5 mm) fabricated in the wall at the middle of the tube. Signals were recorded with a high-speed digital data acquisition system [2] which has a full-scale signal resolution of approximately one part in 8000 and time resolution of 0.4 ms. Temperature of the tube corresponding to the time of the break in the platinum wire gave the melting point of platinum.

The results of three experiments gave an average value of 2044.2 K for the melting point of platinum on the 1968 International Practical Temperature Scale [4] with an average deviation from the mean of the three amounting to 1.1 K. This compares favorably with the accepted value of 2045 K [4].

In each experiment, the contribution to the uncertainty in temperature resulting from the uncertainty in the "temperature-time of break" determination was 0.4 K. The standard deviation of individual temperature measurements in each experiment was less than 0.3 K. Correction due to the radial temperature gradient in the tube was less than 0.1 K. Maximum inaccuracy in temperature measurements at the melting point of platinum, which results from uncertainties in standard lamp, pyrometer calibration, blackbody quality, scattered light, etc., is estimated to be 4 K [2]. Error in the melting point due to alloying effect is negligible since the entire experiment was of very short duration.

Because of the complex nature of the experimental method, it was difficult to determine exactly (1) the time constant for heat transfer between the tube and the specimen, and (2) the effect of the tension due to end weights on the melting point. Crude estimates indicated that this time constant could be of the order of 0.1 ms, which corresponds to an error of the order of 0.2 K in the melting point. It is likely that in the experiments the lowering of the melting point due to tension in the specimen was approximately compensated by an opposite effect which resulted from the finite time constant associated with heat transfer between the tube and the specimen. One may conclude that the melting point of platinum, as determined in this study, is 2044 ± 5 K on IPTS–68.

The results of preliminary work presented in this note have demonstrated the feasibility of measuring the melting point of electrical conductors in the form of thin wires by a pulse heating method of subsecond duration.

References

[1] Cezairliyan, A., Morse, M. S., and Beckett, C. W., Measurement of melting point and electrical resistivity (above 2840 K) of molybdenum by a pulse heating method (to be published in Rev. Int. Hautes Tempér. et Réfract., 1970).

[2] Cezairliyan, A., Morse, M. S., Berman, H. A., and Beckett, C. W., J. Res. Nat. Bur. Stand. (U.S.), **74A** (Phys. and Chem.), 65 (1970).

[3] Foley, G. M., High-speed optical pyrometer, Rev. Sci. Instr., **41**, 827 (1970).

[4] International Practical Temperature Scale of 1968, Metrologia, **5**, 35 (1969).

(Paper No. 74C3&4–301)

JOURNAL OF RESEARCH of the National Bureau of Standards—C. Engineering and Instrumentation
Vol. 74C, Nos. 3 and 4, July–December 1970

A Time-Shared Computer System for Diffractometer Control*

H. A. Alperin

Naval Ordnance Laboratory, White Oak, Maryland 20910

and

E. Prince

Center for Radiation Research, National Bureau of Standards, Washington, D.C. 20234

(July 27, 1970)

A system is described for controlling data acquisition, and for online data reduction, on up to eight neutron and x-ray diffractometers. The system uses a medium-sized computer, with the individual instruments sharing time. Storage of programs, data, and the intermediate results of computations on a rapid-access disk makes roughly 12K of the 16K core memory available to each user in turn for computations. All users' programs are written in FORTRAN. Each user has independent access to the computer, through his own separate typewriter, for input of control parameters and output of sample results. Final output data may be recorded on magnetic tape for permanent filing or for processing offline by a large computer.

Key words: Automatic control; computer control; diffractometer; FORTRAN; neutron diffractometer; real-time data processing; time sharing; x-ray diffractometer.

1. Introduction

During the past 10 years, a number of instruments have been built for the automatic and semiautomatic collection of single-crystal diffraction data, involving the diffraction of both x rays and neutrons. The earlier instruments [Prince and Abrahams, 1959; Abrahams, 1962] were mostly semiautomatic, with input parameters computed on an offline digital computer and transferred to a punched paper tape, which served as a program for the collection of data. The output data would also be recorded on punched tape, to be reduced to integrated intensities and structure amplitudes by the computer. More recently a number of instruments have been built [Busing, Ellison, Levy, King, and Roseberry, 1968; Beaucage, Kelly, Ophir, Rankowitz, Spinrad, and Van Norton, 1966; Fitzwater, 1965; Kruger and Dimmler, 1964] in which a computer was attached directly to a diffractometer, and served to compute settings, acquire the intensity data, and reduce the data to a greater or lesser extent online and in real time.

In controlling diffractometers directly by computers, there have been two distinct approaches. The first, and so far the more common, approach is to use a small computer for each diffractometer instrument. A typical example of this type of system is the one described by Busing et al. [1968]. The other system, which is economical only if there are several diffractometers located physically close together, as is frequently the case with neutron diffractometers at a reactor, is to share time on a large computer. Previous examples of this approach are the system constructed at Brookhaven National Laboratory [Beaucage et al., 1966], at Ames Laboratory [Fitzwater, 1965], and at the Kernforschungszentrum in Karlsruhe [Kruger and Dimmler, 1964]. Each approach has its advantages and disadvantages. In the case of the small computer for each diffractometer, there is the advantage of complete freedom from interactions with users of other instruments in the same installation, but the computing capacity of the small computer is limited. In practice the real-time capability is restricted to control and basic reduction of data, and the data handling itself is limited. The time-sharing approach gives much greater computing capability to each user, the advantage of sharing expensive peripheral equipment, and vastly greater data handling ability, but requires an extensive system program to control the time sharing. However, it must be recognized that even these latter advantages may be effectively lost if the writing, debugging, and modification of the programs that are to be written by the practicing solid-state physicist or structural

*A 10-minute 16-mm sound movie illustrating some aspects of this system may be obtained on free loan by addressing a request to Office of Technical Information and Publications, National Bureau of Standards, Washington, D.C. 20234.

chemist involve special computer knowledge or are inconvenient in any way.

At a research installation such as a reactor, there is usually a wide variety of different types of experiment in progress at any one time. These may include single-crystal structure work, powder diffraction studies, diffraction studies of liquids or amorphous solids, neutron inelastic scattering studies of phonon and magnon dispersion curves, or polarized neutron studies of magnetic materials. Although the apparatus for all of these experiments is similar, the programs for controlling the experiments and analyzing the data may be very different, and the experimenter's ideas of the proper procedure may change as experience accumulates. In order to achieve the necessary versatility and flexibility in a system for controlling diffractometers at the National Bureau of Standards Reactor, it was decided to use the time-sharing approach, with two particular design objectives. First, the individual instruments must have, as much as practicable, truly independent access to the computer; and second, it must be possible for virtually all user programs to be written in FORTRAN compiler language. In order to make the most effective use of available funds, it was further decided to design the system so as to hold capital cost to a minimum, at the expense of some increase in the complexity of the operating system program; and operating costs were to be minimized by designing a system which required no operator to run it.

This paper describes the system which has been developed to meet these objectives. The emphasis is placed on the general ideas behind the system design and, equally important, on the response of the users in terms of some of the features that have been incorporated into the programs written so far.

2. Computer Hardware Configuration

The NBS diffractometer control system uses, for its central processing unit, an XDS 925 computer,[1] with a core memory capacity of 16,384 24-bit words, and a cycle time of 1.75 μs. The core memory is supplemented by a rapid-access disk memory with a capacity of 262,144 words and an average access time of 17 ms. Other peripheral devices include a console typewriter, a paper tape reader and punch, a card reader, and a magnetic tape transport. Figure 1 shows a block diagram of the computer configuration.

The computer communicates with the diffractometers and the experimenters by means of a system interface designed and built to NBS specifications by Xerox Data Systems, Inc. The system interface includes a teletypewriter interface, a master controller, and a station controller for each diffractometer. The teletypewriter interface allows simultaneous communication with the computer from up to eight remote Teletype[2] stations. The master controller consists of two identical units, each of which controls up to four diffractometer stations. It decodes signals going to and coming from the station controllers, and handles certain functions which are common to all stations. These

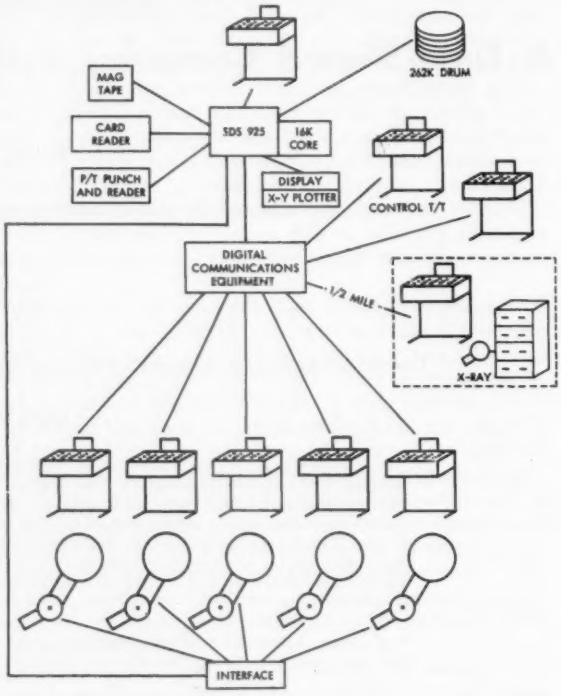

FIGURE 1. *Basic hardware of diffractometer control system showing 5 neutron and 1 x-ray diffractometers interfaced to computer. Each station has its own teletype unit.*

include a pair of digital to analog converters for data display, a 7.5-Hz clock function, light pen detector circuits, and an adjustable timer used for controlling motors. The station controllers contain equipment which is specific to a particular diffractometer. This equipment includes a 16-bit scaler for counting the diffracted beam, a 20-bit scaler for the incident beam monitor, six circuits for detecting "degree marks" which are returned once per revolution of a motor, six circuits for detecting if any motor has hit a limit, five circuits to detect the state of breakpoint switches, and six relay drivers.

3. System Programs

The necessary computer programs may be arbitrarily divided into system programs, which control over all operations, and user programs, which apply to computation and control for a user's particular experiment. System programs are divided into an "offline" (non-real-time) system and an "online" (real-time) system. The offline system described in detail below contains programs needed for general housekeeping,

[1] Xerox Data Systems, Inc., El Segundo, California. Certain commercial equipment is identified in this paper in order to describe adequately the hardware configuration of this system. In no case does such identification imply recommendation or endorsement by the U.S. Government, nor does it imply that the equipment identified is necessarily the best available for the purpose.

[2] Teletype Corp., Skokie, Illinois.

These include the FORTRAN compiler, loader, and library; the assembly routine; programs for such utility functions as copying paper tapes and initializing the system; a program for updating the system; and two programs for transferring control to the online system, one to be used after an orderly shutdown, and another to be used after an accidental or unplanned shutdown.

The online system contains the programs needed to control the experiments and for day-to-day routine operations. It is divided into a core-resident part, and other parts which reside on the disk, to be loaded into core when needed. The core-resident system includes the time-sharing executive routine, referred to as the distributor, subroutines for servicing priority interrupts, all routines required by the FORTRAN runtime package, and a set of subroutines which are used very frequently by users' programs, including all programs for control of diffractometer operations, as well as frequently used computation routines such as SIN, COS, ATAN, and EXP.

To each station there is assigned a specific 72-word block of core memory. Forty of these words are devoted to buffers, 20 words each for input and output, for temporary storage of Teletype messages. The remaining 32 words are pointers, counters, and flag words. One particular flag word, known as the status word, contains bits which are 1's when certain real-time operations (such as the movement of a motor or the counting of neutrons) are in progress, and 0's otherwise. Most of the other flag words are usually equal to -1, but are set to 0 when a real time operation is completed. The distributor repeatedly tests these flag words, and when one is equal to 0 a branch is entered which takes appropriate action. This usually means setting a bit in the status word to 0.

Action is initiated by typing a control message, which is a dollar sign followed by a four- to eight-character code word, and up to seven parameters. A carriage return or an exclamation point terminates the control message, and the control-message-finished flag is set. The distributor will then cause the control message processor to be read into core from the disk, and control is transferred to it. The control message processor is a disk-resident program which interprets control messages entered on a Teletype and initiates appropriate action. In addition to initializing the execution of programs, other actions include the output of information regarding the status of the system and control of the disk files that may be used by the experimenter. When the control message has been processed, control is returned to the distributor, which resumes testing.

After testing all flags, the distributor tests all status words. If the station is active, but the status word indicates that no real time operation is in progress, a user program will be entered. First, the station's COMMON area (i.e., locations where variables listed in a COMMON statement in a FORTRAN program are stored) is read into core from the disk. Attached to the COMMON area are several words which enable the distributor to load the appropriate user program into core from the disk, and then to transfer control to the proper point in the program. The program may retain control for up to five seconds—a FORTRAN function is available to determine if time is almost up—and then must yield control. The COMMON area is now written back on the disk, and control is returned to the distributor. Thus the user saves needed variables (whose values would otherwise be lost upon yielding control to another station) by simply designating them to be in COMMON.

4. User Programs

User programs are two classes, designated level 1 and level 2. A level 2 program is restricted to 128 words of COMMON. In return for this restriction it will be given priority handling by the distributor, which will handle it before any level 1 program. Level 2 programs are intended for operations, such as "manual" operation of the diffractometers, during which a human operator is actually present waiting for results. A level 1 main program (maximum length 5508 words) may call up to a maximum of six segments (each with a maximum length of 2548 words) that will overlay one another in core. There may be up to 1024 words of COMMON. Thus the system can accommodate programs of great complexity, provided that they can be broken up into segments of less than 5 seconds of computing time each.

One special relationship between level 1 and level 2 programs is provided by use of the control message $PAUSE, which causes the level 1 program to halt temporarily. While in this status, a level 2 program, such as one that enables "manual operations" to check on crystal alinement or spectrometer performance, may be executed. Finally, return to the original level 1 program is accomplished with $RESUME.

5. Control of Real-time Operations

Real-time operations (such as moving a motor or starting the neutron counter) are controlled by means of a set of special subroutines that may be called by the user's FORTRAN program. The user's program computes the necessary parameters, calls the subroutines which initiate the required operation, and then yields. The subroutines set the appropriate bits in the station's status word, so that the station remains in a yield status until the real-time operation is completed. When the distributor has reset all of these bits, control then returns to the next statement after the yield. The following sections describe each real-time operation in detail.

5.1. Teletypes

Each station has its own Teletype, which communicates with the computer through an interface which is independent of the computer's main input-output

buffer. The Teletypes are wired in the full duplex mode, so that input from the keyboard and output to the printer are independent. On input the computer identifies the sending station, examines the character to see if it has a special significance, and if it is valid in context, converts the code to its internal code, stores the character in a 20-word buffer in the station's reserved area in the core, and acknowledges receipt of the character by retransmitting the character to the same Teletype's printer. A user program may request input by calling a subroutine TYPEIN, which sets the input-expected bit in the station's status word, and then automatically yields. An exclamation point or a carriage return terminates the message, after which the program may read the message in the buffer by means of the standard FORTRAN ACCEPT statement. If the program has not yielded at a TYPEIN, only control messages (those preceded by $) may be entered. On output, characters are stored in a 20-word output buffer. The program then yields and the computer transmits the characters under interrupt control.

An x-ray diffractometer, located in a building remote from the computer, contains its own control hardware, and thus requires only Teletype communication to operate automatically. The messages sent by the computer are interpreted as instructions by the diffractometer, which sends back data to the computer.

The subroutine TYPEIN (whereby the user program calls for input) also starts the paper tape reader on the Teletype so that if a tape is in position it will be read. When a station becomes inactive (usually because a program has finished execution) the distributor will start the paper tape reader at that station. This feature is very useful because it makes it possible to execute a sequence of programs.

5.2. Neutron counting

Each neutron diffractometer has two pulse-counting channels, one for a monitor detector and one for the diffracted beam, connected to scalers built into the computer interface. The output of the diffracted-beam channel is also connected to a count-rate-meter which drives a strip chart recorder,[3] which provides a continuous time record of the detector output that is useful for monitoring the overall performance of the system during data collection. Either scaler may count either neutrons or 60-Hz timing pulses. The program calls one of the subroutines COUNT(MON) or CNTIME(MON) to count for MON monitor counts from detector or 60-Hz respectively, and then yields. Both scalers are started by a signal from the computer, and count until the monitor scaler overflows. Counting then stops, and the subroutine SCALER(ICOUNT) is used to read the diffracted beam count into location ICOUNT.

5.3. Motor Control

All neutron diffractometer angles are measured by means of worm gears or helical gears and worms driven by "Slo-Syn" stepping motors.[4] To start a motor the program calls a subroutine START(MONUM, TARG) for the fast, slewing speed, or STARTS(MONUM, TARG) for the slow, scanning speed. MONUM is the motor identification number, and TARG is the angle to be reached. The program starts all motors which must be moved and then yields.

Motors may be assigned to any of eight frequencies. The stepping motors run more reliably at fast speeds if they are started by increasing the frequency in several steps. The system makes provision for starting motors in three steps, with frequency ratios of about 1.4. Also, to take care of backlash in the gears, the system causes all motors which are driven in a negative direction to overshoot the target by 0.2 degree, and then approach the final angle in the positive direction.

If the angle-measuring device driven by a motor hits a limit switch, it is an indication either of a programming error or of a malfunction which has caused the true angle to be different from the angel recorded in the computer. In either case the system program stops the motor, makes the station inactive, and prints a message on the station's Teletype.

5.4. Degree Markers

Experience has shown that, if motors are properly installed and have been assigned to appropriate frequencies, slippage is a rare occurrence, but it must be detected if it does occur. For this purpose each motor is fitted with a degree marker, which consists of a lamp, a disk with a slot in it attached to the motor shaft, and a photodiode detector. The assembly is adjusted so that the slot will allow light to hit the photodiode during the step immediately before a whole degree. If an error is detected a correction is made. If the number of errors exceeds a predetermined number, the motor is flagged as malfunctioning. The motor is stopped, and the station is made inactive.

5.5. System Clock

The system clock keeps track of the time of day and the day of the year, and performs two other system functions. It determines whether a station has used the computer for more than 5 seconds at a time, and stops the program if the time limit is exceeded. It also allows the programmer to call a subroutine HOLD (TIME) which automatically yields for a specified time interval and then resumes computing.

5.6. Breakpoint Switches and Relays

The computer interface provides five points per station which can be tested by the computer, using the FORTRAN statement IF (SENSE SWITCH N) to control branches in the program. These points are connected to toggle switches on the typewriter panel, and may also be connected to switches controlled by real-time operations, such as a temperature indicator or a position indicator. Each station is also provided with drivers for five relays, which can be set or reset by means of program instructions. These functions may be combined to perform such operations as measuring intensity versus temperature or changing filters.

[3] Rustrak Instrument Co., Manchester, N.H., Model 88/109B.
[4] Manufactured by Superior Electric Co., Bristol, Conn.

5.7. Data Display

The computer interface provides two analog outputs, which can be set to values in the range ± 10 V by means of program instructions. These outputs are fed into the X and Y inputs of a storage oscilloscope[5] and an $X-Y$ plotter.[6] A FORTRAN subroutine, CONVRT (IX, IY) sets the outputs to levels proportional to the values of IX and IY in the range 0 to 511. Another subroutine, DISPLAY (IYO, ISIZE), if called as the next executable statement after a TYPE statement, will cancel the typing and instead will display the characters of the output record on the oscilloscope screen, enabling the programmer to label a data display with identifying information. The arguments specify the height on the screen where the line of characters will be displayed and the size of the characters.

The experimenter may manipulate the data displayed on the oscilloscope by means of a light pen.[7] A word in core is incremented whenever the pen is in position to be activated by a spot flashed onto the screen. The value of the word is then available as the function LITEPN (N) which is tested by the program immediately after each particular spot has been displayed. The word is automatically reset to − 1 each time the function is called.

5.8. Sequential Files on the Disk

151,552 words of disk memory, slightly more than one half of the total disk memory, are allocated for storage by the users of data and intermediate results of computations. This space is divided into files, which, from the programmer's point of view, simulate binary magnetic tape units. Files are divided into 128-word records, and are of two types: data files, containing 88 records; and scratch files, with eight records. The FORTRAN statements READ TAPE N and WRITE TAPE N will read information from and record information on file N. Two subroutines, RWNDSF(N) and SKPREC(N, ISKP) will, respectively, "rewind" the file N and "skip forward" ISKP records in the file. Control messages are used to reserve up to five files at each station, gain access to a file at another station (read only), or to transfer a file from one station to another. Logical unit numbers may be assigned to files and they may be write-protected if desired.

5.9. Other Input-Output

The computer has a magnetic tape drive unit, a card reader, and paper tape reader and punch which may be used by programs called from a Teletype station located in the computer room. The BCD tape operation statements of FORTRAN, READ INPUT TAPE N and WRITE OUTPUT TAPE N, may be used by experimenters for reading and writing magnetic tapes for permanently storing data or for communicating with other machines.

[5] Tektronix, Inc., Portland, Oregon, Model RM564.
[6] Hewlett-Packard, Pasadena, California, Moseley 7035B.
[7] Sanders Associates, Inc., Nashua, N.H., Photopen EOPT.

6. The Offline System

When the control system was still in the planning stage, it was concluded that it was not feasible to compile and load FORTRAN programs while sharing time with other operations. This would have required modifying the FORTRAN compiler itself to be a real-time program, a task which would have been far too difficult to justify in terms of the benefits that would have resulted. Therefore compiling and loading of programs, along with certain other less frequent operations, are done in a non-real-time, batch processing mode under the "offline system." Care was taken to make the transition from the online to the offline mode (and vice versa) automatic and foolproof; no data or motor angles are lost. The real-time operations are merely suspended upon going offline.

The compiler is a REAL TIME FORTRAN II, which was supplied by XDS and has not been changed in any way. Virtually all user programs are written in FORTRAN language and compiled using this compiler. The only exceptions are certain very short, special-purpose subroutines which perform operations outside of the restrictions of the FORTRAN language, and therefore must be written in assembly language.

In actual operation a source program, on punched cards, is compiled, producing a binary object program on punched paper tape. The program is assigned a number, by which it may be called during real-time operation, and is loaded into core. Library subroutines and links to core-resident subroutines are attached, in absolute address form. When loading is complete, the program and all attached subroutines are written on a program file on the disk, and the program's number is inserted in the program directory, an area on the disk which contains a catalog of the locations of all programs in the program area. The directory will then be scanned by the control message processor to determine the locations from which the program is to be loaded into core at run time.

The offline system also contains various programs for initializing the system, and for certain other utility operations.

7. User Software

The actual use of a computer may change one's approach to the problem at hand, but the implementation of revised ideas is very much a function of the amount of labor involved. The use of FORTRAN has greatly facilitated the development of programs by individual users. The extensive I/0 capabilities of FORTRAN and the use of the COMMON statement to designate the locations of necessary variables have enabled application of some generally useful ideas that have emerged in the course of writing user programs. This section lists some of these ideas, and gives examples of how they have been used so far. The programs mentioned do not represent an inclusive list of the programs that have been written. The program library is still being steadily expanded.

7.1. Routine Tasks

Short, routine tasks frequently repeated require highly simplified input from the Teletype for maximum convenience. One example is a program that carries out simple tasks such as driving motors to a designated angle, counting in place, rocking a crystal through a given angular range, finding the monitor count, finding the location of a peak within a given range, etc. The operation code consists of two letters, such as "FM" for find monitor count rate and "CT" for count.

7.2. Experimental Parameters

Parameters that are used repeatedly in an experiment are entered once, and then saved in COMMON. For example, in the program described above the monitor count is entered with M = (I8). Subsequently, every time "CT" is called, the same monitor count is used.

A more spohisticated example of this same idea is given by a separate program (called PRAM) which accepts all pertinent data for a single crystal, including cell constants, Laue point group, systematic absences, the orientation of the crystal, etc. This program stores these quantities in COMMON, along with certain derived quantities such as the orientation matrix, where they are available to other programs that may now easily compute the setting angles for any reflection, *hkl*, or use other information supplied by PRAM.

7.3. Data Handling

The need for the ability to reduce and manipulate data with a rapid turnaround varies widely from one experiment to another. In some cases it may be sufficient to write data in "raw" form on a magnetic tape, leaving all further processing to a central computing facility. In other cases it may be desirable for the user to exercise human judgement in the course of an experiment. Judgement may be shared between the user and the computer in varying proportions depending on the circumstances. It is important to have available, in addition to the actual online control programs, data-handling programs sufficient to perform whatever manipulations may be required to provide the information that is needed quickly.

As an illustration of a rather complete capacity for handling data, consider the set of programs written for processing powder data (i.e., neutron intensity as a function of counter angle). These data are taken by one program which stores them with suitable header information, which includes a problem number and run number, and five integer parameters which the experimenter may use to label conditions of the run, such as the temperature, magnetic field, etc. This program collects the data, stores them on a data file, and prints out the information as it is accumulated, if desired. This record is not very compact since each line contains only one intensity point. This program may be used repeatedly to collect many runs, which may be repeats or runs under different experimental conditions. A second independent display program will read the data and print it out in compact form, display it on the storage scope, or plot it on the $x-y$ recorder. Scaling may be done automatically by the program or left to the choice of the user. Background points may be indicated by the user by means of the light pen, or on the Teletype, and commands given for the net integrated intensity of a peak to be determined, together with its statistical error. A third program enables the experimenter to collate any data runs by adding or subtracting two or more of them. The results of the collation are also stored on a file and may be subsequently processed by the second program. Printouts of collated runs contain the statistical errors for each data point. There are two additional programs, one for writing data files from the disk onto magnetic tape and the other for recalling data from magnetic tape back onto the disk where it can be reprocessed. The recall program utilized problem and run numbers and the five integer parameters mentioned above to search the tape for the desired data.

The system feature which allows one station to have access (read-only) to another station's files allows all the manipulative and analysis functions described above to be carried out while data collection is still going on at the experimental station.

7.4. Modification of Programs

It would appear to be an axiom of computer usage that the full specifications for a complicated program or system of programs are never completely known beforehand, but rather evolve during the course of writing, testing, and using the programs. A typical example is illustrated by the powder data program mentioned above, which, because of the FORTRAN capability, was easily modified to collect data as a function of sin θ/λ (θ = counter angle, λ = wavelength) where amorphous materials were measured. A further modification enables one to collect data for a single crystal for scans along some specified direction in reciprocal space. In all three cases the data finally stored on the data file are in the form of intensity as a function of some continuous variable. Thus, the manipulative and analysis program described in the previous section could be used as written.

7.5. Automation of Routine Tasks

Certain routine tasks, if automated, will be used more frequently with better overall results for the experiment.

One example of such a task is the measurement of the neutron wavelength and the zero correction to the counter angle. A copper powder sample is used as a standard and four reflections are scanned for their angular positions. The only input required to the program is an approximate value of the wavelength. The program determines the best, least squares value of the wavelength and zero correction.

7.6. Feedback

Utilization of feedback enables great efficiencies to be realized in data taking. For example, when measuring single crystals with moderately large unit cells, for which many hundreds of reflections are required, large amounts of time may be wasted by scanning reflections which are so weak that they are essentially unmeasurable or by measuring strong reflections to an accuracy greater than is needed. A program was therefore written which performs a quick scan over the peak to estimate the intensity first and then proceeds to measure the reflection to the desired accuracy. This program also checks several successive measurements of the intensity for statistical consistency, and causes the data to be remeasured if they are not consistent.

8. Operating Experience

In 22 months of operation the system has proved itself to be highly flexible and reliable. Because the designers and system programmers are also user-scientists, this has permitted modifications to the system program to be made easily when the need was apparent. More than 10 different people have written programs for use on the system with a minimum of difficulty. In some cases the fact that programs are written in FORTRAN has enabled the use of programs which were originally written for quite different machines under quite different circumstances, without any modification whatsoever. The FORTRAN compiler, with its diagnostics, is so effective in eliminating user programming errors that in practice it has been found that all inhibitions to writing new programs for fear they might adversely affect other user programs have been removed. Only two ways have been found for a programming error to cause a system malfunction: writing in an array with an incorrectly computed value for a subscript, and use of an incorrect name for a subroutine. The latter error can cause trouble only if the incorrect name also appears in the library with a special significance.

In the unlikely event that the system does crash, it may be restarted with a single control message and the only variables that must be restored at each station are the motor angles. The user program may test for a restart condition and take special action if that is needed; otherwise the user program will automatically continue from the statement after which it last yielded.

The stepping motors have proved to be highly reliable, provided they are operated within their ratings with respect to speed and torque. When properly adjusted they have been shown to operate for tens of thousands of revolutions without a single slippage error. In a few cases it has been necessary to experiment with a motor to find its proper speed, but the fact that speeds are determined by programs means that they can be changed by simple program changes, often no more than the change of one or two words in a system program.

Because different users can communicate with the computer simultaneously through the individual station Teletypes, instances of interference between users for access to input-output facilities have been extremely rare. The system has proved, so far, to satisfy its design objectives extremely well.

The basic concepts of the time sharing and the FORTRAN capability were developed jointly with Gerd Dimmler of the Brookhaven National Laboratory. His valuable contributions are gratefully acknowledged. We also thank Louis Paolella, Alan Tudgay, and Robert Williams for their assistence in installing the system hardware.

9. References

Abrahams, S. C. (1962), Rev. Sci. Instr. **33,** 973.

Beaucage, D. R., Kelly, M. A., Ophir, D., Rankowitz, S., Spinrad, R. J., and Van Norton, R. (1966), Nucl. Instr. and Methods **40,** 26.

Busing, W. R., Ellison, R. D., Levy, H. A., King, S. P., and Roseberry, R. T. (1968), Report ORNL–4143, Oak Ridge National Laboratory, Oak Ridge, Tenn.

Fitzwater, D. R. (1965), Report IS–1279, Ames Laboratory, Iowa State University.

Kruger, G., and Dimmler, G. (1964), Report KFK–242, Kernforschungszentrum Karlsruhe, Germany.

Prince, E., and Abrahams, S. C. (1959), Rev. Sci. Instr. **30,** 581.

(Paper 74C3 & 4–302)

JOURNAL OF RESEARCH of the National Bureau of Standards—C. Engineering and Instrumentation
Vol. 74C, Nos. 3 and 4, July–December 1970

Tensile Deformation of Vapor-Deposited Copper Reinforced With Tungsten Wires

William D. Jenkins,* William A. Willard, and Donald E. Harne

Institute for Materials Research, National Bureau of Standards, Washington, D.C. 20234

(July 29, 1970)

Short-time tensile tests were made at room temperature on sheet specimens of vapor-deposited copper containing zero to 26 volume percent continuous tungsten wires having diameters of 0.0005, 0.001, and 0.005-inch. Specimens were annealed at 25, 300, and 600 °C (298, 573, and 873 K) prior to testing. Strength, ductility, shape of the stress-strain curves, and types of fractures were influenced by volume fraction and number of layers of wires as well as by wire diameter and alinement. Strength values for the composites with 2 to 3 percent volume fractions of wires exceeded those predicted by the law of mixtures whereas at higher volume fractions, either conformance to the law was observed or lower values than those predicted were obtained. Increase in strength was accompanied by a decrease in electrical conductivity. All the properties investigated were markedly affected by increasing the annealing temperature. Tungsten wires failed in a ductile manner after considerable localized deformation ("necking") in various sections of the wires.

Key words: Composites; copper; electrical conductivity; fracture; law of mixtures; metallic bonding; tensile properties; tungsten; vapor-deposition; wires.

1. Introduction

The possibility of producing structural materials having mechanical properties better than those currently available has led to a number of investigations involving metal-fiber composites. However, clarification of basic principles associated with composite behavior can be made only after an accumulation of a significant amount of data obtained in carefully controlled tests and with composites in which the matrix and fibers are mutually compatible. One such composite is a system containing a copper matrix with tungsten wires. Cu–W composites were used, in part, by Kelly and Davies [1][1] in deriving some basic principles of fiber-reinforcement. Several other investigators have also made mechanical property and electrical resistivity measurements on this composite [2, 3, 4, 5, 6]. Their materials were made by liquid infiltration or by electroforming processes. Data in the present investigation were obtained from specimens made from vapor-deposited copper and vapor-deposited copper containing tungsten wires. The purposes of this investigation were to: (1) determine the effects of volume fraction, diameter, and number of layers of wires and wire alinement on room-temperature mechanical properties; (2) determine the effect of annealing on these properties; (3) relate mechanical behavior to the shape of the stress-strain curve; (4) ascertain conformance of the data to the "law of mixtures"; (5) correlate strength values with electrical conductivity; (6) observe the types of fractures obtained; and (7) determine the mechanism by which the tungsten wires deformed or fractured.

2. Materials and Testing Procedures

Sheets of vapor-deposited copper and vapor-deposited copper containing tungsten wires were prepared and supplied in the condition as vapor-deposited (referred to hereafter also as "VD" or "as annealed at 25 °C"). The copper sheets were approximately 15 inches (38.1 cm) long, 1 in (2.54 cm) wide and 0.01 in (0.0254 cm) thick. The composite sheets contained continuous tungsten wires. The length and width of these sheets were the same as those for the copper; however, the thickness was dependent on the number of layers of wires (1, 2, or 3), volume fraction of wires (ranging from 2.1 to 26%), and wire diameters (0.0005, 0.001 or 0.005 in) (0.0127, 0.0254, or 0.127 mm), as shown in table 1. With one exception, the wires were alined in the longitudinal direction. In the exception, the wires were deliberately misalined in order to ascertain the effects of misalinement on mechanical properties. Blanks 4.25 in (10.8 cm) long and 1 in (2.54 cm) wide were cut from the sheets. The blanks were then cut in half in the longitudinal direction to make duplicate adjacent specimens having dimensions of 4.25 by 0.5 in (10.8 by 1.27 cm). These were machined into tensile specimens, each having a 0.2-in

*Present address: 1829 Ingleside Terrace N.W. Washington, D.C. 20010.
[1] Figures in brackets indicate the literature references at the end of this paper.

(0.51 cm) width over a 1-in (2.54 cm) gage length. The pairs of specimens were then divided into three groups: one group to be tested in the vapor-deposited condition, the second group was annealed in vacuum for 15 min at 300 °C, and the third group was annealed in vacuum for 15 min at 600 °C. Cross sections of the vapor-deposited copper before and after annealing at 600 °C are shown in figure 1. Microstructures of some of the

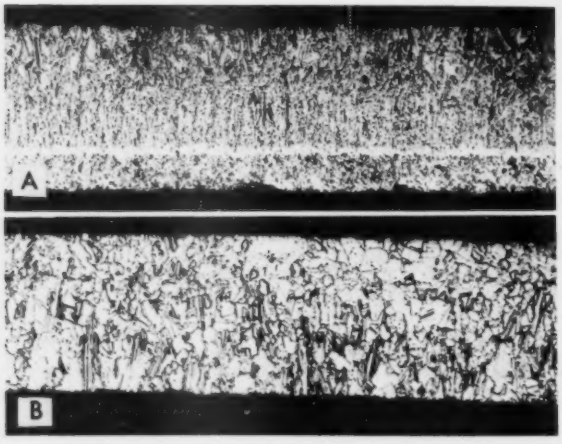

FIGURE 1. *Microstructure of vapor-deposited copper.*

Cross sections, etched in equal parts NH_4OH and H_2O_2 (3%); × 100.
A. As vapor-deposited (annealed at 25 °C)
B. Annealed at 600 °C.

as received composites are shown in figure 2. Fairly evenly spaced tungsten wires in the copper matrix are evident in figure 2A, B, and C. Poorly spaced wires are shown in figure 2D for a composite which was examined but not tested. The absence of any observable (at × 500 magnification) chemical reactions at the Cu-W interface is shown in figure 2E. Composite sheets having large voids such as those shown in figure 3A were also discarded prior to making the tensile specimens, while those having structures as shown in figure 3B, C, and D were considered to be usable. Reactions of the etchant with the interface material were more apparent in the annealed material (fig. 3C and D) than in the material in the condition as vapor-deposited (fig. 3A). Moreover, well-defined grains, evident in the annealed copper (fig. 1B) were not observed in the annealed composite (fig. 3D).

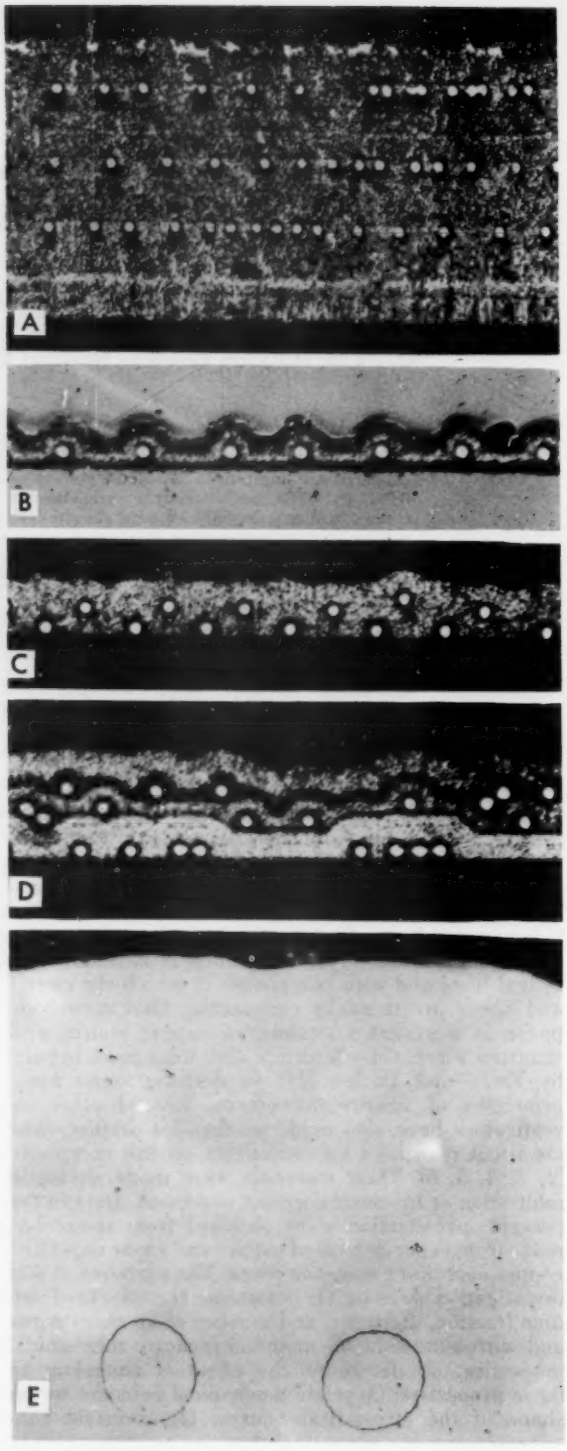

FIGURE 2. *Microstructures of vapor-deposited copper with tungsten wires. Cross sections.*

	Wire diameter, inch	Number of layers of wires	Etchant	Magnification
A	0.0005	3	1:1 NH_4OH and H_2O_2 (3%)	× 100
B	.001	1	do	× 100
C	.001	2	do	× 100
D	.001	3	do	× 100
E	.001	1	None	× 500

The specimens were tested in tension in air at a temperature of about 25 °C. The movement of the cross-head of the hydraulic machine was controlled to produce a rate of straining of about 0.1 percent per minute. A fixture was specially designed and built in

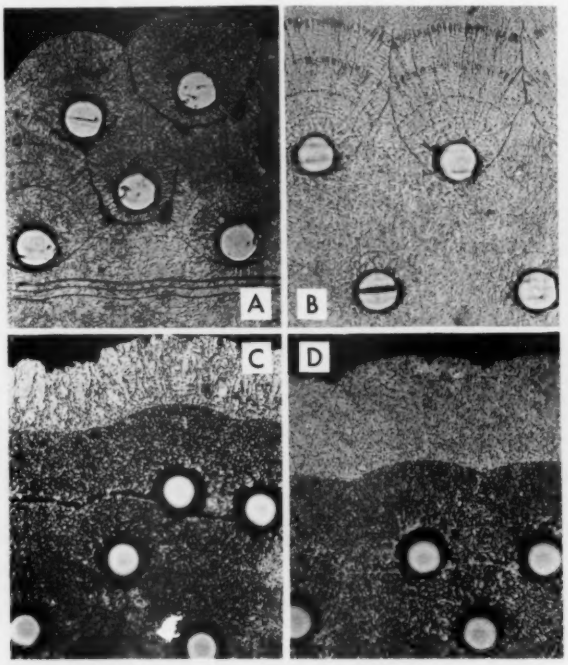

FIGURE 3. *Microstructures of vapor-deposited copper with tungsten wires.*

Cross sections, etched in equal parts NH_4OH and H_2O_2 (3%) × 250.
A, B. – Annealed at 25 °C.
C. – Annealed at 300 °C.
D. – Annealed at 600 °C.

this laboratory to insure alinement and nonbending of the specimens as they were placed in the grips (fig. 4A). The same view with fixture removed and specimen ready for testing is shown in figure 4B.

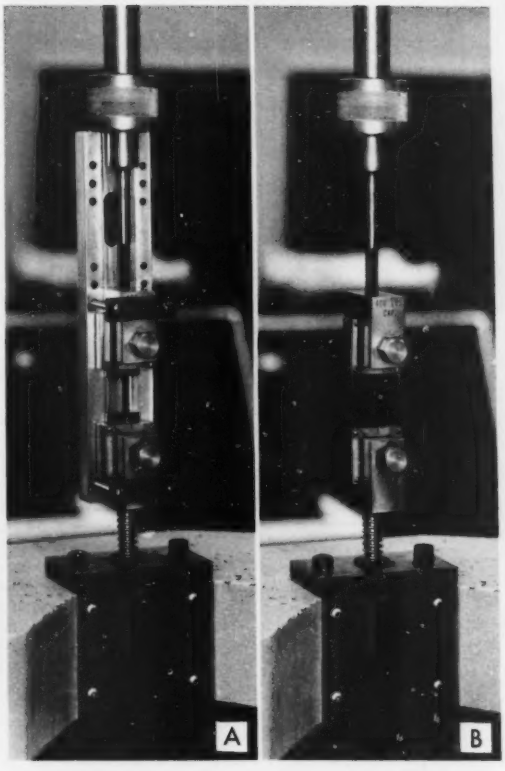

FIGURE 4. *Photographs of part of the apparatus used for making tension tests on the* Cu-W *composite specimens.*

A. Set-up with specially designed fixture for insuring alinement and nonbending of specimen during placement of specimen in grips.
B. Same view as A with fixture removed.

3. Results and Discussion

Test results are shown in Tables 1 and 2 and in figures 5 through 18. The effects of annealing on the stress-extension curves and on the mechanical properties of the copper are shown in figures 5 and 6. Annealing the copper at 300 °C had little or no effect on the stress-extension curves from zero to 15 ksi (103.4Mn/m²). However, the tensile strength of the vapor-deposited copper and the annealed (at 300 °C) copper was approximately the same. This occurred in spite of the fact that the yield strength of the annealed specimen was much lower than that of the vapor-deposited specimen. Increasing the annealing temperature to 600 °C caused a greater decrease in yield than in tensile strength. This decrease in strength was accompanied by a large increase in elongation.

McDanels et al. [2] have presented data which indicated the existence of four stages of stress-strain behavior during tensile testing of copper-tungsten composites. These stages were: elastic deformation of both fiber and matrix (stage 1), elastic deformation of fiber and plastic deformation of matrix (stage 2), plastic deformation of both fiber and matrix (stage 3), and failure of fiber and matrix (stage 4). Weeton et al [3] indicated that the shape of the stress-strain curve, especially in stage 4, depended on the manner in which the fibers fractured.

Stress-extension curves for some of the specimens used in the present investigation are shown in figures 7 through 12. It is observable that the point of occurrence of each of the stages and the flatness of the curves are affected by such test conditions as the number of layers, volume percent and diameter of the wires as well as the annealing temperature and wire misalinement. During stages 1 and 2 (region from zero stress to the yield point) the slopes of some of the curves are only slightly affected by annealing at 300 °C (figs. 7, 8, 10, and 11). However, during the third stage (the region between yield and maximum load), the shape of

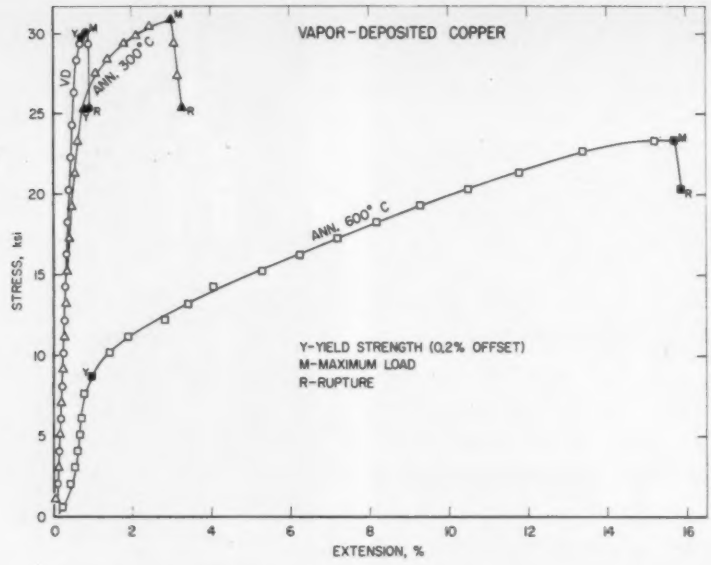

FIGURE 5. *Effect of annealing temperature on stress-extension curves of vapor-deposited copper specimens.*

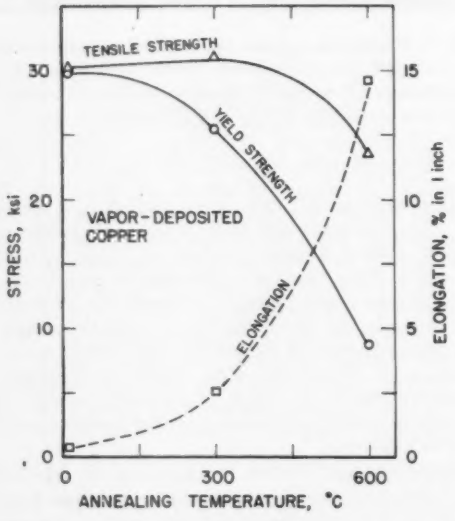

FIGURE 6. *Effect of annealing temperature on some tensile properties of vapor-deposited copper.*

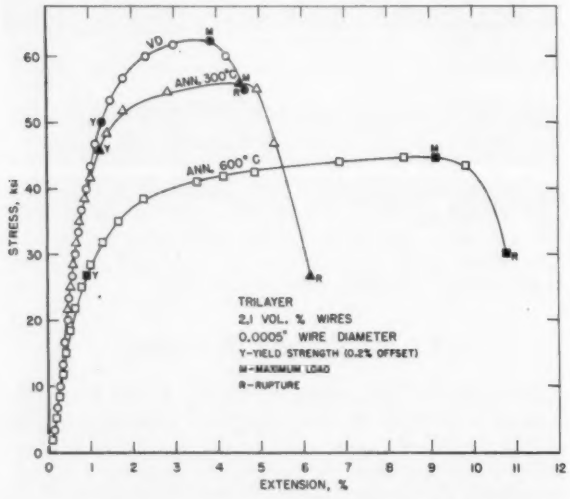

FIGURE 7. *Effect of annealing temperature on stress-extension curves of vapor-deposited copper specimens containing 2.1 volume percent tungsten wires.*

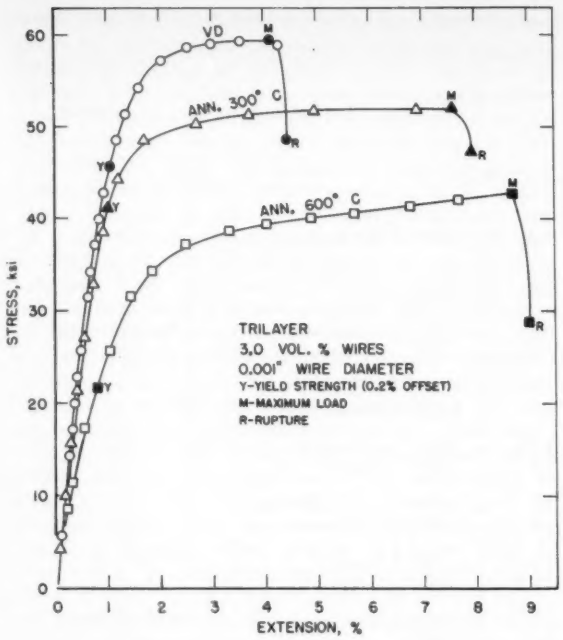

FIGURE 8. *Effect of annealing temperature on stress-extension curves of vapor-deposited copper specimens containing 3 volume percent tungsten wires.*

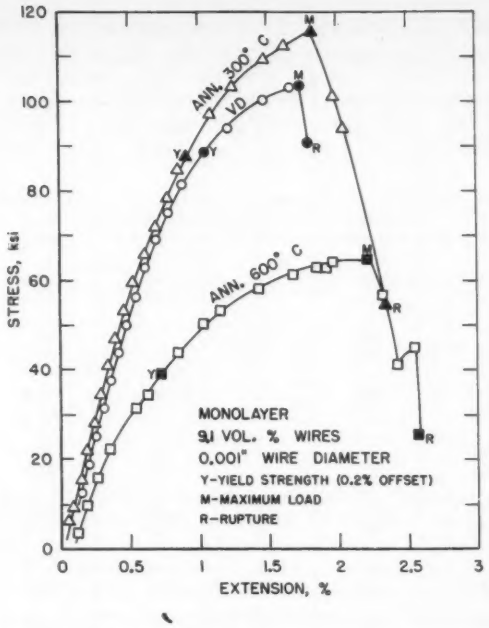

FIGURE 10. *Effect of annealing temperature on stress-extension curves of vapor-deposited copper specimens containing 9.1 volume percent tungsten wires.*

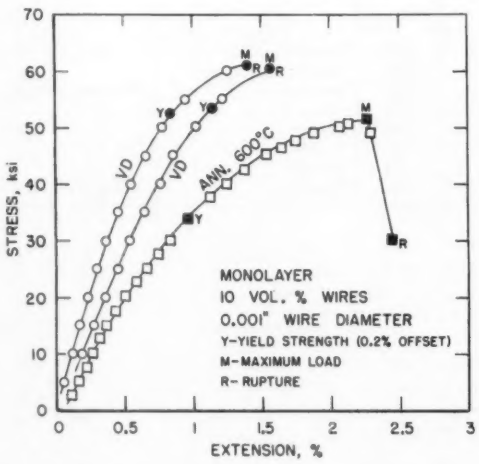

FIGURE 9. *Effect of annealing temperature on stress-extension curves of vapor-deposited copper specimens containing 10 volume percent misalined tungsten wires.*

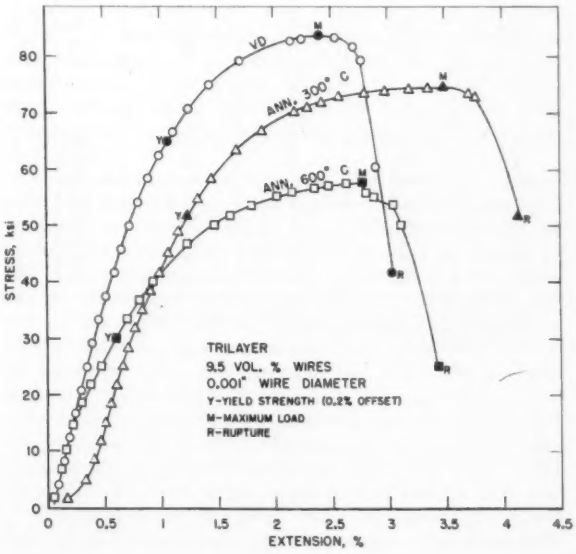

FIGURE 11. *Effect of annealing temperature on stress-extension curves of vapor-deposited copper specimens containing 9.5 volume percent tungsten wires.*

TABLE 1. *Test conditions and results of room temperature tensile tests made on composites having a copper matrix with continuous tungsten wires*

Volume fraction wires, %	Wire diameter, inch	Number of layers of wires	Yield strength, 0.2% offset, ksi[c]	Tensile strength, ksi	Elongation % in 1 inch	S/S_T [a]	Type of fracture	Remarks
				Annealed at 25 °C				
2.1	0.0005	3	48.5	63.2	2.1	1.486	Tensile	
2.1	.0005	3	50.5	63.2	3.3	1.486	Shear	
3.0	.001	3	42.5	54.2	1.0	1.179	Tensile	
3.0	.001	3	45.4	59.4	3.3	1.292	Shear	
10	.001	1	51	60	0.7	0.725	Premature	Wires Misalined
10	.001	1	53	60	.6	.725	Premature	Do.
9.1	.001	1	89.5	104.8	.7	1.338	Tensile	
9.1	.001	1	87.5	106.1	1.2	1.354	Tensile	
9.9	.001	2	68	82	1.3	0.994	Premature	
9.9	.001	2	62	81.2	1.6	.985	Tensile	
9.5	.001	3	65	83.5	1.9	1.040	Shear and Tensile	
9.5	.001	3	63	79.2	1.9	0.987	Tensile	
9.7	.001	3	56	77.4	1.8	.953	Tensile	
9.7	.001	3	55	72.4	1.5	.891	Premature	
26	.005	2	96	125.7	1.1	.983	Tensile	Wires pull out
26	.005	2	94	113.2	0.6	.886	[b]	Do.
				Annealed at 300 °C				
2.1	0.0005	3	46.5	56.6	5	1.456	Tensile	
3.0	.001	3	41.5	51.9	6.9	1.107	Shear	
9.1	.001	1	87.5	116.4	1.4	1.470	Shear	
9.9	.001	2	45	59.3	1.55	0.711	Tensile	
9.5	.001	3	51.5	74.6	2.8	.919	Tensile	
9.7	.001	3	32	52.1	5	.635	Tensile	
				Annealed at 600 °C				
2.1	0.0005	3	27	45.1	9.7	1.255	Tensile	
3.0	.001	3	22	42.6	7.8	1.078	Tensile	
10	.001	1	33.5	50.7	1.3	0.661	Tensile	Wires misalined
9.1	.001	1	38.5	64.4	1.8	.891	Shear	
9.9	.001	2	33	57.3	1.5	.749	Tensile	
9.5	.001	3	36	57.6	2.7	.787	Tensile	
9.7	.001	3	32	53.7	3	.714	Tensile	
26	.005	2	80	112.1	1.8	.912	Tensile	Wires pull out

[a] S/S_T = Tensile strength divided by theoretical tensile strength.
[b] Fracture initiated outside of gage length.
[c] 1 ksi = 6.895 MN/m².

all the curves are affected by prior annealing. During the fourth stage (region between maximum load and rupture), a number of different rupture mechanisms appeared to occur, and they were strongly dependent on test conditions. For example, smooth curves in this region indicated that the wires retained some of their bond strength after fracturing and acted as discontinuous fibers would be expected to act (fig. 7). As the volume percent or size of the wires increased (e.g. figs. 8 and 12), the stress-extension behavior indicated that nearly all the fibers fractured in the region of maximum load since very little extension occurred between maximum load and fracture. Misalinement of the fibers contributed to premature rupture.[2] This behavior was observed with duplicate vapor-deposited specimens (VD curves, fig. 9) in which the wires were deliberately misalined. Catastrophic failure was not observed for the specimen with poorly alined wires and annealed at 600 °C (fig. 9). A strengthening effect occured during some portions of the fourth stage as shown by a reversal in the 600 °C curve in figure 10; whereas, some other specimens exhibited a discontinuous weakening effect during this stage (600 °C curve in fig. 11). Duplicate tests indicated slight differences in slope of the stress-extension curves in the first stage (VD curves, fig. 9) even though the tensile strength of the specimens from the same sheet was the same (table 1).

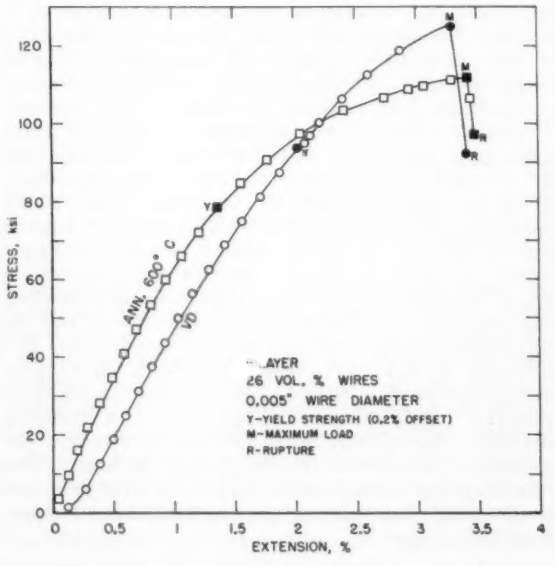

FIGURE 12. *Effect of annealing temperature on stress-extension curves of vapor-deposited copper specimens containing 26 volume percent tungsten wires.*

[2] Premature rupture indicates that the specimen fractured completely prior to the attainment of tensile strength.

Previous investigations [1, 3, 5] have shown that a number of factors influence the strength and ductility of composites. The influence of test conditions on yield and tensile strength and elongation for composite specimens used in the present investigation is shown in figures 13, 14, and 15 and in table 1. As indicated in figures 13A and 14A, a decrease in the tungsten wire diameter from 0.001 to 0.0005 in resulted in an increase in the yield and tensile strength of the composite. This observation was consistent with the fact that the tensile strength of the smaller wire was 12 percent higher than that of the larger wire. This was not unexpected as the larger wire probably had more internal defects than the smaller one.

TABLE 2. *Test conditions and results of tensile tests made on the vapor-deposited copper matrix material*

Annealing temperature	Yield strength, 0.2% offset	Tensile strength	Elongation
°C	*ksi*	*ksi*	*% in 1 inch*
25	30.2	30.3	0.36
25	29.1	30.2	.35
300	25.5	31.1	2.5
600	8.8	23.5	14.6

McDanels et al. [2] have discussed the effects of orientation of fibers on mechanical properties and concluded that composites with randomly oriented fibers should have lower strengths than similar composites in which the fibers (wires) were alined in the direction parallel to the direction of loading. This conclusion was confirmed by the data obtained in the present investigation as shown in figures 13B and 14B. However, strengthening effects due to alining were less pronounced as the annealing temperatures were increased.

As shown in figures 13C and 14C, sheet specimens with one layer of wires had higher strength than those with two or three layers of wires. This effect was less evident as the annealing temperature was raised to 600 °C. Increasing the number of layers of wires from two to three had little or no effect on the yield and tensile strength. Moreover, increasing the annealing temperature for the monolayer from 25 to 300 °C had no effect on the yield strength (fig. 13C) and a slight increase tensile strength was observed (fig. 14C).

Jeck and Signorelli [4] suggested that decreasing the thickness of the matrix between fibers increases the shear strength of the matrix. As shown in figures 13D and 14D, decreasing the thickness of matrix material (Cu) between the tungsten wires increased the yield and tensile strengths of the composites. The data indicate that a triaxial strengthening effect exists even for the annealed material.

The greatest increase in strength above that of the vapor-deposited copper was obtained with the composite specimens having 26 volume percent of 0.005-in diam wires. These specimens also showed the least tendency to lose strength on increasing the annealing temperature from 25 to 600 °C. This latter observation

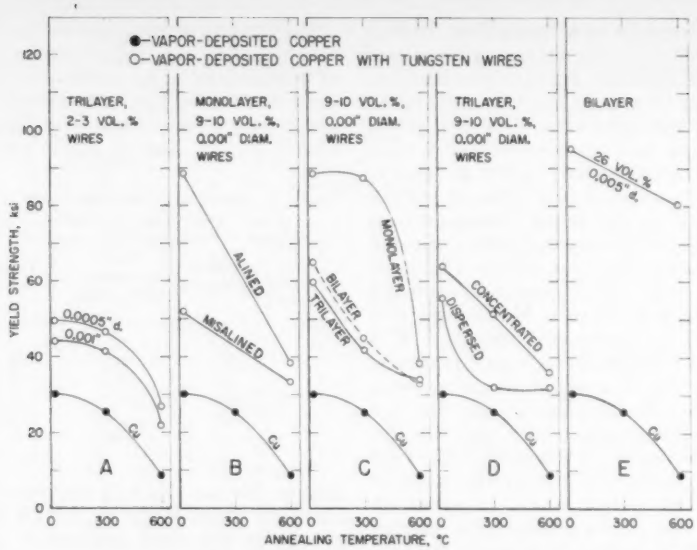

FIGURE 13. *Effect of annealing temperature on the yield strength of vapor-deposited copper specimens and vapor-deposited copper specimens containing tungsten wires.*

is due to the fact that this composite contained the least amount of matrix material. Moreover, the strengthening occurred in spite of a 36 percent decrease in tensile strength of the 0.005-in diam wires below that of the 0.0005-in diam wires.

The influence of test conditions on elongation of the specimens used in the present investigation is shown in figure 15. Elongation of all the composites was greater than that of the copper for the specimens annealed at 25 °C; whereas the reverse was true for those annealed at 600 °C. With few exceptions elongation increased with an increase in annealing temperature, a decrease in volume percent wires, better wire alinement, an increase in number of layers of wires, and interwire distance. Due to the scarcity of data no conclusions could be drawn concerning the effects of wire diameter on elongation.

The law of mixtures, in which the strength of a composite is said to be equal to the sum of the tensile strength of each component multiplied by its volume fraction, has been shown to be valid for a number of composites. However, deviations from the law have been found for some complete systems and at various volume fractions of wires for the same system. Weeton and Signorelli [3] summarized a number of factors known to produce synergistic effects in a composite. Conversely, deleterious effects may be attributed to the fact that matrix and fibers (wires) may not necessarily behave in the same manner individually as they do collectively in a composite. Both synergistic and deleterious effects were observed in the present investigation (fig. 16). Strengths above those calculated from the law of mixtures were observed at low wire content while the opposite was observed for the high volume percent wire content. Tensile strength-theoretical tensile strength ratios associated with both the deleterious and synergistic effects were lowered by raising the annealing temperature to 600 °C.

Properties other than strength and ductility may be important in engineering design of structural components. Electrical conductivity and resistivity are two of these properties. Using Cu-W composites made by liquid infiltration, McDanels [6] indicated that electrical conductivity was a linear function of fiber content. The relationship showing changes in electrical resistivity and conductivity of the present composites and the strength and volume percent of tungsten wires is shown in figures 17 and 18. An initial rapid rate of increase in electrical resistivity with increase in volume percent of wires or tensile strength was followed by a slower increase as these variables were increased (fig. 17A and B). As shown in figure 17C, no consistent relations existed between electrical resistivity and the tensile strength-theoretical tensile strength ratio. The decrease in electrical conductivity with increase in strength is shown in figure 18. All of these curves show inflection points after which the rate of decrease in electrical conductivity with increase in strength decreases as the yield or tensile strength increases. The curves appear to level off at about 65 percent decrease in electrical conductivity below that of the vapor-deposited copper.

4. Metallography

Some of the copper and Cu-W composite specimens were examined after rupture. The results are shown in figures 19 through 22. Rupture of the copper specimens, with no wires, initiated at one edge and progressed through the specimen to the opposite edge of

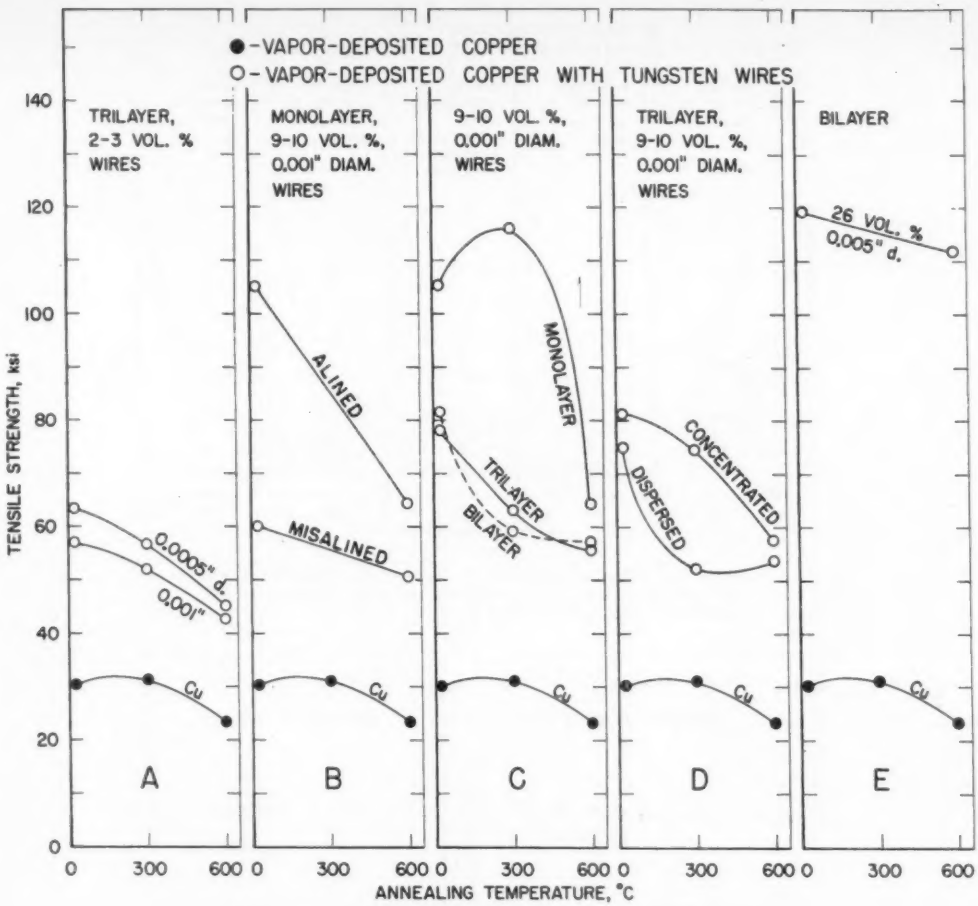

FIGURE 14. *Effect of annealing temperature on the tensile strength of vapor-deposited copper specimens and vapor-deposited copper specimens containing tungsten wires.*

the specimen (fig. 19B). The rate at which the fractures progressed decreased with increase in annealing temperature. Each of the fractures, shown in figure 19, was classified as tensile in that they occurred after the attainment of maximum load (fig. 5) and did not exhibit shear-type characteristics for which the stress-extension curves would be similar. The fracture surface became more jagged as the annealing temperature increased (fig. 19). This tendency was accompanied by an increase in the number of surface cracks that did not link up to become a part of the complete fracture.

In table 1 and figure 20, the types of fractures of the composites are classified as premature, tensile, and shear. Premature fractures were associated with those specimens which ruptured before the attainment of the normal maximum load as indicated by stress-extension curves, such as the VD curves shown in figure 9. No premature fractures were observed for specimens annealed at 300 or 600 °C. Moreover, where comparisons were possible, prematurity was accompanied by low ductility (table 1 and fig. 20A and B). As indicated in table 2 and illustrated in figure 20C, most of the composite specimens exhibited a tensile-type fracture. From the amount of data available, ductility values associated with tensile fractures appeared to fall between the low values for the premature and the high values for the shear-type fractures. A typical shear-type fracture is shown in figure 20D, while a part shear-part tensile fracture is shown in figure 20E. Even though the fracture of the latter specimen occurred outside the gage length and was accompanied by some wire-pullout, none of these factors affected either the tensile strength or elongation, as shown by a comparison with the data obtained on a duplicate specimen that fractured in a tensile manner (table 1). However, when extreme wire pull-out was observed during the tests (fig. 20F), no useful data could be obtained and the test results had to be discarded.

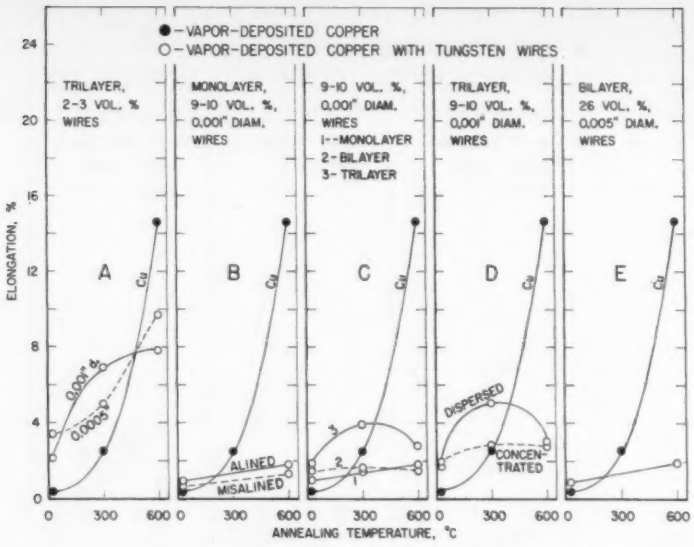

FIGURE 15. *Effect of annealing temperature on elongation values of vapor-deposited copper specimens and vapor-deposited copper specimens containing tungsten wires.*

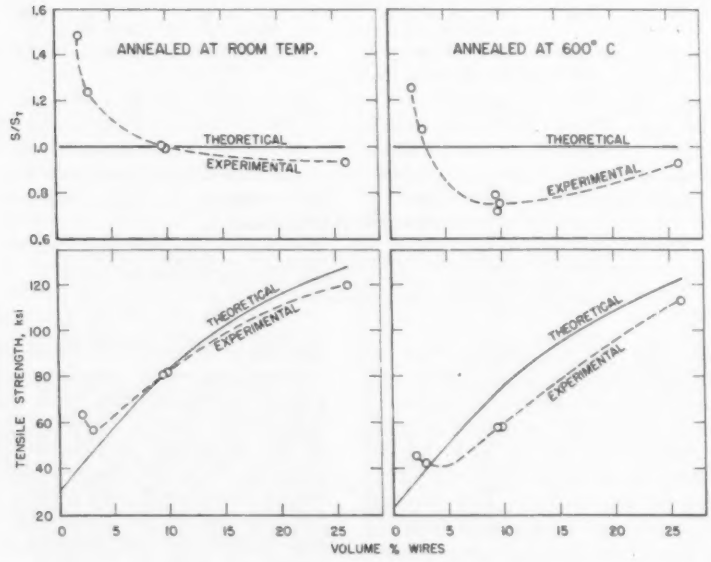

FIGURE 16. *Effect of volume percent tungsten wires on tensile strength of* Cu-W *composite specimens and on the ratio of the tensile strength* (S) *to the theoretical tensile strength* (S_T) *based on the law of mixtures.*

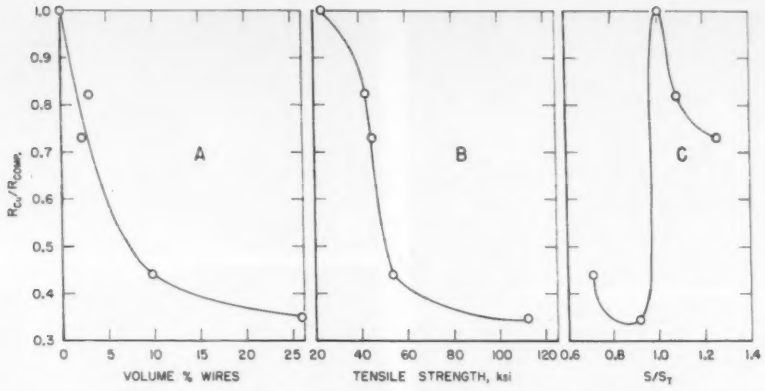

FIGURE 17. *Effect of volume percent tungsten wires, tensile strength and the tensile strength—theoretical tensile strength ratio on the electrical resistivity of* Cu-W *composites.* R_{Cu}, *Resistivity of the vapor-deposited copper.* R_{Comp}, *Resistivity of the* Cu-W *composites.*

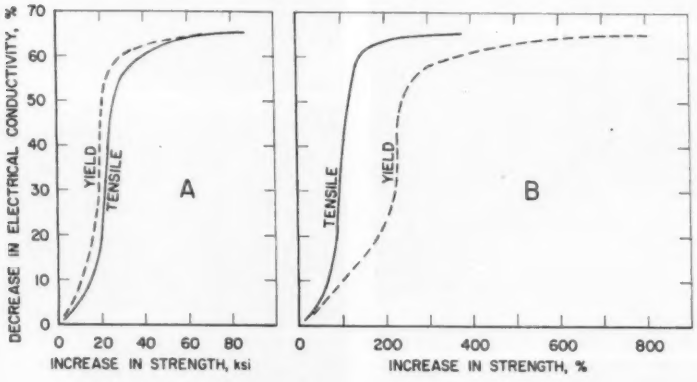

FIGURE 18. *Relationship between strength and electrical conductivity of* Cu-W *composites.*

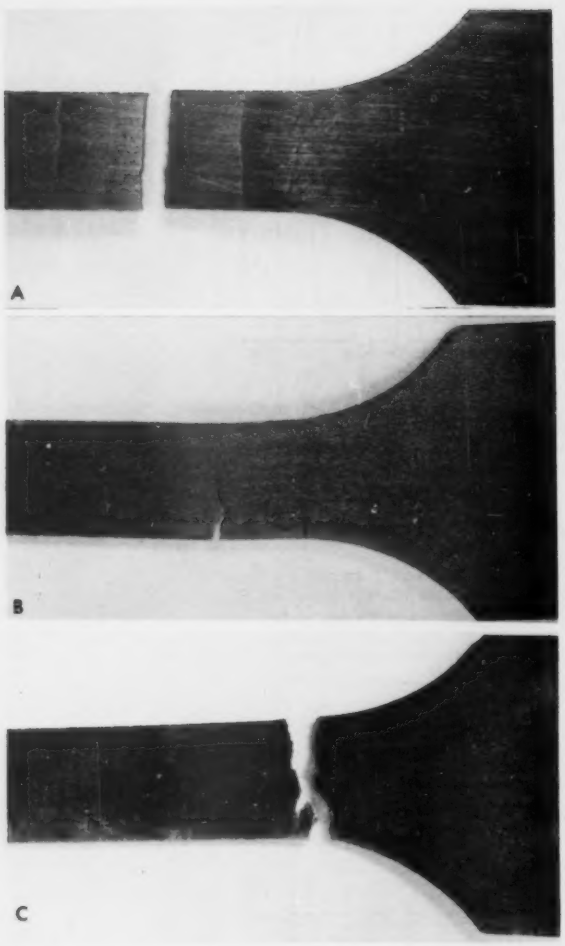

FIGURE 19. *Vapor-deposited copper specimens after fracture.* × 3⅓

A. Annealed at 25 °C
B. Annealed at 300 °C
C. Annealed at 600 °C

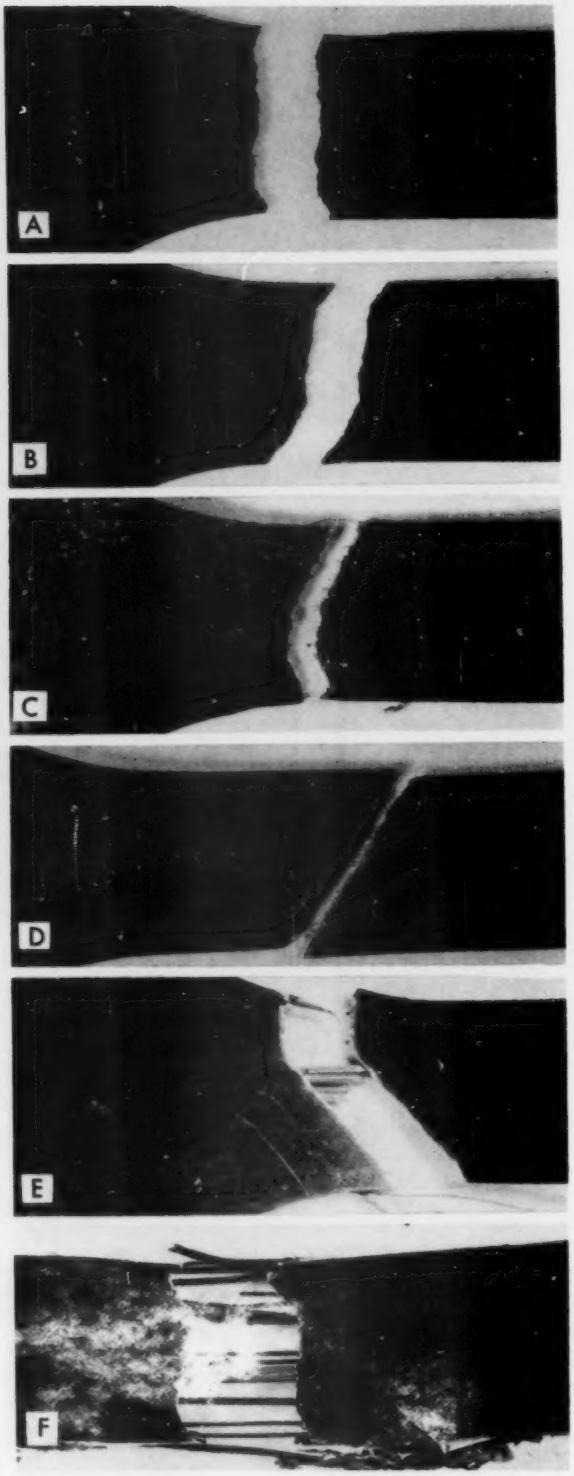

FIGURE 20. *Vapor-deposited copper specimens containing tungsten wires, after fracture.* × 5

(Data obtained on F not used in this investigation.)

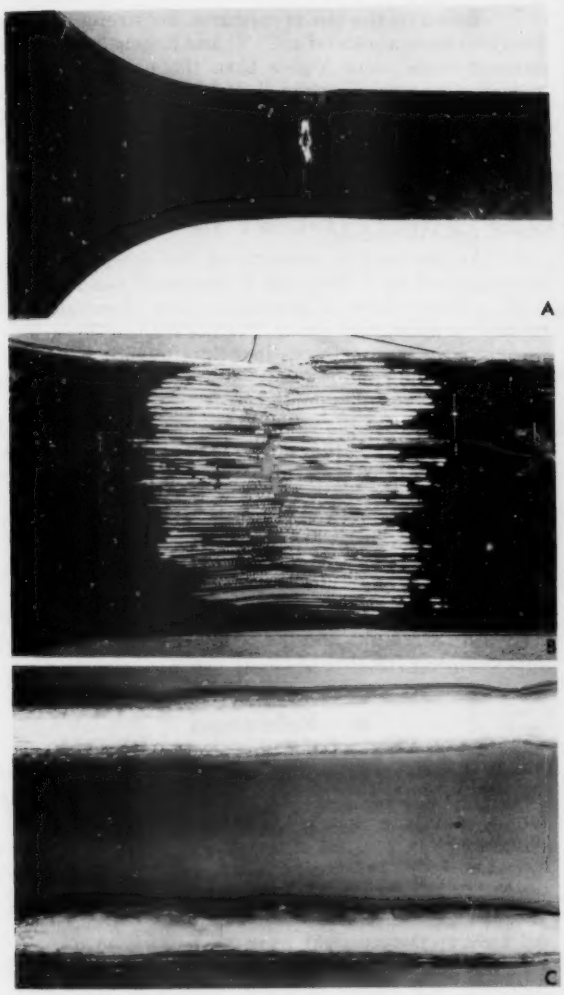

FIGURE 21. *Vapor-deposited copper specimen containing 9.5 volume percent tungsten wires.*

Test stopped before complete fracture.
A. Surface showing region of initiation of fracture. × 3.3
B. Same region as A, after dissolution of some of the copper by HNO_3 (conc.). × 6.6
C. A deformed and a fractured tungsten wire from area shown in B. × 330

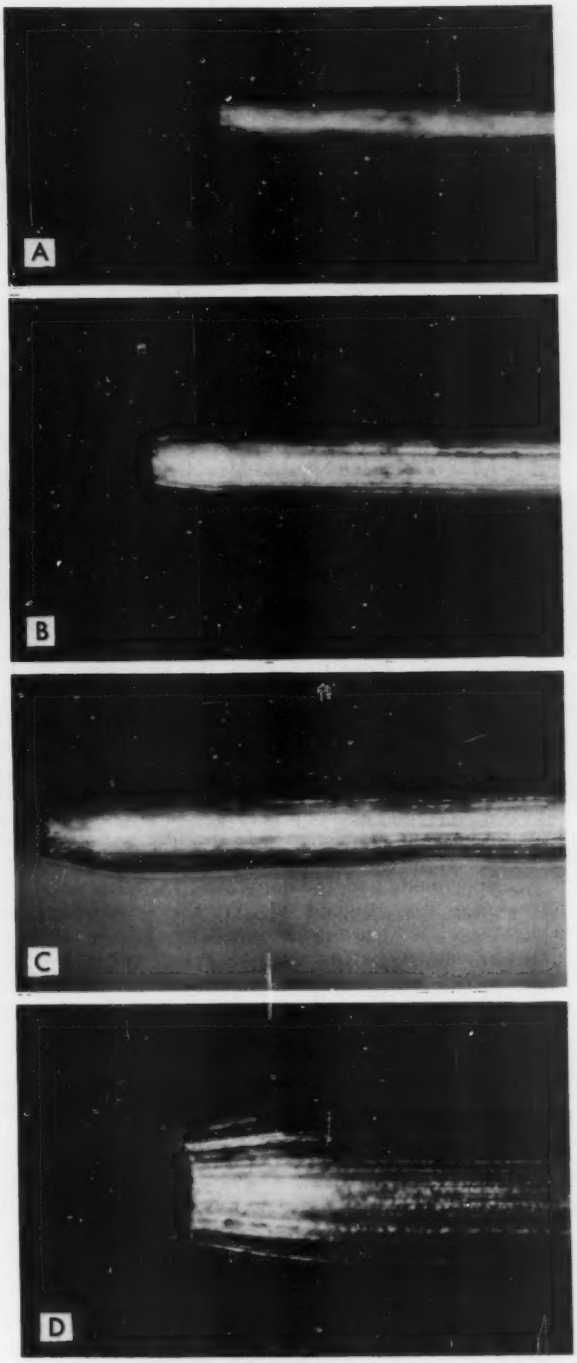

FIGURE 22. *Fractured tungsten wires from* Cu–W *composite specimens after complete fracture in tension.*

	Initial wire diameter, inch	Magnification
A	0.0005	× 500
B	.0005	× 1000
C	.001	× 500
D	.005	× 200

Fracture of most of the composite specimens was initiated away from the edges of the specimens as illustrated in figure 21A for a specimen for which the test was stopped after the attainment of maximum load and before complete rupture. After the copper was dissolved away by nitric acid, the tungsten wires were exposed in the region of the crack (fig. 21B). Some of the wires had ruptured and some had been deformed and remained intact. Although the fractures occurred after extensive localized deformation ("necking"), a number of necks occurred in regions away from complete fracture (fig. 21C). Figure 22 indicates that the mechanisms of deformation and fracture of the tungsten wires imbedded in the copper matrix were essentially the same for all sizes of the wires used in this investigation.

The authors are deeply grateful to Glenn W. Geil for his helpful discussions and to Mrs. Gertrude M. Davis for her assistance in the preparation of this manuscript.

5. Summary

1. Short-time tensile tests were made at room temperature on vapor-deposited copper specimens containing zero to 26 volume percent of continuous tungsten wires. Prior to testing, the specimens were annealed at 25, 300, or 600 °C.

2. A decrease in strength, due to an increase in annealing temperature, was generally accompanied by an increase in ductility.

3. An increase in strength was attributed to an increase in volume fraction of tungsten wires, decrease in wire diameter or decrease in the number of layers of wires.

4. Specimens having poorly alined wires tended to have lower strength and ductility than specimens in which the wires were alined.

5. Specimens having wires close together tended to have higher strength and lower ductility than those with wires more widely dispersed.

6. The shape of the stress-strain curves and the types of fractures obtained were influenced by all the variables considered.

7. Based on the law of mixtures the strength values for specimens annealed at 25 °C and having 2–3 volume percent wires were higher than the calculated theoretical strengths. For the 9–10 volume percent wire composites they were equal to the theoretically calculated values and for the 26 volume percent they were lower than the theoretical values.

8. Additional deviations from the law of mixtures were caused by annealing the specimens at 300 or 600 °C prior to testing.

9. An increase in strength of the composites was accompanied by a decrease in electrical conductivity.

10. Three types of fractures were observed: premature, tensile, and shear. Premature fractures were associated with specimens less ductile and shear fractures with specimens more ductile than those that fractured in a tensile manner.

11. Fracture of the vapor-deposited copper initiated near one edge of the specimen; whereas fracture initiated near the center portion of the composite specimens.

12. Tungsten wires in the composites failed after considerable necking of the wires.

13. The number of "necks" in the individual wires appeared to be a function of wire diameter.

14. The tungsten wires appeared to have a spread in fracture strengths and the composite failure resulted from complete fracture of all the wires.

6. References

[1] Kelly, A., and Davies, G. J., The principles of the fibre reinforcement of metals, Met. Rev. **10**, No. 37, 1–78 (1965).

[2] McDanels, D. L., Jeck, R. W., and Weeton, J. W., Stress-strain behavior of tungsten-fiber-reinforced copper composites, NASA TN D–1881 (1963).

[3] Weeton, J. W., and Signorelli, R. A., Fiber-metal-composite materials, NASA TN D–3530 (1966).

[4] Jeck, R. W., and Signorelli, R. A., The effect of interfiber distance and temperature on the critical aspect ratio in composites, NASA TN D–4548 (1968).

[5] Cooper, G. A., Electroformed composite materials, Journal of Matls. Sci. **2**, 409 (1967).

[6] McDanels, D. L., Electrical resistivity and conductivity of tungsten-fiber-reinforced copper composites, NASA TN D–3590 (1966).

(Paper 74C3&4–303)

JOURNAL OF RESEARCH of the National Bureau of Standards—C Engineering and Instrumentation
Vol. 74C, Nos. 3 and 4, July–December 1970

"Connector-Pair" Techniques for the Accurate Measurement of Two-Terminal Low-Value Capacitances

Aurel Millea [1]

Institute of Basic Standards, National Bureau of Standards, Boulder, Colorado 80302

(August 24, 1970)

A method is described that allows two-terminal capacitance measurements to be performed with uncertainties of $\pm 0.0001 - 0.0002$ pF, the ultimate accuracy limit being imposed only by the repeatability performance of the connectors. This technique has been used for the calibration of coaxial capacitance standards and the measurement of the fringe capacitance of coaxial open-circuit terminations; other applications are also possible in the field of high-frequency coaxial measurements.

Key words: Capacitance measurement; coaxial adaptor; coaxial connector; fringe capacitance; standard capacitor; two-terminal capacitor.

1. Introduction

Two-terminal capacitance standards of relatively low nominal value (beginning with 1 pF), equipped with coaxial connectors, are often used in high frequency measurements. Such capacitors are currently manufactured as working standards for calibrating impedance bridges. Coaxial precision capacitors are the most suitable reference standards for a general system of high frequency immittance calibration [1].[2] There is therefore an increasing need for accurate calibration of these capacitance standards.

Generally, precision standard capacitors intended for high frequency operation are calibrated at a low frequency and a frequency dependent correction is separately evaluated for taking into account the effect of the residual inductance [2]. Thus, the final accuracy of the capacitor calibration is to a great extent (and sometimes almost entirely) determined by the accuracy of the low frequency measurement. The main difficulty in this measurement is to establish a precise reference plane separating the capacitor from the measuring circuit. This plane must be mechanically identifiable and precisely reproducible; the capacitance measurement will be repeatable only in this case, avoiding the "connection errors." The best presently known way to meet these requirements is to equip both the capacitor and the measuring instrument with precision coaxial connectors [3].

It is generally accepted that the effective capacitance of a standard two-terminal capacitor is the capacitance added to the measuring circuit when the capacitor is connected to the terminals of the instrument (usually a bridge). It must be assumed that before connecting the capacitor, the instrument terminals were in a conventionally adopted "reference state," for example in open-circuit, with a special open-circuit termination or in a hypothetical radial-field (TEM-field) configuration. The latter convention is to be preferred, since it gives a definition of the capacitance independent of the bridge terminals. The capacitance is defined assuming (a) a radial field in the vicinity of the connector reference plane and (b) the capacitor electrodes limited by the connector reference plane. In principle, this definition gives a precise meaning to the two-terminal capacitance concept, making it independent of the instrument used for its measurement. Two techniques have been developed for the measurement of two-terminal capacitance, in accordance with this definition:

(a) The measurement is performed in two steps, first balancing the bridge with terminals open-circuited and then rebalancing with the capacitor connected. The result is:

$$C_x = \Delta C_m + C_f$$

where ΔC_m is the difference between the two readings on the bridge and C_f is the fringe capacitance of the open-circuit connector [4]. Special techniques are required to determine the value of C_f with a satisfactory accuracy.

(b) A three-terminal to two-terminal adaptor, equipped with a suitable output connector, is inserted between a three-terminal bridge and the capacitor.

[1] The author is permanently with the Institute of Metrology, Bucharest, Romania.
[2] Figures in brackets indicate the literature references at the end of this paper.

403-833 O - 70 - 4

The capacitance to be determined is:

$$C_x = C_m - C_{ad}$$

where C_m is the measured total direct capacitance and C_{ad} is the direct capacitance of the adaptor. This method has been developed at the National Bureau of Standards [2]; the adaptor is of a coaxial guard-electrode type, and C_{ad} was calculated in terms of the dimensions of the active section.

Both methods have the disadvantage that their accuracy depends directly on the accuracy with which the values of C_f and C_{ad} respectively are known. Experience has shown that good quality connectors allow a very good repeatability to be achieved; nonrepeatability errors are typically one order of magnitude smaller than the uncertainty of C_f and C_{ad}. Therefore, existing techniques are limited to an accuracy considerably lower than the precision attainable in two-terminal capacitance measurements by using precision coaxial connectors.

The "connector-pair" techniques described here require no corrections to be made nor any fringe capacitances or adaptor capacitances to be known. Two coaxial cables are used, each terminated with a precision connector of the same type as the capacitor to be measured. The capacitance is measured successively with each of these cables. The unknown capacitances of the cable and connector are then eliminated by connecting both cables to the bridge and making an additional measurement with the cable connectors coupled together. To avoid errors due to capacitance changes when cables are curved, a three-terminal bridge is used and the cable outer conductors are connected to the ground terminal of the bridge. Simple, non-precision two-terminal to three-terminal adaptors are introduced to connect the capacitor to the coaxial cables.

Thus, the measuring circuit contains only connector pairs; in each measurement, two of the three connectors involved are coupled together, in all possible combinations. Obviously, an essential condition for this is the sexless character of connectors.

The same principle can be applied in other measurements encountered in high frequency coaxial measurements: for example, determination of the direct capacitance of precision three-terminal to two-terminal adaptors, fringe capacitance measurements of precision coaxial connectors and measurement of the capacitance of precision coaxial lines.

2. Two-Terminal Capacitance Measurement

The measuring arrangement is shown in figure 1.

The capacitor, whose capacitance C_x is to be measured, is connected to the output of a three-terminal to two-terminal adaptor. This adaptor has been simply improvised by combining two NBS-Woods type coaxial connectors [5] with a thin dielectric sheet introduced between the outer conductor flanges.[3] A precision transformer-arm bridge is used, in three-terminal connection. Therefore, the measured capacitance is composed of C_x and the direct capacitance of the adaptors, C_A and C_B respectively.

The measurement procedure is as follows:

(a) The first adaptor with its cable and the capacitor C_x are connected to the bridge terminals (fig. 1a); the capacitance measured by the bridge is

$$C_1 = C_A + C_x \quad (1)$$

(b) Introducing the second adaptor into the circuit (fig. 1b) the measured capacitance is

$$C_2 = C_B + C_x \quad (2)$$

(c) Finally, with both adaptors connected to the bridge and their output connectors coupled together (fig. 1c) one obtains

$$C_3 = C_A + C_B. \quad (3)$$

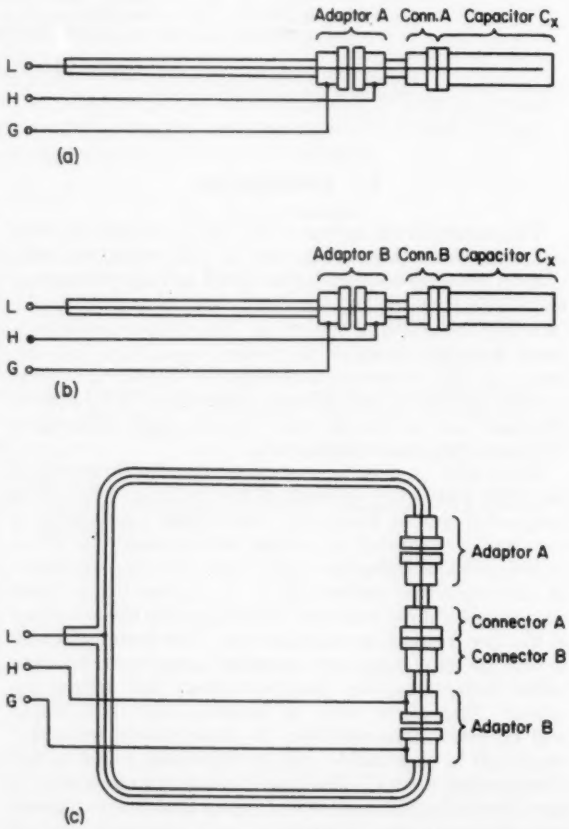

FIGURE 1. *"Connector-pair" technique for two-terminal capacitance measurement:* (a) *First adaptor with capacitor connected to the bridge;* (b) *Second adaptor with capacitor connected to the bridge;* (c) *Both adaptors connected, with connectors coupled together.*
L—"low"-terminal of the bridge (detector input); H—"high"-terminal of the bridge (transformer output); G—"ground"-terminal of the bridge.

[3] Any other types of such adaptors can be used, the only conditions being a rigid construction and good shielding.

Thus, from (1), (2) and (3):

$$C_x=\frac{1}{2}(C_1+C_2-C_3). \tag{4}$$

It is seen that the value of C_x is simply given by combining three measured capacitance values. In all cases there are only coupled connectors in the measuring circuit, thus assuring the required radial field conditions in the zone of the connector reference planes. In this way, the capacitor is connected in the normal manner and the radial field condition is achieved without using any extraneous devices.

The capacitance of five standard two-terminal capacitors, of nominal values ranging from 1 pF to 5 pF, was measured by this method. All capacitors and adaptors were equipped with 14 mm precision coaxial connectors. Each measurement was carried out at least ten times; generally, the repeatability was within ± 0.0001 pF and in a few cases within ± 0.0002 pF, except the 5 pF capacitor which exhibited a larger spread of the measured values.

Measurements were repeated using different adaptors (at least six adaptors in each case); no significant changes of the measured C_x values were noticed. However, care had to be taken to avoid imperfect coupling of connectors; in view of this, all measurements were repeated with connectors joined in two or three different positions.

For comparison, the capacitors were calibrated by using the three-terminal to two-terminal adaptor method [2]. In these measurements, the value of the direct capacitance of the NBS precision adaptor was taken as $C_{ad}=0.8528$ pF (see next section). Values determined by the two methods agree within the uncertainties of both methods.

The results are summarized in table 1. The "estimated measurement uncertainty" includes non-

TABLE 1. *Measured capacitance of two-terminal capacitance standards*

Nominal value pF	Measured value pF		Estimated measurement uncertainty pF
	By the method described	By the "adaptor" method	
1	1.0007	1.0007	±0.0001
2	2.0014	2.0013	±.0002
.....	2.6675	2.6675	±.0001
.....	2.6690	2.6691	±.0002
5	4.999	4.999	±.001

repeatability errors, systematic errors due to mechanical imperfections of individual connectors and errors introduced by the bridge. In most cases, errors caused by connector imperfections and bridge errors were negligible, so that the uncertainty figures given in table 1 practically coincide with the nonrepeatability values mentioned above; these figures represent an estimation based on computations of 3σ (three times the standard deviation).

3. Measurement of the Direct Capacitance of Precision Three-Terminal to Two-Terminal Adaptors

The same technique allows the direct capacitance of a three-terminal to two-terminal adaptor to be accurately measured. For this purpose, the adaptor is subjected to a measurement procedure similar to that previously described, together with two auxiliary three-terminal to two-terminal adaptors. Each adaptor pair is successively introduced in the circuit shown in figure 1c; the following equations are obtained:

$$C_1=C_{ad}+C'_{ad}; \tag{5}$$

$$C_2=C_{ad}+C''_{ad}; \tag{6}$$

$$C_3=C'_{ad}+C''_{ad}; \tag{7}$$

where: C_1, C_2, and C_3 are the measured capacitance values, C_{ad} is the direct capacitance of the adaptor to be measured and C'_{ad}, C''_{ad} are the direct capacitances of the auxiliary adaptors.

Equations (5), (6), and (7) give

$$C_{ad}=\frac{1}{2}(C_1+C_2-C_3). \tag{8}$$

One of the auxiliary adaptors may be replaced by a simple coaxial capacitor. In this case, the measurement is performed following step by step the procedure illustrated in figures 1a, 1b, and 1c.

More than two auxiliary adaptors may be also used, in all possible combinations, to obtain a number of equations exceeding the number of unknown quantities (for example, in the case of three auxiliary adaptors, 6 equations may be written for C_{ad}, C'_{ad}, C''_{ad}, and C'''_{ad}). The use of more than three auxiliary adaptors permits determination of the same adaptor capacitance by a number of different combinations and, thereby, reveals any systematic errors which may exist.

The direct capacitance of the NBS precision two-terminal to three-terminal coaxial adaptor [2] was determined by this method. Six auxiliary adaptors were used, in various combinations. As in the previously described measurements, the repeatability was within ±0.0001 pF; no significant systematic errors could be detected.

The value obtained is

$$C_{ad}=0.8528\pm0.0002 \text{ pF},$$

the estimated uncertainty including adaptor and connector instabilities.

The value previously determined by calculation, based on dimensional measurements, is

$$C_{ad}=0.8513 \text{ pF}.$$

4. Connector Fringe Capacitance Measurements

The fringe capacitance of precision coaxial connectors has an important role in both lumped and distributed parameter measurements. For certain configurations this fringe capacitance may be calculated. A high frequency method for measuring the fringe capacitance of precision coaxial connectors was described by Woods [4] and a low frequency one by Hersh [6]. The high frequency method consisted of measuring the difference of connector capacitances with open end and terminated by a precision quarter-wavelength short-circuited line. The low frequency method was based on three-terminal measurements with a guard electrode, an insulating gap being inserted in either the inner or the outer conductor of the coaxial connector. Both methods are rather cumbersome and of a limited accuracy, primarily because of certain perturbing effects that must be evaluated (for example, the "short-circuit" end of the $\lambda/4$ line, the insulating gap separating the guard electrode).

The "connector-pair" technique is particularly suitable for accurate fringe capacitance measurements, since the connector is under normal working conditions and no corrections or estimations are to be made.

Consider the measuring circuit shown in figure 2a, similar to that previously described. The measured capacitance is

$$C_1 = C_A + C_{fA} + C_B + C_{fB} \tag{9}$$

where C_A and C_B are the direct capacitances of the adaptors, and C_{fA} and C_{fB} are the fringe capacitances of connectors at adaptor outputs.

Now, if the connectors are coupled together, as in figure 2b, fringe capacitances disappear and the bridge measures

$$C_1' = C_A + C_B. \tag{10}$$

From (9) and (10) the sum of the fringe capacitances is

$$C_{dA} + C_{fB} = C_1 - C_1' = \Delta C_1. \tag{11}$$

Having three adaptors, with the same type of output connectors, these measurements can be performed three times, taking successively every possible combination of two connectors. The resulting equations

$$\begin{aligned} C_{fA} + C_{fB} &= \Delta C_1; \\ C_{fB} + C_{fC} &= \Delta C_2; \\ C_{fC} + C_{fA} &= \Delta C_3; \end{aligned} \tag{12}$$

give the following expressions for the fringe capacitances:

$$\begin{aligned} C_{fA} &= \frac{1}{2}(\Delta C_1 - \Delta C_2 + \Delta C_3); \\ C_{fB} &= \frac{1}{2}(\Delta C_1 + \Delta C_2 - \Delta C_3); \\ C_{fC} &= \frac{1}{2}(-\Delta C_1 + \Delta C_2 + \Delta C_3). \end{aligned} \tag{13}$$

Therefore, the fringe capacitance of any coaxial connector (only sexless) can be determined by connecting it to the output of a three-terminal to two-terminal adaptor and by using two other auxiliary adaptors to perform the three measurements described. More than two auxiliary adaptors may also be used, in all possible combinations, to obtain a redundant system of equations that reduces measurement uncertainties.

Table 2 shows the measured values of fringe capacitances on several 14 mm precision coaxial connectors.

The fringe capacitances were determined in two cases: connectors with a special open-circuit termination and without termination (open end). Larger uncertainties in open-end condition take account of noncontrollable influence of surrounding objects.

It may be seen that for each individual connector the value of the fringe capacitance is quite stable, the measurements giving repeatable results. However, there is a relatively large spread of the C_f values for different connectors of the same type. It is believed that the value of C_f depends primarily on the location

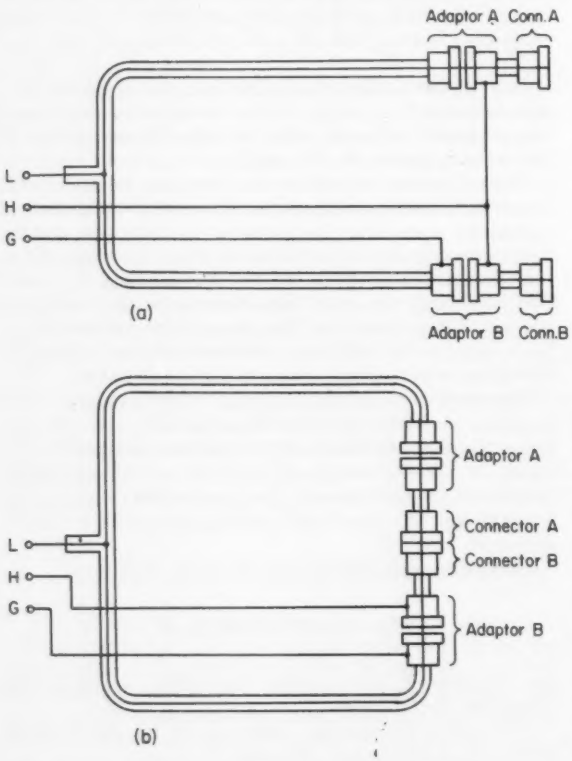

FIGURE 2. *Connector fringe capacitance measurement:* (a) *Connectors in open-circuit;* (b) *Connectors coupled together.*

TABLE 2. *Measured values of the fringe capacitance of 14 mm precision connectors*

Connector	With special open-end termination		Open-end	
	Fringe capacitance pF	Uncertainty pF	Fringe capacitance pF	Uncertainty pF
No. 2	0.1662	±0.0002	0.1484	±0.001
No. 5	.1672	±.0002	.1490	±.001
No. 9	.1625	±.0002	.1452	±.001
No. 10	.1696	±.0002	.1513	±.001
NBS adapt.	.1655	±.0002	.1480	±.001

of the center conductor top with respect to the reference plane. With different terminations, C_f values are practically unchanged (variations noticed were smaller than 0.0001 pF).

The measured values of C_f are generally lower than indicated in the literature [7] for this type of connector: 0.172 ± 0.008 pF with the special open-circuit termination and 0.155 ± 0.008 pF with open end.

5. Measurement of the Capacitance of Two-Port, Four-Port or Six-Port, Precision Coaxial Devices

The capacitance of two-port, four-port, or six-port coaxial devices such as precision coaxial lines, angles, ramifications, cubes, etc., can be also determined by this method. In every case, the capacitance is measured under rigorous radial field conditions for all ports of the device.

The total capacitance of a precision coaxial line may be measured by inserting the line between the coaxial connectors of two three-terminal to two-terminal adaptors. The line capacitance value is simply obtained by substracting the sum of the adaptor direct capacitances, measured with the adaptor connectors coupled together. This technique avoids errors due to inequalities of connector fringe capacitances, occuring in conventional methods based on open-circuit terminations.

The capacitance of a precision 50 Ω line of 10 cm length with 14 mm connectors at both ends was measured, using several pairs of adaptors in the measuring circuit. The value obtained was 6.6683 ± 0.0005 pF.

6. Some Remarks Concerning the Measurement of Small Capacitances With Two-Terminal Bridges

Most two-terminal bridges require an initial balance (or "zero adjustment") which is commonly performed with open terminals. As long as the measured capacitance value is relatively large or the accuracy required is low, the effect of the fringe capacitance of the bridge terminals is usually neglected, and the "initial balance capacitance" is conventionally taken as zero. In precision measurements of low-value capacitances, however, this effect can be important and the initial balance must be related to a precisely known capacitance value. The most simple possibilities are to use for the initial balance either an open-circuit termination or a standard low-value two-terminal capacitor.

As previously mentioned, fringe capacitance values of precision coaxial connectors vary within relatively wide limits (table 2). However, the capacitance of a standard coaxial capacitor is quite stable and free of connector errors. In other words, the capacitance added to the measuring circuit by an open-circuit termination depends upon the connector; even for the same type of connector, a spread of ± 0.01 pF may occur from one individual connector to another, while the capacitance added to the measuring circuit by a coaxial capacitor is practically independent of the bridge terminal connector. Consequently, it is better technique to use a small value standard capacitor for the initial balance of a two-terminal bridge (or, in general, a two-terminal capacitance measuring instrument) than an open-circuit termination.

For example, consider the case of a two-terminal bridge with a 14 mm precision connector. If a 1 pF standard capacitor is used, the initial balance can be performed in a simple way, with an accuracy of typically ± 0.001 pF or better. If an open-circuit termination were used instead, (a) the initial balance would correspond to a fractional capacitance value (equal to the fringe capacitance of the bridge terminal connector) and (b) this value would be variable from one bridge to another, typically between 0.16 pF and 0.17 pF.

When two-terminal capacitances are measured by a substitution method, connecting to the bridge the capacitor to be measured and then a standard capacitor of the same nominal value, the bridge serves only for determining the small difference between the two capacitance values. In this case there is no need for an additional initial bridge balance.

7. Conclusions

The "connector-pair" technique described offers a relatively simple way to increase the accuracy of two-terminal low-value capacitance measurements up to the limits imposed by the connectors themselves. The main application of this technique is in calibration of coaxial impedance standards. However, capacitance being one of the electrical quantities measurable with the highest accuracy, other applications are also possible, in the field of high frequency measurements, transducers, etc.

The author acknowledges the helpful suggestions of R. N. Jones, Circuit Standards Section, National Bureau of Standards, Boulder.

8. References

[1] Huntley, L. E., and Jones, R. N., Lumped parameter impedance measurements, Proc. IEEE **55**, No. 6, 900–911 (June 1967).

[2] Jones, R. N., and Huntley, L. E., A precision, high frequency calibration facility for coaxial capacitance standards, Nat. Bur. Stand. (U.S.), Tech. Note 386, 27 Pages (March 1970).

[3] Jones, R. N., and Huntley, L. E., Precision coaxial connectors in lumped parameter immitance measurements, IEEE Trans. on Instrumentation and Measurements **IM-15**, No. 4, 375–380 (Dec. 1966).

[4] Woods, D., A coaxial connector system for precision R.F. measuring instruments and standards, Proc. IEE (London) **108 B**, No. 38, 205–213 (March 1961).

[5] Woods, D., Admittance standardization and measurement in relation to coaxial systems, IRE Trans. on Instrumentation **I-9**, No. 3, 258–268 (Sept. 1960).

[6] Hersh, J. F., private communication.

[7] Orr, R. and Zorzy, J., More coaxial capacitance standards, General Radio Experimenter **42**, No. 5, 19–23 (May 1968).

(Paper 74C3&4-304)

JOURNAL OF RESEARCH of the National Bureau of Standards—C. Engineering and Instrumentation
Vol. 74C, Nos. 3 and 4, July–December 1970

The Use of Dew-Point Temperature in Humidity Calculations

Lawrence A. Wood

Institute for Materials Research, National Bureau of Standards, Washington, D.C. 20234

(August 21, 1970)

The dew-point temperature has a number of desirable features as a means of expressing humidity. The Antoine Equation, $\log e_w = A - B(T+C)^{-1}$, where e_w is the partial pressure and T is the temperature of saturated aqueous vapor, represents the Goff-Gratch formulation quite well over the range of temperature from 0 to 140 °F. The pressure e_w, in inches of mercury, is obtained by taking the constants $A = 6.70282$, $B = 3150.515$ (°F)$^{-1}$ and $C = 391.0$ °F, calculated from values given by Dreisbach. It is shown that the dew-point DP is related to the relative humidity RH by the relation:

$$(DP+C)^{-1} = (T+C)^{-1} + B^{-1} \log (RH)^{-1}.$$

Lines of nearly constant positive slope represent constant relative humidity values on graphs of dew-point against temperature. The value of the slope decreases from unity for $RH = 100$ percent to about 0.76 for $RH = 10$ percent, corresponding to the linear equation

$$DP = [1 + 0.1471 \log (RH)^{-1}]^{-2}(T-70) + DP_{70} \text{ where } DP_{70} = [2169 + 319 \log (RH)^{-1}]^{-1} \times 10^6 - 391.$$

Psychrometric charts showing dew-point and dry-bulb temperature as coordinates with lines representing constant relative humidity and constant wet-bulb temperature (obtained from the Ferrel Equation) are extremely useful, since given values for any two of these four variables serve to locate a point, from which the values of the other two variables can be read directly.

Key words: Antoine Equation; dew point; humidity; hygrometry; psychrometric chart; relative humidity; vapor pressure of water; wet-bulb temperature.

1. Introduction

In calculations of the humidity of air containing moisture, the dew-point temperature has a number of desirable features as a means of expressing the absolute humidity. In many instances in which the temperature of the air is changed the dew point remains relatively constant. One illustration of this is the rise of temperature when cold outdoor air in winter is heated and brought indoors without humidification. The dew point remains relatively constant also during the normal daily rise and fall of temperature of outdoor air. In fact, the usual morning weather reports could provide a number which would be much less subject to change during the day if the value of dew point were to be reported in place of the relative humidity.

The present paper stresses the advantages of using dew point in expressing humidity, derives some applicable equations, and presents illustrative charts and tables to facilitate the operation.

The results given here should be useful for engineering purposes of measurement and control of humidity in the range above about 5 percent relative humidity at pressures near a normal atmosphere, where the requirements for precision at temperatures between 0 and 140 °F, do not exceed about 0.5 percent in relative humidity or a few tenths of a degree F in temperature. These requirements are intermediate between the approximate values sometimes used in rough calculations based on readings with hair hygrometers or similar instruments and the more precise values required in research in hygrometry.

The temperature range was chosen to include the complete range of uncontrolled variation of atmospheric temperature. When a reference temperature near normal room temperature is required, a value of 70 °F has been chosen, to be at the midpoint of the range.

2. Definitions and Tabulations of Values

The present paper makes use of the definitions adopted by the Conference of Directors, International Meteorological Organization, meeting in Washington in 1947, with the revised definition of relative humidity adopted by the International Joint Committee on Psychrometric Data, meeting in Philadelphia in 1950.

These are presented in detail in the Smithsonian Meteorological Tables, Sixth Edition 1951 [1].[1] The same definitions are accepted by the American Society of Heating, Refrigeration, and Air Conditioning Engineers (ASHRAE) and published in the ASHRAE Guide and Data Book [2].

An extensive study of the thermodynamic properties of moist air completed in 1945 and 1946 by Goff and Gratch [3, 4, 5] led to formulation of tables of consistent numerical values. These values have been accepted and promulgated by both the Directors of the International Meteorological Organization and the ASHRAE. They have been published in several handbooks [1, 2, 6].

The numerical values of vapor pressure used in the present work are those shown in Table 95 of the Smithsonian Meteorological Tables [1], which gives values of aqueous saturation vapor pressure at intervals of 0.1 °F at the standard atmospheric pressure of 29.921 inches of mercury (760.00 mm of mercury, 101,325 N m^{-1}).

Relative humidity *RH* is defined as the ratio of the mol-fraction of water vapor in a given volume of moist air to the mol-fraction of water vapor in the same volume of saturated moist air at the same temperature and pressure. For the ideal gas mixtures assumed here, this definition is equivalent to defining relative humidity as the ratio of the partial pressure e of water vapor in moist air to the partial saturation pressure of water vapor e_w at the temperature of the air [2]. The partial pressure of saturated water vapor is affected only slightly by the presence or absence of air [1]. At atmospheric pressure near room temperature the difference is of the order of 0.5 percent, and will be neglected in the present work.

Dew-point temperature is defined as the temperature at which the partial vapor pressure of water in moist air would be sufficient to saturate the air. In other words, the partial vapor pressure at the given temperature is equal to the partial saturation vapor pressure at the dew-point temperature.

[1] Figures in brackets indicate the literature references at the end of this paper.

3. Dew-Point and Relative Humidity

Let us consider first only three variables, limiting ourselves to standard atmospheric pressure and postponing for the present all discussion of wet-bulb temperatures. The variables are (dry-bulb) temperature, relative humidity, and dew point. In a search of the literature I could find no tables showing explicitly the dew point as a function of temperature and relative humidity, although small graphs with temperature in Celsius degrees have been given in the German literature [7]. Consequently table 1 has been drawn up in order to show the dew point for different temperatures at 10° intervals from 0 to 140 °F and for relative humidities at 10 percent intervals from 10 to 100 percent. Values of the saturation vapor pressure of water are shown in the second column of the table. They are taken from the Goff-Gratch formulation, as presented in the Smithsonian Meteorological Tables [1]. The units of pressure are inches of mercury, each equivalent to 3386.389 N/m^2.

Table 1 was prepared by calculating the vapor pressure as the product of the saturation vapor pressure e_w and the relative humidity *RH*. The dew point was then read to the nearest 0.1° from the Tables as the temperature at which this value of vapor pressure is equal to the saturation vapor pressure.

4. Antoine Equation for Vapor Pressure

Of the many empirical forms of equations for the pressure of the saturated vapor of a liquid [8] the one proposed by Antoine for water [9, 10] and later extended to other liquids [11] possesses a number of ad-

TABLE 1. *Saturated aqueous vapor pressure and dew point (°F)*

T	e_w	10%	20%	30%	40%	50%	60%	70%	80%	90%	100%
°F	*in Hg*										
0	0.04477	−44.2	−31.6	−24.1	−18.6	−14.2	−10.6	−7.5	−4.7	−2.2	0.0
10	.07080	−35.8	−23.1	−15.3	−9.5	−4.9	−1.1	+2.2	+5.1	+7.7	+10.0
20	.10960	−27.9	−14.6	−6.5	−0.4	+4.4	+8.4	11.8	14.8	17.5	20.0
30	.16631	−20.1	−6.2	+2.3	+8.6	13.6	17.8	21.4	24.6	27.4	30.0
40	.24767	−12.2	+2.2	11.1	17.6	22.9	27.3	31.0	34.3	37.3	40.0
50	.36240	−4.4	10.5	19.8	26.7	32.1	36.7	40.6	44.1	47.2	50.0
60	.52160	+3.3	18.8	28.5	35.6	41.3	46.1	50.2	53.8	57.1	60.0
70	.73916	11.0	27.1	37.2	44.6	50.5	55.5	59.8	63.6	66.9	70.0
80	1.0323	18.6	35.4	45.8	53.5	59.7	64.9	69.3	73.3	76.8	80.0
90	1.4219	26.2	43.6	54.4	62.4	68.9	74.2	78.9	83.0	86.7	90.0
100	1.9334	33.7	51.8	63.0	71.3	78.0	83.6	88.4	92.7	96.5	100.0
110	2.5968	41.2	59.9	71.5	80.2	87.1	92.9	98.0	102.4	106.4	110.0
120	3.4477	48.7	68.0	80.1	89.0	96.2	102.3	107.5	112.1	116.2	120.0
130	4.5274	56.1	76.0	88.5	97.8	105.3	111.6	117.0	121.8	126.1	130.0
140	5.8842	63.4	84.0	97.0	106.6	114.4	120.9	126.5	131.5	135.9	140.0

vantages [12]. Consequently it has been extensively used in recent years. It may be written

$$\log e_w = A - B(T+C)^{-1} \quad (1)$$

where e_w is the partial pressure and T the temperature of the saturated vapor, while A, B, and C are empirical constants.

When e_w is expressed in millimeters of mercury and T in degrees Celsius, the constants for water between 0 and 60 °C have been evaluated by Dreisbach [13a, 13b] as

$A = 8.10765$,
$B = 1750.286$, (deg C)$^{-1}$ and
$C = 235.0$ deg C.

When e_w is expressed in inches of mercury and T in degrees Fahrenheit the constants for water between 32 and 140 °C may be calculated from those just given. This calculation gives:

$A = 6.70282$,
$B = 3150.515$, (deg F)$^{-1}$ and
$C = 391.0$ deg F.

With these constants the Antoine Equation yields values of vapor pressure which, for our purposes, are in completely adequate agreement with those given in the Goff-Gratch tabulation [1, 2, 6]. The differences are less than about 0.00040 in of mercury for temperatures in the range 40 to 120 °F and less than about 0.00100 in of mercury in the ranges 0 to 40 °F and 120 to 140 °F.

If differences of this magnitude are not to be tolerated recourse must be had to equations of much greater complexity containing many more constants [1]. Computer programs have been developed to deal with this situation [14].

5. Dew Point and Relative Humidity

Since the dew point temperature DP and the relative humidity RH are defined in terms of vapor pressures, an equation involving them may be easily derived from eq (1). The vapor pressure at temperature T is $(RH)e_w$ and is equal to the saturation vapor pressure at the dew point temperature DP. Thus by applying eq (1) at the dew point temperature we obtain

$$\log (RH)e_w = A - B(DP+C)^{-1}. \quad (2)$$

Subtracting eq (2) from eq (1) we have:

$$\log (RH)^{-1} = B[(DP+C)^{-1} - (T+C)^{-1}]$$

$$(DP+C)^{-1} = (T+C)^{-1} + B^{-1} \log (RH)^{-1}. \quad (3)$$

This form of equation suggests a plot of $(DP+C)^{-1}$ against $(T+C)^{-1}$. When C is again taken as 391.0 °F. the lines obtained for constant relative humidity are straight and have unit slope, as predicted. From the intercepts a value of B^{-1} may be obtained.

In the present work, however, a nongraphical method has been employed to obtain B^{-1} with greater sensitivity. This involved calculating the difference of $(DP+C)^{-1}$ and $(T+C)^{-1}$ from the values of dew point as a function of temperature as given in table 1. The constant C was taken as 391.0 °F, as before. The average value of this difference for all temperatures from 0 to 140 °F for a given relative humidity was divided by $\log (RH)^{-1}$ to obtain B^{-1}.

No significant trends could be noted in this difference as a function of temperature or in the values of B^{-1} as a function of relative humidity. The mean value of B^{-1} obtained in this way was 318.6×10^{-6} (deg F)$^{-1}$. The reciprocal of the value of B in the Antoine Equation as given above by Dreisbach [13], is 317.4×10^{-6} (deg F)$^{-1}$. The agreement between these two independent values is highly satisfactory. In the remainder of this paper we shall take the value of B^{-1} as 319×10^{-6} (°F)$^{-1}$. Both the graph of eq (3) and the constancy of the individual values of B^{-1} confirm the validity of the equation in representing experimental values of dew point.

According to the present results, the values of the constants as given by Dreisbach for the range 32 to 140 °F appear to be valid also for the saturated vapor pressure of subcooled water in the range 0 to 32 °F.

When the dew point for a given relative humidity is plotted as a function of temperature it is found that the data can be represented by a family of almost linear curves. Figure 1 shows such a plot, where the points represent the data of table 1. The lines shown are straight lines with slopes decreasing from unity at $RH = 100\%$ to about 0.76 at $RH = 10\%$.

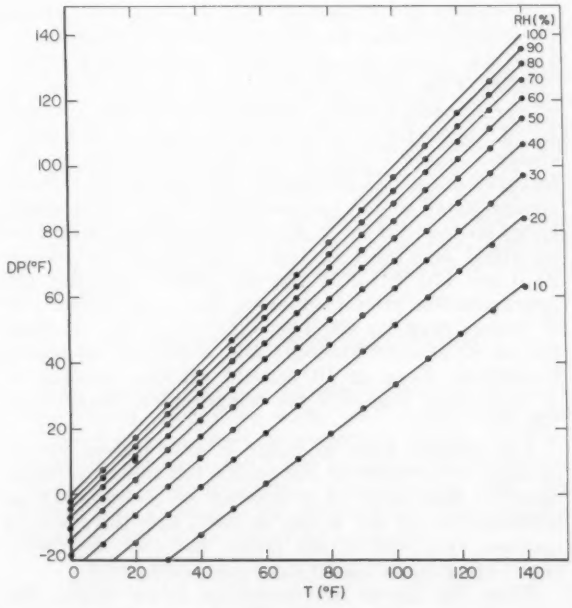

FIGURE 1. *Dew point* DP *as a function of temperature* T *at different values of relative humidity* RH.

403-833 O - 70 - 5

Numerical values of the slope may be calculated from an equation obtained by differentiation of eq (3). This is:

$$d(DP)/dT = [1 + B^{-1}(T+C) \log (RH)^{-1}]^{-2}. \quad (4)$$

When the numerical values just obtained for the constants B^{-1} and C are inserted it is found that the slope for the curve corresponding to 90 percent relative humidity should be about 0.986 at 70 °F. The slope is about 0.2 percent greater than this at 0 °F and about 0.2 percent less than this at 140 °F. The predicted slope of the curve corresponding to 10 percent relative humidity should be about 0.76 at 70 °F. It should be about 4 percent greater than this at 0 °F and about 4 percent less than this at 140 °F.

In view of this close approach to linearity of DP as a function of T at constant RH it is sometimes convenient to express the relation between dew point and temperature in strictly linear form involving DP_0, the dew point at some reference temperature T_0, and a constant slope equal to the slope at T_0.

$$DP = [1 + B^{-1}(T_0 + C) \log (RH)^{-1}]^{-2}[T - T_0] + DP_0 \quad (5a)$$

where

$$DP_0 = [(T_0 + C)^{-1} + B^{-1} \log (RH)^{-1}]^{-1} - C. \quad (5b)$$

For work near room temperature it is convenient to take the reference temperature $T_0 = 70$ °F. With the constants $C = 391.0$ °F and $B^{-1} = 319 \times 10^{-6}$ (deg F)$^{-1}$ these equations become:

$$DP = [1 + 0.1471 \log (RH)^{-1}]^{-2}[T - 70] + DP_{70} \quad (6a)$$

where

$$DP_{70} = [2169 + 319 \log (RH)^{-1}]^{-1} \times 10^6 - 391. \quad (6b)$$

It should be recognized that this equation, in explicit form to yield the dew point, is an approximation. Equation (3) on the other hand depends only on the validity of the Antoine form and the proper evaluation of its constants B and C. However, calculation of values by eq (6) over the range of temperatures and humidities shown in table 1 leads to the conclusion that the differences are not significant for the degree of precision contemplated in the present work. The largest differences are found at the highest and lowest temperatures, as would be expected, and at the lowest humidities. At 0 and 140 °F for 10 percent relative humidity the approximation yields values of dew point about 1 to 2° higher than eq (3). This difference falls to about 0.5° at 40 percent humidity and is still less at higher humidities. Even at 10 percent relative humidity it is no greater than 0.6° for temperatures from 30 to 130 °F.

The straight lines in figure 1 were drawn, not to conform necessarily to the points, but rather to represent the dew point as a function of temperature as predicted by eq (6). It can be seen that the lines do conform very well to the points and that the differences are approximately those just mentioned.

When the linear approximation is not made, the values predicted by eq (3) differ by only a few tenths of a degree from those given in table 1 and thus deviate only imperceptibly from the experimental points shown in figure 1.

6. Wet-Bulb Temperature Isotherms

The lowering of temperature of a thermometer surrounded by a wick from which water is evaporating is often used to measure humidity [15]. There are numerous possibilities for error and uncertainty, but the method gives useful results when the proper precautions are taken.

Humidity is calculated from readings of wet-bulb temperature by the use of the Ferrel Equation [1, 15, 16, 17]

$$e_T = e'_{wT'} - 367 \times 10^{-6}[1 + 0.00064(T' - 32)]p(T - T') \quad (7)$$

where e_T is the partial pressure of water vapor at the dry-bulb temperature T, $e'_{wT'}$ is the partial pressure of saturated water vapor at the wet-bulb temperature T' and p is the total pressure. The quantity e_T calculated by this equation is divided by e_{wT}, the saturation vapor pressure at temperature T to obtain the relative humodity RH. From this, the dew point may be calculated by the methods given in the preceding sections of this paper. The total atmospheric pressure p appears in the Ferrel Equation, and due regard must be paid to variations in it, in calculations of humidity by this method. As in the preceding sections, the value here will be assumed to be the standard atmosphere of 29.921 in of mercury.

On a chart with dew point as ordinate and dry bulb temperature as abscissa one can show a family of curves corresponding to constant wet-bulb temperature. In figure 2 these curves have been drawn at 10° intervals. The values shown are those calculated from eq (7) in the manner just described. It will be noted that the slopes are always negative and that their absolute value increases with increase of dry-bulb temperature or with decrease of wet-bulb temperature. Several of the constant humidity lines of figure 1 are also shown in figure 2.

Dew point values as calculated from the Ferrel Equation to the nearest degree only, are tabulated directly as a function of wet- and dry-bulb temperatures in tables issued by the Weather Bureau [17]. Although the results are based on saturated vapor pressure values antedating those of Goff and Gratch [3, 4, 5], the dew points tabulated agree, to the nearest degree, with those calculated in the manner just described for the range studied in the present work.

7. Psychrometric Charts

A psychrometric chart with dew point as ordinate and temperature as abscissa, like figure 1, is very useful in humidity calculations. If wet-bulb temperatures are required, it can show superposed, as in figure 2, both the family of curves for constant wet-bulb temperature with negative slopes and the family of lines of positive slope representing constant relative humidity.

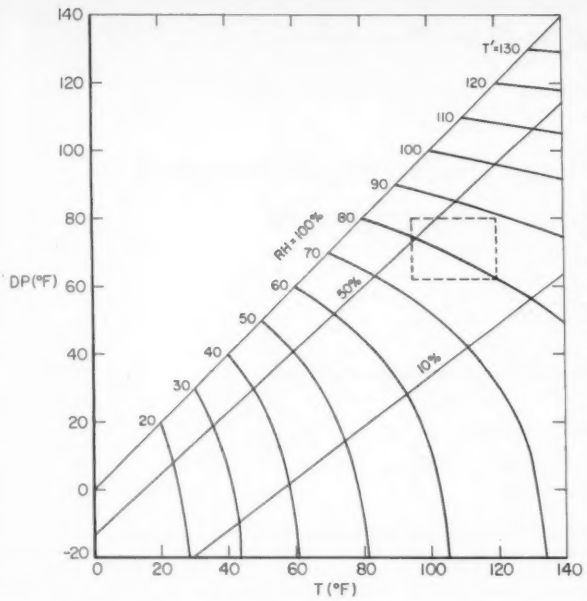

FIGURE 2. *Dew point* DP *as a function of temperature* T *at different values of wet-bulb temperature* T'.

The lines for relative humidities of 10 percent, 50 percent, and 100 percent from figure 1 are shown for comparison.
The rectangular box shows the range of values covered in figure 3.

The psychrometric charts usually available in the handbooks and other references [2, 6] are similar to these but show as ordinate the partial vapor pressure or the absolute humidity in mass per unit volume of dry air or the humidity ratio (also called mixing ratio) in mass per unit mass of dry air, rather than the dew point. In all these charts the graphs representing constant relative humidities are curves of constantly increasing slope, rather than the linear graphs shown in figures 1 and 2. Consequently, the calculation of the points, the drawing of the curves, and the visual interpolation are all considerably more difficult. However, the curves representing constant wet-bulb temperature are usually linear in contrast with those in figure 2.

As a measure of humidity the use of the dew point has another advantage over that of vapor pressure or mass per unit volume, since the conversion from British units to metric units involves only a change from temperatures in degrees Fahrenheit to temperatures in degrees Celsius. For example, figure 1 requires only a relabeling of the two coordinates in degrees Celsius to conform to the metric system; figures 2 and 3 require, in addition, only the conversion of the wet-bulb temperatures to degrees Celsius.

Our psychrometric chart shows four variables—dry bulb temperature and dew point as coordinates with relative humidity and wet-bulb temperature as lines. Given values for any two of the variables serve to define a point on the chart, from which the values of the other two variables may be read directly. Such a chart is simpler and easier to use than various nomograms which are available for humidity calculations [16].

In practical problems of humidity measurement and control the ranges of interest are usually much smaller than those shown in figures 1 and 2. Under such circumstances it is very convenient to use eqs (6) and (7) as a basis for drawing a grid consisting of lines of constant relative humidity and constant wet-bulb temperature on a psychrometric chart.

A typical example is shown in figure 3, which has been applied to the measurement and control of the humidity and temperature of the air surrounding a carbon arc. The relative humidity lines are drawn at intervals of 2 percent and the wet-bulb temperature curves at intervals of 1 °F on graph paper measuring 250 × 180 mm. Visual estimation of tenths of the intervals between curves makes possible interpolation of values to 0.2 percent relative humidity and 0.1 °F wet-bulb temperature. Each millimeter on the scales for coordinates represents tenths of degrees for dew point and dry bulb temperature.

In one application of the chart it was desired to find the wet-bulb temperature corresponding to 30 percent relative humidity at 117 °F. The chart showed the dew point to be 77.5 °F, and the corresponding wet-bulb temperature was then estimated as 87.0 °F by visual interpolation along a line through the dew point approximately normal to the two nearest wet-bulb isotherms.

In another typical application the wet-bulb temperature was observed to be 84.5 °F at a temperature of 110 °F. The dew point was then read from the chart as 76.0 °F and the relative humidity as 35.0 percent.

On another occasion it was desired to know how high the relative humidity could be at 115 °F without having condensation when the air was cooled to room temperature 77 °F. This was read from the chart as 31.4 percent, together with the corresponding wet-bulb temperature of 86.3 °F.

Finally, a fourth problem involved determining the temperature to which one must heat air with a dew point of 70 °F in order to reduce its relative humidity to 30 percent. The value was read to be 108.5 °F, with a corresponding wet-bulb temperature of 80.7 °F.

In all four problems the values of the desired qunatities were found by locating a single point on the chart, and the whole operation was completed in a much shorter time than when alternative methods were used.

8. Summary and Conclusions

The Antoine Equation has been shown to represent with good accuracy the values of the saturated vapor pressure of water over the range 0 to 140 °F, as formulated by Goff and Gratch and promulgated by meteorological and air-conditioning organizations. The dew point DP is related to the temperature T and relative humidity RH by the following equation:

$$(DP+C)^{-1}=(T+C)^{-1}+B^{-1}\log(RH)^{-1}$$

where B^{-1} and C, constants in the Antoine Equation, have the values 319×10^{-6} (°F)$^{-1}$ and 391 (°F) respectively. The dew point DP may also be calculated with

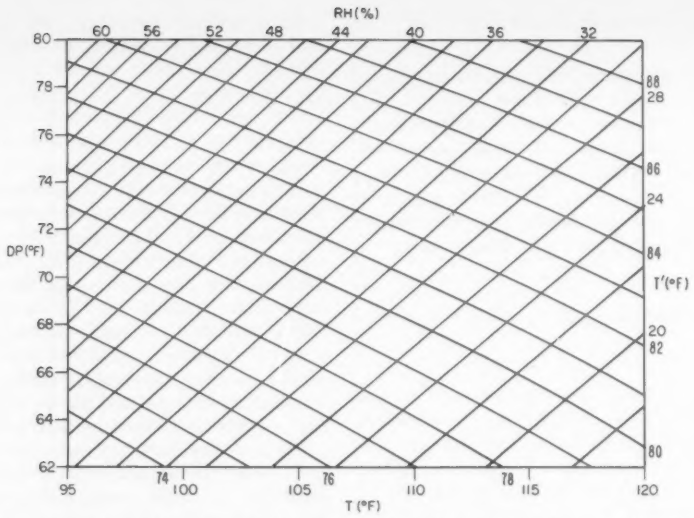

FIGURE 3. *Typical psychrometric chart of dew point* DP *and temperature* T *used in humidity calculations.*

The range of values covered is that of the rectangular box shown in figure 2.
Lines of positive slope correspond to constant relative humidity ($RH = 18$ to 60%).
Lines of negative slope correspond to constant wet-bulb temperature ($T' = 74$ to 88 °F).

satisfactory accuracy from the linear equation

$$DP = [1 + 0.1471 \log (RH)^{-1}]^{-2}(T - 70) + DP_{70}$$

where

$$DP_{70} = [2169 + 319 \log (RH)^{-1}]^{-1} \times 10^6 - 391.$$

It is convenient and useful to plot the dew point of moist air as a function of the temperature of the air. Points corresponding to constant relative humidity are well represented by lines of constant positive slope with the value of the slope decreasing from unity at 100 percent relative humidity to about 0.76 at 10 percent relative humidity. On the same chart showing dew point as ordinate and temperature as abscissa, points corresponding to constant wet-bulb temperature appear on lines of variable negative slope. The absolute value of this slope increases with increase of (dry-bulb) temperature and with decrease of wet-bulb temperature. Psychrometric charts showing dry-bulb temperature and dew point as coordinates with relative humidity and wet-bulb temperature as lines are extremely useful in humidity calculations, since given values for any two of these four variables serve to locate a point, from which the values of the other two variables can be read directly.

9. References

[1] List, Robert J., Smithsonian Meteorological Tables, 6th Revised Edition (Smithsonian Institution, Washington, D.C., 1951).

[2] ASHRAE Guide and Data Book, 1965–66, p. 29, American Society of Heating, Refrigerating and Air Conditioning Engineers, New York, 1965.

[3] Goff, J. A., and Gratch, S., Thermodynamic Properties of Moist Air, Am. Soc. Heating and Ventilating Engineers Trans. **51**, 125 (1945); Heating, Piping, and Air Conditioning ASHVE Journal **17**, 334 (1945).

[4] Goff, J. A., and Gratch, S., Low Pressure Properties of Water in the Range −160 to 212 °F, Am. Soc. Heating and Ventilating Engineers Trans. **52**, 95 (1946).

[5] Goff, John A., Chairman, Standardization of Thermodynamic Properties of Moist Air, Final Report of Working Subcommittee, International Joint Committee on Psychrometric Data, Am. Soc. Mech. Eng. Trans. **71**, 903 (1949); Am. Soc. Heating Ventilating Eng. Trans. **55**, 463 (1949).

[6] Perry, John H., Editor, Chemical Engineers Handbook, 3rd Edition, p. 760, McGraw Hill, New York, 1950.

[7] Lieneweg, F., Absolute und relative Feuchtbestimmungen mit den Lithiumchlorid Feuchtemesser, Siemens-Zeitschrift **29**, No. 5/6, 212 (1955). Reproduced in book, W. Lück Feuchtigkeit: Grundlagen, Messen, Regeln, P. Oldenbourg, Munich and Vienna, 1964; and also in book D. Sonntag Hygrometrie, Ein Handbauch der Feuchtigkeitsmessung, No. 6, p. 985 (Akademie-Verlag, Berlin, 1966).

[8] Partington, J. P., An Advanced Treatise on Physical Chemistry, Vol. **2**, p. 265 (Longmans, Green, and Co., London, 1951).

[9] Antoine, C., Vapor Pressures, New relation between pressures and temperatures, Comptes Rendus **107**, 681 (1888).

[10] Antoine, C., On the vapor pressure of water up to 200 atmospheres, Comptes Rendus **113**, 328 (1891); **116**, 870 (1893).

[11] Antoine, C., Calculation of pressures of various vapors, Comptes Rendus **107**, 778 and 836 (1888).

[12] Thomson, G. W., The Antoine Equation for vapor-pressure data, Chem. Rev. **38**, 1 (1946).

[13a] Dreisbach, R. R., Physical Properties of Chemical Compounds, Vol. III, p. 474, Advances in Chemistry Series No. 29, American Chemical Society, Washington, 1961.

[13b] Lange, N. A., Handbook of Chemistry, 10th Edition, p. 1438 (McGraw-Hill, New York, 1961).

[14] Kusuda, T., Algorithms for psychometric calculations of thermodynamic properties of moist air, Nat. Bur. Stand. (U.S.), BSS 21, 53 pages (Jan. 1970). U.S. Government Printing Office, Washington, D.C. 20402.

[15] Wexler, A., and Brombacher, W. G., Methods of Measuring Humidity and Testing Hygrometers, Nat. Bur. Stand. (U.S.), Circ. 512, 18 pages (1951).

[16] Bindon, H. H., A Critical Review of Tables and Charts Used in Psychrometry, Vol. **1**, p. 3 in Book Humidity and Moisture, Measurement and Control in Science and Industry, Arnold Wexler, Ed. (Reinhold, New York, 1964).

[17] Marvin, C. F., Psychrometric Tables for Obtaining Vapor Pressure, Relative Humidity, and Dew Point, U.S. Dept. of Commerce, Weather Bureau, U.S. Government Printing Office, Washington, D.C. (1941).

(Paper 74C3 & 4–305)

JOURNAL OF RESEARCH of the National Bureau of Standard—C Engineering and Instrumentation
Vol. 74C, Nos. 3 and 4, July to December 1970

Bolovac Application for HF and Microwave Power Measurement and Standardization

M. C. Selby*

Institute for Basic Standards, National Bureau of Standards,

Boulder, Colorado 80302

(August 25, 1970)

The bolometric voltage and current (BOLOVAC) standard for frequencies to 18 GHz and higher, recently developed at the National Bureau of Standards (NBS), can also be used to measure power, offering the following advantages over a number of other methods in use today:

(1) It eliminates:
- (a) the uncertainty resulting from neglecting termination mismatch
- (b) measurement of reflection coefficients and computations using complex equations
- (c) "Limits-of-error" charts, thus rendering definitive results
- (d) use of impedance charts
- (e) dc or af calibrations of power meters
- (f) need of corrections such as "effective efficiency" and "calibration factor."

(2) It covers a wide frequency range (0.5 MHz to 18 GHz or wider)

(3) It should result in substantial reduction of calibration time in many instances

(4) It can be applied to calibrate feed-through power measurement methods for power levels ranging into kilowatts.

In measuring power, the Bolovac (1) measures the voltage across a known resistance component of a given load, or (2) measures the voltage in any plane of a coaxial line of known characteristic impedance and known voltage distribution along the line, or (3) absorbs the rf power as any other absorption-type power mount does. In the first two cases resistance and voltage distribution measurements may be made separately or these measurements may be combined with the power measurement procedure. In the third case the rf power is absorbed in a special disk-type bolometric detector of the Bolovac and is equal to the dc- (or af) bias-power substituted in that detector; this bias power is measured with conventional power substitution bridges. Any appreciable unaccounted for power losses occur outside the Bolovac and can be determined employing conventional techniques as well as the Bolovac itself. The Bolovac needs no rf calibration. A Bolovac may have a power range of 20 dB or higher, depending on accuracy desired, and a maximum power approaching its safe power dissipation, e.g., 0.5 W or higher. This paper is limited to the application of the Bolovac to power measurements only and presents analytical and practical aspects of this application.

Key Words: Bolometric power standards; Bolovac power measurements; calibration of power meters; RF and microwave power measurements; standard of power through 18 GHz.

1. Introduction

The bolometric voltage and current (BOLOVAC) standard [1][1] was developed originally to furnish accurate hf and microwave voltages and currents. It was the first successful attempt to extend the direct measurement of these quantities well into the microwave range [18 GHz or higher]. This device turns out to be as useful for power measurement and standardization either as a feed-through or absorption type with apparent advantages over some of the widely used methods at present.

In measuring power, the Bolovac (1) measures the voltage across a known resistive component of a given load, or (2) measures the voltage in any plane of a coaxial line of known characteristic impedance and known voltage distribution along the line, or (3) absorbs the rf power as any other absorption-type power mount does. In the first two cases resistance and voltage distribution measurements may be made separately or these measurements may be combined with the power measurement procedure. In the third case

[1] Figures in brackets indicate the literature references at the end of this paper.

*Electromagnetics Division, National Bureau of Standards, Boulder, Colorado 80302.

the rf power is absorbed in a special disk-type bolometric detector of the Bolovac and is equal to the dc- (or af) bias-power substituted in that detector; this bias power is measure with conventional power substitution bridges. Any appreciable unaccounted for power losses occur outside the Bolovac and can be determined employing conventional techniques as well as the Bolovac itself. Perhaps the major contribution of the Bolovac is in that it resolves the difficulty introduced by the most serious source of uncertainty in power measurement, namely, the mismatch error [2, 3]. Directional couplers accomplish the same purpose but do so over a relatively narrow range of frequency for individual couplers. In addition, the directivity, the coupling factor and the side-arm power meters of each coupler must be calibrated. On the other hand, as will be seen below, the application of the Bolovac inherently eliminates the mismatch uncertainty, has a wide frequency range (e.g., 0.5 MHz to 18 GHz), and needs no rf calibration.

The application of known rf voltages to power measurements introduces a number of other advantages, namely, the elimination of:

(1) measurement of power-meter correction factors, e.g., effective efficiency and calibration factor,

(2) measurement of source and load complex reflection coefficients,

(3) computation involving complex formulas containing these reflection coefficients,

(4) using "limits-of-error" charts as an alternative to measuring phase angles of reflection coefficients and

(5) complex computations or the application of impedance charts in measuring load impedances.

Basically the Bolovac measures voltages at all the frequencies mentioned and makes the above advantages possible. A brief description of the Bolovac is given later in the text. However, because the advantages of its application are listed at the outset in this introduction, it seems appropriate to list also its present limitations.

The relative difficulties and disadvantages encountered to date at the National Bureau of Standards (NBS) in the construction and application of the Bolovac are briefly as follows.

(1) The voltage sensor of the Bolovac is a split bolometric thin-film disk. Such disks do not seem available commercially. The NBS so far has succeeded in developing a fabrication technique for disk values up to about 10 Ω; 50-Ω films were produced, but are not yet successfully assembled. These 50-Ω disks are particularly desirable.

(2) Impedance measurements are needed to determine the resistive components of the loads connected to the Bolovac (this is not needed when the Bolovac is used as an absorption-type power meter). However, the text below shows that these impedance measurements do not involve phase measurements and do not require complex computations, or the use of complex impedance charts.

(3) Attention must as usual be given to such common difficulties as reproducibility and losses of connectors, stub tuners or slotted lines; the Bolovac, however, may be employed to determine such losses.

(4) As in all other cases of bolometric measurements, the application of the Bolovac requires a resistance bridge and a precalibrated dc- or af-biasing power source. The use of thermoelectric or photoemissive sensors [1, 4] will still require dc calibration, so that, these applications are essentially equivalent to dc-power substitution calorimetry.

Considering the above advantages and limitations, the application of the Bolovac holds promise for radical improvements in coaxial power measurements.

This paper deals with the application of the Bolovac to power measurements. Additional papers are planned to deal in detail with its other applications.

The ultimate objective in measuring rf or microwave power is to determine the net power flow from a given source to a given load with maximum possible accuracy. When the load is an intermediary tool, (e.g., an uncalibrated power meter of any kind), toward that ultimate objective, the operation may be referred to as "calibration." Fairly sophisticated calibration techniques are used at the NBS. These require

(1) high-qualtiy, relatively expensive, calorimetric, substitution or other standards,

(2) considerable space,

(3) personnel with proper technical qualifications,

(4) intercomparisons between independent and quasi-independent methods, and

(5) considerable time [3].

A basic difference between these methods and the one employing the Bolovac, is that none of the present methods measures rf voltages at frequencies above about 10 MHz. Another basic difference is that the Bolovac, when used as a power absorption device, has no dc-for-rf power substitution error and has essentially all of the net rf power flowing to the Bolovac absorbed in its bolometric disk; thus only dc or af reference standards are needed to calibrate a power bridge employing a Bolovac as a mount. The major advantage in measuring power with the Bolovac, is the prospect of its application in facilites one or more calibration echelons removed from the NBS with little or no loss in the accuracy available at NBS. Two factors seem to make this possible:

(1) the previously mentioned elimination of complex reflection-coefficient measurements including associated relatively complex computations and

(2) elimination of accuracy degradation between calibration echelons.

Because the greatest uncertainties are introduced by the reflection coefficients (referred to as "mismatch errors") and because their elimination has been a major goal in past efforts to improve power measurements, these errors are discussed below at some length.

Calibration and measurement steps commonly used at present. The NBS calibrates at present two figures of merit for coaxial absorption type meters, namely:

$$\eta_e = \text{effective efficiency} = \frac{P_{\text{ind}}}{P_{\text{in}}} \quad (1)$$

K_c = calibration factor $= \dfrac{P_{ind}}{{}_fP} = \eta_e(1-|\Gamma_m|^2)$ (2)

where

P_{ind} = dial reading of the power meter which in many cases is the dc or af power substituted for rf power in the bolometers of a bolometric type meter.

P_n = net power absorbed by the meter
= incident power, ${}_fP$, minus reflected power, ${}_rP$.

Γ_m = complex reflection coefficient of the power meter.

Uncertainties of about ±1 to 2 percent for η_e and K_c [3, 7] are quoted by the NBS at frequencies to 18 GHz. Similar calibration terms are measured for feed-through type meters with the same uncertainties for frequencies to 4 GHz and ±2 to 3 percent for higher frequencies.

If a load with reflection coefficient, Γ_1, is substituted in a laboratory outside the NBS for a calibrated power meter having a reflection coefficient, Γ'_m, connected to a generator with reflection coefficient, Γ_g, the relationship between the net power absorbed by the standard meter, P'_n and that absorbed by the load, P_1, is [2, 3, 8].

$$P_1 = \frac{P'_{ind}}{\eta'_e}\left[\frac{1-|\Gamma_1|^2}{1-|\Gamma'_m|^2}\cdot\frac{|1-\Gamma_g\Gamma'_m|^2}{|1-\Gamma_g\Gamma_1|^2}\right]. \quad (3a)$$

Here P'_{ind} is the indicated power on the calibrated meter with effective efficiency, η'_e, and reflection coefficient Γ'_m. Of course the load, itself, can be another power meter.

Two special cases are of particular interest:

(a) when the load matches the characteristic impedance, Z_0, of the line, $\Gamma_1 = 0$, then the net power absorbed by the load, designated for this case as P_0, is given by

$$P_0 = \frac{P'_{ind}}{\eta'_e}\frac{|1-\Gamma_g\Gamma'_m|^2}{1-|\Gamma'_m|^2}. \quad (3b)$$

(b) When the load is a conjugate match of the generator impedance, $\Gamma_1 = \Gamma_g^*$, then the net power, designated for this case as P_c, is given by

$$P_c = P_0\frac{1}{(1-|\Gamma_g|^2)}. \quad (3c)$$

Examination of eqs (3) shows that both the magnitude and phase of the Γ'_g have a great effect on the accuracy of power measurements. It is not uncommon to have $|\Gamma|$ values as high as 0.2 to 0.5 (corresponding to VSWR, S, of 1.5 to 3) in the frequency range to 18 GHz. Their phases may vary from zero to ± 180°. It is relatively simple to measure the magnitude $|\Gamma|$ (or S) of a load but more troublesome to measure its phase angle. It is even more difficult to measure the magnitude and phase of Γ_g, particularly when it must be made under operating conditions of the generator. The present common practice is to measure only the magnitudes of the Γ'_g, to assume their phases to be zero, and to use eqs (3). The latter assumption introduces a serious uncertainty, sometimes referred to as "termination uncertainty." For example, when $|\Gamma_1| = 0.2$ and $|\Gamma_g| = 0.3$, the effect of neglecting their phases will introduce an error in P_n that could be as high as 25 percent. Values of these worst-case uncertainties for various combinations of $|\Gamma_1|$ and $|\Gamma_g|$ are given in various published charts and monographs; however, these values can not be used to correct a given value of P_n. Only measured phase angles of the Γ'_g could make this possible. Unfortunately such measurements are seldom, if ever, made [3], particularly in measurement facilities outside the NBS and other top level laboratories. The logical conclusion is to use power-measurement methods that do not require the measurement of the phases of Γ'_g. The Bolovac provides such a method. Moreover, the procedures available with the Bolovac make it possible to incorporate the measurement of the absolute magnitude of Γ_1 into a routine, relatively simple step of the power measurement procedure and, in addition, eliminate the need of measuring Γ_g altogether. This will be discussed further.

The degradation of accuracy as standard power meters are calibrated in a series of echelons starting with a top standardization laboratory and ending with the field of operation is also of major concern. A degradation of 2, 3, or 4 to 1 in accuracy is generally prescribed between echelons [8, 10]. Thus, for example, an uncertainty of 1 percent in the indication of a meter calibrated at the NBS may inflate into an uncertainty of 27 percent by the time it reaches the operational field through 3 intermediary calibration echelons [10], each having a degradation of 3:1. Use of the Bolovac (which does not require rf calibration) could eliminate this degradation of accuracy.

2. Basic Principles. Physical and Electrical Characteristics of the Bolovac

The Bolovac may be looked upon as an rf voltmeter measuring voltages in an orthogonal plane, (i.e., the only plane where voltages are defined) of a coaxial line operating in a TEM mode [1]. Transmission (including slotted) lines throughout this text are assumed to have negligible losses unless specified otherwise. Figure 1 shows the basic elements of the Bolovac connected through a transmission line to an rf source. These elements are (1) a bolometric thin-film disk orthogonally located in a coaxial assembly, (2) bias feed-through type terminals to connect this disk to a resistance bridge, (3) bias blocking capacitors built into the feed-through terminals, and (4) "input" and "output" connectors. The disk consists of a thin resistive annular film and electrodes connecting the film to the coaxial conductors. To prevent shorting the bias power, the outer conductor and the film of the disk are split along a diameter. The rf voltage, V_B, appearing across the thin film is determined con-

ventionally by the bridge measuring the reduction of biasing power dissipated in the bolometric thin-film disk located in that plane. The two halves of the disk are connected in series for dc and in parallel for rf. The rf resistance of the disk is equal to its dc resistance at all frequencies in question to 0.001 percent or better [1]. Thus, if the dc resistance of the disk is 200 Ω per side, its rf resistance is 50 Ω. Providing there is sufficient rf signal to permit adequate bridge balancing, correct voltages are measured regardless of the impedance presented to the disk by the generator and the load. In its use the Bolovac disk is located within 0.001 to 0.002 in of the input plane of a device under test.

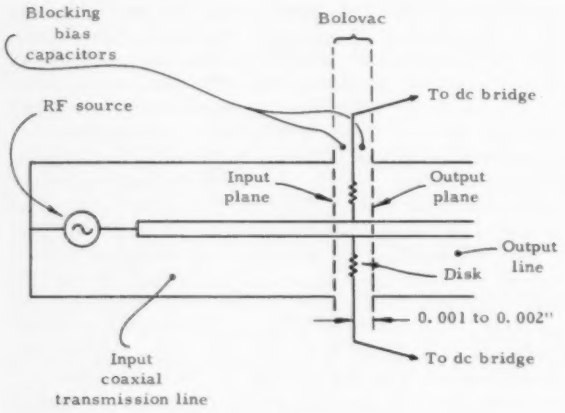

FIGURE 1. *Schematic diagram of Bolovac connected between input and output coaxial transmission lines.*

The application of the Bolovac, as a voltage measuring device, to power measurement may be described as follows. Figure 2 shows a schematic presentation of a power meter or load M having its input at plane m. The equivalent lumped circuit admittance, Y_p, to the right into plane m is shown as an equivalent resistance R_p shunted by a reactance X_p. The net power absorbed by the load is

$$P_n = V_B/R_p, \tag{4}$$

where V_B is the voltage measured by the Bolovac at plane m. If the line is lossless, the same V_B can be measured at any other plane $n\lambda/2 (n = \text{integer})$ away from plane m, e.g., plane A.

The value of R_p may be measured in various ways, e.g., with a slotted line of negligible loss as shown in figure 3, in which case it is given by

$$R_p = \frac{V_{max}}{V_{min}} Z_0 (V_m/V_{max})^2 = SZ_0 (V_m/V_{max})^2 \tag{5}$$

where

Z_0 = characteristic impedance of the slotted line
S = V_{max}/V_{min}
V_m = the voltage at plane m or at a plane in the slotted line $n\lambda/2$ away from plane m
V_{min} = is the voltage minimum in the line
V_{max} = is the voltage maximum in the line

The uncertainties in measuring R_p and P_n, including the effect of slotted-line losses, are discussed below under error analysis.

Equation (5) derived in appendix A shows that the computation of R_p does not involve complex values nor the aid of the Smith or other impedance charts. The accuracy of R_p depends on the accuracy of Z_0 and of two rf voltage ratios. The state-of-the-art of impedance and rf voltage-ratio measurements permits relatively high accuracies [7].

When the Bolovac is used with an equal arm bridge (see appendix B), the value of the voltage appearing across R_p is

$$V_B = 0.25 (V_0^2 - V_1^2)^{1/2} \tag{6a}$$

where V_0 and V_1 = dc-bias bridge voltages without and with rf respectively.

Appendix B gives other forms of eq (6).

Once R_p is known, the load is connected directly to the Bolovac and, combining eqs (4), (5), and (6a), the net power flow into the load is given in terms of

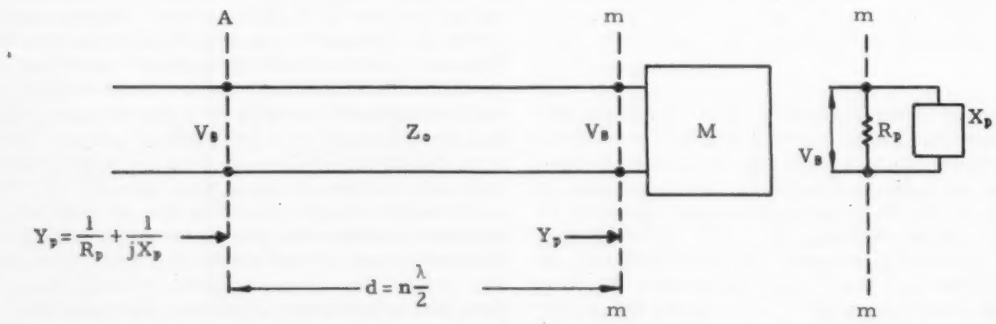

FIGURE 2. *Bolovac connected to a power meter or load, M, directly (at plane* m*) or through a lossless line (at plane* A*).*

Z_0, dc voltages, and ratios of rf voltages by

$$P_n=\frac{\left(V_B\frac{V_{max}}{V_m}\right)^2}{SZ_0}=\frac{1}{16SZ_0}\quad(V_0^2-V_1^2)(V_{max}/V_m)^2. \tag{7}$$

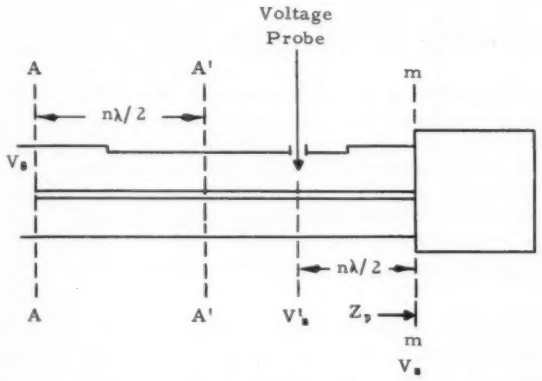

FIGURE 3. *Calibration of power meter with Bolovac and slotted line.*

Since a lossless line is assumed, a simpler computation may be used in one step, i.e., leaving the slotted-line between the Bolovac and the meter. In this case

$$P_n=\left(V_B'\frac{V_{max}}{V_B'}\right)^2/SZ_0 \tag{8}$$

where V_B'= the voltage in plane A', fig. 3, $n\lambda/2$ away from the Bolovac disk, assumed to be equal to V_B.

The Bolovac, its connector and the slotted lines are constructed to have the cross section of the line between A and A' uniform.

Again, V_B' in eq (8) may be replaced by its equivalent in (6a) when an equal arm bridge is used with the Bolovac.

Thus, the Bolovac permits the measurement of the net power absorbed by the meter under calibration without the necessity of measuring "substitution" power, complex reflection coefficients, η_e, and K_c.

If for any reason, e.g., to check manufacturers' specifications it is desired to find the incident power, η_e, and K_c, eqs (1) and (2) may be used, recalling that

$$_fP=\frac{P_n}{1-|\Gamma_m|^2}=\frac{P_n}{1-\left(\frac{S-1}{S+1}\right)^2}. \tag{9}$$

Because indicated or substituted bias power of the meter under test is not needed for its calibration by the Bolovac, one may dispose of the dc or af calibration of the power meter. However, this presently required calibration may be desirable for secondary purposes, e.g., for uniformity in production and repair of the indicating or "instrument" part of power meters without the bolometer mounts. The instruments are then interchangeable with the same mount. When the meter is calibrated in terms of substituted bias power, eq (1) may be used to find η_e.

It may be of interest to note that eq (8) can be used to determine the rf voltage in a given plane of a coaxial system in terms of known power absorbed by a load. For example, a calibrated power meter (or a Bolovac used as a power meter) placed as a termination of a feed-through type sampling oscilloscope yields the net power flow past the input plane to the oscilloscope. The voltage in this plane is V_B. The ratios S and V_{max}/V_B' are measured in a slotted line terminated by the above sampling oscilloscope-Bolovac combination. However, one must keep in mind several sources of possible errors, namely, (1) discontinuities in the slotted line between the input plane and the plane in the slotted line Where V_B' is located, (2) losses between the V_B' plane and the power meter and (3) the correction factor, if any, of the power meter.

Direct application of the Bolovac as a source of voltage eliminates these errors and reduces the measurement time from hours to minutes per frequency.

3. Applications

3.1. Measuring Net Power Flow in a Transmission Line With a Bolovac

In practice one is generally interested in measuring the power flow in a transmission line under one of the three following impedance matching conditions:

(1) Maximum power available from a source (when a conjugate match exists along the line). This power will be designated as P_c.

(2) Power flow when there are no standing waves in the line, (i.e., when the source looks into a load having an impedance equal to the characteristic impedance of the line). This power will be designated as P_0.

(3) Net power flow, P_n, under any matching conditions including the above.

Measurement of P_c and P_0 is usually of interest when one wishes to evaluate the power-delivery capabilities of a source. Measurement of P_n is generally desired when one wishes to know the net power absorbed by the load. The latter, as indicated above, may be a power meter under calibration.

To determine P_c or P_0 of an "unknown" source with the Bolovac, any power meter in series with a slotted line and a stub tuner is first used as a load. The input end of the slotted line is connected to the source, and the stub tuner is connected at the output end of the line. To measure P_c the stub is adjusted for maximum indication of the power meter. To measure P_0, the stub tuner is adjusted for flat voltage distribution along the line. In either case the source is replaced by a Bolovac. The level of V_B is adjusted to reproduce the respective meter reading. The value of V_B, S and V_B/V_{max} are measured and eq (7), or equivalent, yields the value of P_c or P_0.

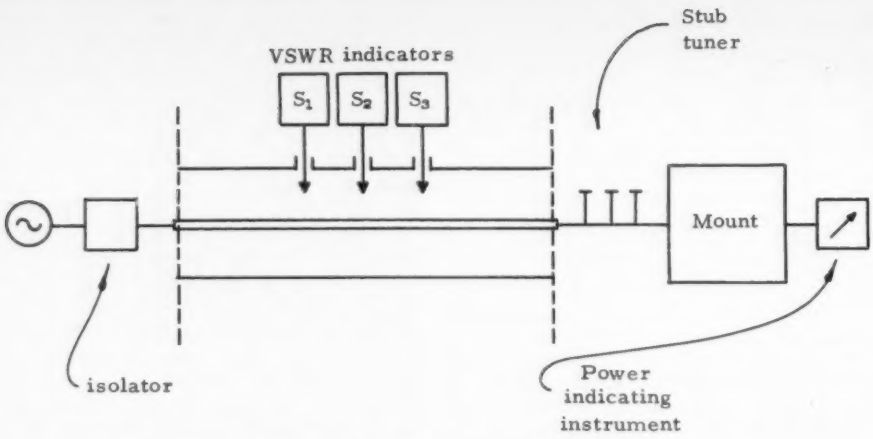

FIGURE 4. *Setup to obtain a Z_0-match of a power meter.*

A relatively simple procedure is suggested in appendix C to accomplish the Z_0-match adjustment of the stub without resorting to the hitherto employed "hit or miss" time-consuming and tedious procedure. The price to pay for this relief is the employment of three temporary probes in the slotted line as described in the appendix and illustrated in figure 4.

3.2. Monitoring Net-Power Flow in a Transmission Line

The net power, P_n, may be computed using (7), provided (1) one voltage, V_B, is measured with the Bolovac at any plane in the line and (2) the ratios S and V_{max}/V_B are measured. There are several ways to obtain V_B and the above ratios. For example:

(1) A slotted line section with a probe precalibrated with a Bolovac [5] may be permanently installed in the system. A multiple probe (MP) line-section, discussed later may be used instead.

(2) A Bolovac plus the slotted or MP line section may be permanently installed in the system. This eliminates the need of probe calibration. However, it is desirable to have a Bolovac with a value of $R \gg Z_0$ to reduce the loading effect of the Bolovac to a minimum. The availability on the market of high-resistance thin thermistor films seems to make this feasible.

3.3. Application of the Bolovac as a Load or as an Absorption Type Power Meter

The Bolovac may be used as an absorption-type power meter as illustrated in figure 5. For this purpose the Bolovac is turned end for end, so that its normally "output" side (fig 1) becomes its input side facing the generator end. A single sliding short is connected to the other (normally input) side of the Bolovac and is set for antiresonance at the specific frequency at which the measurement is made. It can be shown [11, 12, 13] that the antiresonant input impedance of a good quality 50-Ω 7 mm coaxial sliding short will be of the order of 10,000 Ω or higher at frequencies to 18 GHz. The input impedance of the Bolovac is then essentially one-fourth the equivalent dc resistance of the disk at any frequency under consideration here, for values of R_s of 50 Ω or lower.

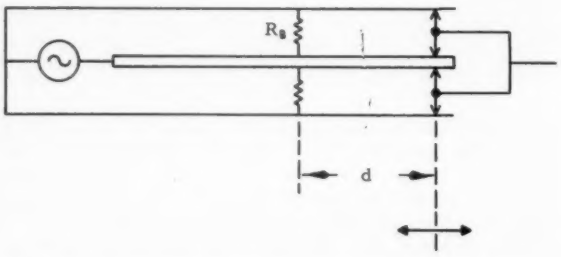

FIGURE 5. *Application of the Bolovac as an absorption-type power meter.*

Since η_e for the Bolovac is unity, the net absorbed power is given by

$$P_n = V_B^2/R_B' \doteq V_B^2/R_B = P_{dc}\,(\text{sub}) \qquad (10)$$

where P_{dc} (sub) = dc power substituted in the Bolovac and R_B' = equivalent disk rf resistance shunted by the admittance of the sliding short. One may connect the Bolovac in series with a three-stub tuner to a source, adjust the tuner for maximum V_B and find P_n. To find P_c the losses in the tuner are added to P_n. For the case of $R_B = Z_0$ one achieves a zero reflection-coefficient power meter for the antiresonant frequencies of the sliding short. Moreover such a Bolovac with the sliding short constitutes a Z_0-termination over its entire frequency range to an accuracy limited by structural perfection of the disk. With other R_B values the Bolovac makes available a standard mismatch which does not require rf calibration.

The antiresonant settings of the sliding short can be predetermined for a number of frequencies in order to obviate the necessity of making the adjust-

ment each time the frequency is changed. Several such shorts will cover a wide frequency range. The mechanical setting of the short is not critical because the antiresonant impedance curve is relatively flat around its maximum. A procedure to determine an antiresonant position is to first find two adjacent resonant positions at which V_B is minimum. The antiresonant position of the short is then located halfway between the two resonant positions. Once calibrated, the set of the sliding short is ready for use with any Bolovac at any time.

A power meter may be calibrated by substitution of a Bolovac operating in the power-absorption mode as illustrated in figure 5. This method seems particularly attractive because of its relative simplicity and because it does not need a slotted line. The procedure is as follows. The power meter is connected to a stable source in series with a three-stub tuner. The latter is adjusted for conjugate match, i.e., for maximum indication of the power meter. The meter is then replaced by the Bolovac and the stub tuner readjusted for maximum V_B of the Bolovac. Since the maximum available power, P_c, from the source is generally constant, the indicated meter power is equal to P_{dc} (sub). Because the input S value of the Bolovac might be quite different from that of the meter the tuner losses will not be the same and generally a small correction can be introduced for the difference.

It should be pointed out that the sliding short is not necessary for the measurement of P_n with the Bolovac used as an absorption power meter. However, in this case the input resistive component, R'_B, of the Bolovac (without the sliding short) has to be measured and computed with eq (5). P_n is then given by eq (4) substituting R'_B for R_p.

3.4. Application of the Bolovac for Feed-Through Power Measurement

It was pointed out above that the major source of uncertainty in present-day absorption (as opposed to feed-through) type power measurements is the mismatch error introduced by the terminal reflection coefficients in the transmission line. One method of eliminating this difficulty is to use directional couplers. Because the Bolovac, like directional couplers, eliminates the need of measuring Γ_g and Γ_l, its potential application for feed-through power measurement is briefly discussed here. It is assumed that the reader is familiar with directional couplers and will be in a position to assess the relative applicational merits of the couplers vis-a-vis the Bolovac.

A high resistance Bolovac, e.g., one with a disk resistance for example, 100 times Z_0, permanently placed in a transmission line, will continuously measure the voltage in a certain plane of the line. A probe in a slotted section of this line will furnish the voltage ratios required in eqs (7) and (8) to compute the net, incident, or reflected power flow in the line. With additional electronic instrumentation it may be possible to read these power components directly. Multiple-probe line sections may be used instead of slotted sections for fixed frequencies or limited frequency ranges. Application of MP lines for power and impedance measurements have been treated analytically in the past [14, 15, 16, 17, 18] and need not be discussed here.

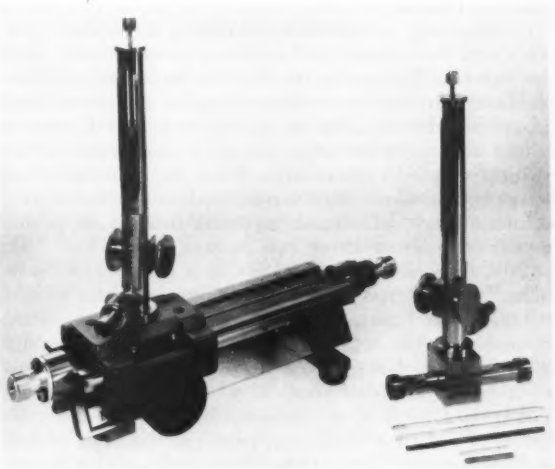

FIGURE 6. *NBS-built multiple-probe (MP) line (right) and commercial slotted line are shown.*

Commercial probes are used with both lines. Some of the self-supporting and end supported center conductors and connecting pins for the MP line are in the foreground.

Figure 6 shows an experimental NBS MP section in comparison with a commercial slotted line; the latter, though more expensive, has a range of 2 to 18 GHz as compared to two fixed frequencies (5 and 10 GHz) useable with the MP line with equal accuracy. The frequency limitation of an MP line is a result of the requirement that the fixed probes be an eighth of a wavelength apart. Figure 7 shows the equivalent schematic diagram of an MP line and appendix D gives equations of immediate interest in its application. An MP line may be built with a number of probe holes located so that the above spacing is attainable at several harmonic frequencies, such as 1, 2, 4, 8 and 3, 6 and 12 GHz. Thus approximately the same number of

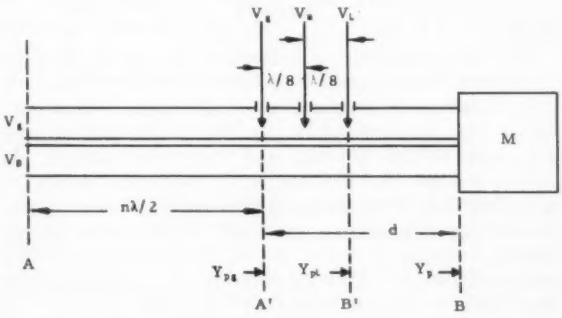

FIGURE 7. *Three-probe MP line for impedance and power measurements.*

calibration frequencies commonly furnished at present for commercial power meters may be obtained with one MP line.

While high-resistance disks are not yet available, low-resistance Bolovacs can be used in connection with feed-through power measurements in two ways:

(1) One way is to calibrate existing directional couplers and their associated side-arm power meters with the Bolovac. The power meters may be calibrated independently first with the Bolovac using the procedures described above. Coupling ratios may next be determined in a conventional manner employing one of the calibrated power meters to read the main-line net power and another meter to read the side arm net power. Bolovacs may, of course be used instead of power meters to measure these two powers.

(2) A second way is to calibrate a probe-type "voltmeter" in a slotted line or an MP line in terms of line voltage as a function of frequency. The procedure recommended in reference [5], can be used, where the known voltage is furnished by the Bolovac. The sinusoidal voltage distribution in a shorted slotted line section is used in that procedure to calibrate a "voltmeter." P_n is then computed from the readings of this probe-voltmeter. The dynamic linearity of this probe type voltmeter may also be checked versus the sinusoidal voltage distribution in the line. Coupling factors between P_n in the slotted line and the probe voltmeter of the order of 30 to 40 dB were obtained at the National Bureau of Standards at frequencies of 4 to 12 GHz with a normal probe penetration (of about 25% of interconductor spacing). The dynamic range depends on the range of the power meter used with the probe. Commercial meters are available with ranges of a microwatt to 100 mW or a range of 50 dB. This range may be further increased by employing attenuator pads in series with the probe power meter. An overlapping calibration range, with and without the pad, will assure range continuity. Thus voltage magnitudes and their ratios may be made available enabling the measurement of kilowatts of feed-through power during operation.

4. Error Analysis, Dynamic Range, Results

The error analysis of reference [1] shows that the total limit of uncertainty in the Bolovac voltages is ±0.1 percent at frequencies to 18 GHz. This uncertainty may be realized in any laboratory with a properly constructed Bolovac and associated bridge. As stated before, the Bolovac with its bridge needs no rf calibration. It is assumed that dc (or audio) voltage measuring capabilities required to measure bridge biasing voltages V_0 and V_1 for eq (7) with high accuracy are available, in which case the rf power absorbed by the Bolobac is as accurate as P_{dc} (sub).

In some applications of the Bolovac for power measurements additional sources of uncertainty are those contributed by (1) the slotted lines or MP lines needed to determine the resistive components of the load or of the rf-power-absorbing system and (2) the losses in auxiliary components such as the slotted lines, stub tuners, and connectors which are not a part of the specified load.

The limits of uncertainty in measuring resistive components of loads at the NBS are given in the references [7, 19]. For frequencies up to 18 GHz with 7 mm 50-Ω slotted line techniques and precision LPC–7 connectors the uncertainties are

$$\Delta S = 1.002 + 0.002f(\text{GHz}). \tag{11}$$

For mated configuration of latest improved type-N connectors these are

$$\Delta S = 1.004 + 0.004f(\text{GHz}). \tag{12}$$

The uncertainties at lower echelon laboratories may be found in reference [19]. These depend on many factors including the quality of the facilities and competence of personnel. For S values of 1.2 or less at frequencies to 8 GHz the uncertainty in R_p may be 1 percent or less. At 18 GHz it may be as high as 3 percent. For higher S values the uncertainty does not increase appreciably.

Power losses in stubs, slotted lines and connectors are of the order of 1 to 5 percent at frequencies to 18 GHz and can be determined with an uncertainty of 1 to 5 percent [7, 20].

As said before, component losses can be measured with the Bolovac or a precalibrated power meter. For example, the net power flow in a system may be measured with the Bolovac and the loss is given by the power drop of the power meter when the component is inserted between the slotted line and the meter. Or when the bolovac is used as an absorption power meter the maximum available (conjugately matched) power from a stable source is measured before and after the lossy component is inserted in the system. Allowances must be made for the effect of the magnitude of S on the losses of components, particularly of stub tuners. For this purpose two absorption-type Bolovacs having widely different values of R_s may be used with the same source of P_c.

The disk is the heart of the Bolovac. Though a number of commercial firms are making thin-film disk resistors, the NBS was to date not successful in locating a supplier of the needed disks having a sufficiently high temperature-coefficient of resistivity, and had to develop its own disks. A separate paper is planned to describe the in-house fabrication of the disks. Briefly the characteristics of those realized to date are as follows:

Film material—platinum, gold and carbon
Electrodes —gold in most cases
Dimensions —as required for 50Ω, 7 mm coaxial line
Resistance of disk—0.2 to 10 Ω (0.4 to 20 Ω per side) gold units, a couple of 25-Ω platinum units, and a number of 50-Ω carbon units

Substrate —glass, quartz, or 2-mil high-temperature plastic

Power dissipation (continuous) in the assembly—
0.25 to 0.5 W. The maximum power dissipation is several times higher; however, the long-term resistance drift is greater as the power dissipation is increased. This drift does not interfere with the application of the Bolovac.

Incremental resistance (bolometric)—
approximately 1 to 5 Ω per watt

Dynamic range of individual disks—
approximately 10:1 in voltage (20 dB) for precisions of the order of 1 to 2 percent. Precision increases rapidly as the range is kept narrower. The voltage at the low end is limited by the bridge stability and ratio of rf power to total bias power. At the high end it is limited by the ratio of the fractional bias power required to restore balance.

Maximum accuracy with an equal arm bridge is realized when the rf power is 2/3 of the total power dissipated in the disk [21].

The range of power obtained so far in a 50-Ω system is approximately 200 microwatts to half a watt at first-order agreements with calorimetrically calibrated power meters of 0.5 to 5 percent at frequencies of 10 MHz to 18 GHz respectively. Efforts to optimize structural details, particularly of the disks, were limited. Voltages of 25 mV at 1 percent uncertainty [2] and of 300 mV at 0.1 percent were measured at 10 MHz with Bolovacs using two thermistors instead of the usual disk. Experimental evidence indicates that one can measure 0.1 V with low resistance (0.1 to 0.2Ω) disks with the same uncertainty. The advantages here are that the disks can be used to 18 GHz as against 1 GHz for the thermistors. Also the disks are much superior mechanically.

It can be shown that the effect of the antiresonant impedance of good sliding shorts shunting Bolovac disks of resistance values below 100 Ω is negligible. Since higher resistance Bolovacs will hardly be considered for use as absorption power meters, there is no need dwelling on this effect.

One may wind up the discussion of the error analysis by pointing out the major sources of uncertainties in associated equipment. These are residual VSWR of slotted and MP lines, and the limited reproducibility caused by connector contacts and variations in their discontinuities. As frequencies increase, this problem is aggravated. The next largest source is the instability of rf source outputs when relatively long-time intervals (1 to 3 min) are required to transfer an amplitude value from the Bolovac to a source like an rf micropotentiometer, particularly when accuracies better than 0.5 percent are needed. In the latter case it may be best to reduce the time element by coaxial switching.

There are numerous commercial bridges presently used with bolometric power mounts. These can be used or adapted for use with Bolovacs. A high-precision miniaturized bridge recently developed at the NBS may be of interest for this purpose. [22]

[2] The uncertainty consists of a limit of systematic errors of 0.5 percent and a one-sigma-value of 0.5 percent for random errors.

5. Conclusion

The application of the Bolovac to standardize power meters and to measure power transmitted in TEM coaxial lines introduces a superior technique for all echelons of calibration and measurement. One of its major advantages is the elimination of the error contributed by impedance mismatch at the source and load ends of the transmission line. The work at the NBS so far was limited to 7 mm—50-Ω coaxial lines and frequencies to 18 GHz. Mechanical precision of 14 mm—50-Ω Bolovac disks (for frequencies to 9 GHz) should be higher than that of the 7 mm units. On the other hand 3.5 mm disks (for frequencies to 36 GHz) will probably be inferior by comparison. However, the application of the Bolovac to 36 GHz appears feasible and desirable. One must not lose sight of the fact that the same Bolovac makes it possible to apply known voltages for experimental and practical treatment of problems other than power measurement at microwave frequencies [4, 5, 6]. For example, the Bolovac was recently used to measure deflection amplitude versus frequency of an oscilloscope to 18 GHz for the first time in terms of voltage directly, instead of indirectly in terms of the time consuming and laborious method of measuring power and impedance.

Appreciation is hereby expressed to C. M. Allred and C. C. Cook for a constructive review of the paper, to P. E. Werner for his efforts in disk fabrication development, and to W. J. Blank and R. P. Chariton for performing countless painstaking observations and measurements.

6. Appendix A. Net Power Flow in a Transmission Line is $(V_{max}V_{min})/Z_0$ (ref. 11, p. 564)

Net power flow through plane m, figure 3, is then

$$P_n=\frac{V_m^2}{R_p}=\frac{V_{max}V_{min}}{Z_0}=\frac{V_{max}^2}{SZ_0}=\frac{1}{SZ_0}\left(V_m\frac{V_{max}}{V_m}\right)^2$$

$$=V_m^2\frac{1}{SZ_0}\left(\frac{V_{max}}{V_m}\right)^2\therefore R_p=SZ_0\left(\frac{V_m}{V_{max}}\right)^2 \qquad (5)$$

where

V_m = rf voltage in plane m

V_{max} = voltage maximum in a lossless coaxial line feeding power to the load M.

R_p = reciprocal of the equivalent conductance of the load M at plane m.

7. Appendix B. Rf Voltage Measured by Bolovac

In case of an equal-arm bridge the biasing power dissipated in the bolometer arm is

$$P_0 = (\tfrac{1}{2}V_0)^2/R_m$$

where

V_0 = initial biasing voltage applied to the bridge at balance
R_m = bias resistance of the Bolovac.

When rf is applied to the bolometer arm and the biasing voltage is reduced to rebalance the bridge

$$P_1 = (\tfrac{1}{2}V_1)^2/R_m$$

where P_1 = biasing power after rf is applied.

The rf power dissipated in the bolometer arm is

$$(P_0 - P_1) = P_{rf} = \frac{1}{4R_m}(V_0^2 - V_1^2) = V_{rf}^2/R_{rf}.$$

Let R_{T1} and R_{T2} be the resistance of the two halves of the disk respectively and let

$\alpha = \dfrac{R_{T1}}{R_{T2}} \geq 1$; then for $\alpha = 1$, R_{rf} of the disk $= \dfrac{1}{4} R_m$ and

$$4V_{rf}^2 = \tfrac{1}{4}(V_0^2 - V_1^2)$$

$$\therefore V_B = V_{rf} = 0.25\,(V_0^2 - V_1^2)^{1/2}. \qquad (6a)$$

One may read voltages directly across the Bolovac instead of across the bridge (employing a relatively high input-resistance dc voltmeter, e.g., a presently available four or five digit voltmeter). In this case for any bridge, let

V_{B0} = bias voltage drop across the Bolovac without rf
V_{B1} = bias voltage drop across the Bolovac with rf
$\Delta V_{B0} = V_{B0} - V_{B1}$

$$P_{rf} = P_{B0} - P_{B1} = \frac{1}{R_m}\,[2V_{B0}\Delta V_{B0} - (\Delta V_{B0})^2]$$

and for $\alpha = 1$, $P_{rf} = \dfrac{4V_{rf}^2}{R_m}$

$$V_{rf} = \tfrac{1}{2}[2V_{B0}\Delta V_{B0} - (\Delta V_{B0})^2]^{1/2}. \qquad (6b)$$

For relatively large values of $V_{B0}/\Delta V_{B0}$, (say 5000:1),

$$V_{rf} \doteq \tfrac{1}{2}(2V_{B0}\Delta V_{B0})^{1/2} \qquad \text{(to 0.01\%)}.$$

For $\alpha > 1$, $R_{rf} = \dfrac{\alpha}{(1+\alpha)^2}\,(R_m)$ (6c)

and

$$V_{rf} = \frac{\alpha^{1/2}}{(1+\alpha)}\,[2V_{B0}\Delta V_{B0} - (\Delta V_{B0})^2]^{1/2} \qquad (6d)$$

or for large $V_{B0}/\Delta V_{B0}$

$$V_{rf} \doteq \frac{\alpha^{1/2}}{(1+\alpha)}\,(2V_{B0}\Delta V_{B0})^{1/2}. \qquad (6e)$$

8. Appendix C. Method of Adjusting the Uniformity of the Voltage Distribution in a Slotted Line for a Z_0-Match

1. The three probes (fig. 4) are located in succession at any one plane of the line. The gain of each associated VSWR(s) indicator is set to read the same as the others.

2. The three probes are then placed in the line spaced within a distance preferably of $\lambda/4$. In case of physical space limitations one or two of the probes may be moved a distance $\lambda/2$ from its originally intended position.

3. The stub tuner is adjusted for maximum output indication of the power meter, i.e., for a conjugate match. This procedure is useful because the generator impedances are reasonably close to Z_0 and thus a roughly approximate match is obtained.

4. The readings of the three S indicators are then equalized by readjusting the stubs. In our experience it has been found very helpful to watch the power meter indication as the stubs were readjusted for the Z_0 match in order to prevent abrupt large changes in its reading.

The procedure suggested above was performed at the National Bureau of Standards by inexperienced personnel in a small fraction of the time required by a single-probe procedure.

9. Appendix D. Measurement of Power With a Multiple-Probe Line

Referring to figure 7 [18]

$$Y_{pg} = G_{pg} + jB_{pg} = \frac{1}{R_{pg}} - j\,\frac{1}{x_{pg}} \qquad (13)$$

$$P_B = V_g^2 G_{pg} \qquad (14)$$

$$G_{pg} = \frac{V_L}{V_g}\frac{1}{Z_0}\left[1 - \frac{1}{4}\left(2\,\frac{V_m}{V_L}\frac{V_m}{V_g} - \frac{V_L}{V_g} - \frac{V_g}{V_L}\right)^2\right]^{1/2}, \qquad (15)$$

$$jB_{pg} = \frac{1}{jx_{pg}} = \frac{j}{2Z_0}\left(1 + \frac{V_L^2}{V_g^2} - \frac{2V_m^2}{V_L^2}\right) \qquad (16)$$

$$G_{pL} = \frac{V_g}{V_L}\frac{1}{Z_0}\left[1 - \left(\frac{V_L}{2V_g} - \frac{V_m}{V_L}\frac{V_m}{V_g} + \frac{V_g}{2V_L}\right)^2\right]^{1/2} \qquad (17)$$

$$jB_{pL} = \frac{1}{jx_{pL}} = \frac{j}{2Z_0}\left(1 + \frac{V_g^2}{V_L^2} - \frac{2V_m^2}{V_L^2}\right) \qquad (18)$$

where

V_g is the voltage in the plane of the probe next to the generator. When the Bolovac is used as shown in figure 3, $V_g = V_B$.

V_m and V_L are the voltages in the planes of the other two probes respectively.

The *pg* subscripts identify impedance and admittance components in the plane of the probe closest to the source.

The *pL* subscripts identify impedance and admittance components in the plane of the probe closest to the load M.

The above impedance equations are written in terms of voltage ratios to emphasize that only voltage ratio measurements are needed and are obtainable with greater accuracy than absolute voltages. The distance $B' - B$, figure 7, may be made equal to an integral number of half wavelengths to render G_{pL} equal to that at any chosen input plane of the load, M. The power absorbed by the load must of course be computed in terms of a known voltage and input conductance in one and the same plane, e.g., in plane A', figure 7.

10. References

[1] Selby, M. C., Bolometric voltage and current (Bolovac) standard for high and microwave frequencies, J. Res., Nat. Bur. Stand. (U.S.) (Eng. and Instr.), **72C**, No. 1 (Jan.–Mar. 1968).

[2] Beatty, R. W., Macpherson, A. C., Mismatch errors in microwave power measurements, Proc. IRE **41**, pp. 1112–1119 (Sept. 1953).

[3] Rumfelt A. Y., and Elwell, L. B., Radio Frequency Power Measurements, Proc. of IEEE **55**, No. 6, Survey and Extensive Bibliography, p. 837 (June 1967).

[4] Selby, M. C., Electrothermic instruments for measuring voltage or current, Patent No. 3,487,305; December 30, 1969.

[5] Selby, M. C., Voltage measurement at high and microwave frequencies in coaxial lines, Proc. of IEEE **55**, No. 6, 877–882 (June 1967).

[6] Beatty, R. W., A microwave engineer's point of view toward voltage measurements, private communication (June 1967).

[7] Beatty, R. W., Coaxial power impedance and attenuation calibration methods at NBS. The Microwave Journal **111**, 65–75 (May 1968).

[8] Microwave power measurement, Hewlett-Packard Application Note, No. 64, HP AN 64.

[9] Personal communication with personnel of NBS and other laboratories.

[10] Government specification affecting calibration laboratories, National Conference of Standards Laboratories, April 1969. Report by A. E. Hess, RF Calibration System Analysis Project, NBS Boulder, Colorado, Project No. NBS 2720482, January 21, 1969.

[11] Ryder, John D., Networks, lines and fields, Second Edition, 1959 (Prentice-Hall, Inc.), p. 343.

[12] International Telephone and Telegraph Corp., Reference data for radio engineers, Fourth Edition (1957), p. 574.

[13] NBS Monograph 96, Electrical parameters of precision coaxial, air-dielectric transmission lines, p. 14 (June 30, 1966).

[14] Sucher, M., and Fox, J., Handbook of microwave measurements, I (John Wiley & Sons, New York), p. 122ff.

[15] King, D. D., Measurements at centimeter wavelengths (Van Nostrand Series), pp. 197–199 (1952).

[16] Duffin, W. J., Three-probe method of impedance measurement, Wireless Engineer **29** (Dec. 1952), p. 317.

[17] Ginzton, E. L., Microwave measurements (McGraw-Hill Book Co., Inc., 1957), p. 236.

[18] An adaptation of the three-voltmeter method for measuring power and voltage at high frequencies, Electric and Musical Industries, Ltd., Hayes, Middlesex.

[19] IEEE Technical Committee Report on the State-of-the-Art of Measuring unbalanced transmission line impedances, R. L. Jesch, Chairman, June 3, 1970. (To be published.)

[20] Ragan, G. L., Microwave transmission circuits, R. L., Series No. 9 (McGraw-Hill Book Co., Inc., 1948), p. 150.

[21] Selby, M. C., Single-bolometer series-parallel circuit for accurate voltage and power measurement, Instrument Society of America, Preprint No. 21. 6–1–64, October 1964.

[22] Larsen, N. T., and Clague, S. R., The NBS type II power measuring system, to be presented at the ISA, 25th Annual Conference, October 26–29, 1970.

(Paper 74C3 & 4–306)

JOURNAL OF RESEARCH of the National Bureau of Standards—C Engineering and Instrumentation
Vol. 74C, Nos 3 and 4, July–December 1970

Publications of the National Bureau of Standards*

Selected Abstracts

Allan, D. W., Guetrot, A., Higbie, L. S., Lavanceau, J. D., **An application of statistical smoothing techniques on VLF signals for comparison of time between USNO and NBS,** *Proc. 23d Frequency Control Symp., Atlantic City, N.J., May 6–8, 1969, p. 248 (1969).*

Key words: Effect of mass on frequency; flicker noise; NBS; noise correlation; NSS; optimum filter; phase noise; radio propagation; time comparison; USNO; VLF propagation; WWVL.

Recent developments have provided a method for obtaining submicrosecond time comparisons over continental distances. The method was applied to a time comparison between the master clocks at the United States Naval Observatory (USNO) and at the National Bureau of Standards (NBS) in Boulder, Colorado.

There were the following developments. First, if two signals show a reasonable degree of correlation in their fluctuations, then one may derive an optimum linear combination of the two with a mean square error less than for either signal individually. The two signals studied were the transmissions on 21.4 kHz from NSS in Annapolis, Maryland, and on 20.0 kHz from WWVL in Fort Collins, Colorado. It is necessary that receivers be located for both signals at the locations of the controling clocks. Existence of positive correlation was shown. The positive cross correlation probably was due to the near reciprocal path and the very close transmission frequencies.

Second, the phase fluctuations due to the propagation medium were consistent with a spectral density of the random phase noise proportional to $|f|^{-1}$, commonly called flicker of phase noise. This persisted for Fourier frequencies from one cycle per day down to one cycle per several weeks. The fluctuations on the linear combination of the two signals still behaved as flicker of phase noise but at a lower level.

The phase or time fluctuations of the master clocks however followed a spectral density law proportional to $|f|^{-3}$, flicker of frequency noise, for frequencies lower than one cycle per day.

Third, an optimum linear filter (Wiener filter) giving the minimum mean square error estimate (MMSEE) of the signal has been determined for a random walk of phase signal (spectral density proportional to $|f|^{-2}$) imbedded in white noise (spectral density proportional to $|f|^{0}$). The same filter was shown to be still optimum for spectral densities proportional to $|f|^{-3}$ for the signal and $|f|^{-1}$ for the noise.

Application of the above filter to the appropriate linear combination, defined through correlation properties, of NSS and WWVL signals showed an improvement of 15 dB in the rms day-to-day phase fluctuations. The day-to-day rms time deviations were about 70 ns on the final results. The output estimate of the filter, compared with portable clock measurements, gave a disparity of the order of the final output noise.

The experiment provided an opportunity to determine if there is an effect of mass on frequency and within the uncertainties of the experiment a null result was obtained.

Alvarez, R., Paulsen, P. J., Kelleher, D. E., **Simultaneous determination of trace elements in platinum by isotope dilution and spark source mass spectrometry,** *Anal. Chem.* **41,** *No. 7, 955–958 (June 1969).*

Key words: Cation-exchange; electrodeposition; high-purity metal analysis; multi-element; spark source mass spectrometry; stable isotope dilution; trace determinations.

An isotope dilution technique using the spark source mass spectrograph was investigated for applicability to simultaneous, multi-element trace determinations. Isotopically altered Ag, Cu, Ni, Pb and Pd were separated from a 250-mg sample of platinum by cation exchange, and electrodeposited onto gold electrodes for sparking in the spectrograph. Electrodeposition provided the spiked analytes in an adherent form, relatively free of anions and organic residue from the ion exchange resin, both of which could complicate the spectrum. Contamination, the principal limitation of the method, was minimized by isothermally distilling the reagent acids and by isolating the operations from the laboratory environment. After determining the isotope ratios, the concentrations were computed, ranging from 0.5 ppm (μg/g) for Ni to 14 ppm for Pb. Improved precision and accuracy was obtained compared to conventional spark source analysis. The results were compared with those of other methods and the platinum material was issued by NBS as Standard Reference Material 681.

Bates, R. G., **Measurement of pH,** *Handbook of Biochemistry, H. A. Sober, ed., pp. J190–J194 (Chemical Rubber Company, Cleveland, Ohio, 1967).*

Key words: Acidity; glass electrode; indicators; pH; standardization.

The operational definition of pH, in the form endorsed by the International Union of Pure and Applied Chemistry, is presented. The preparation of standard reference solutions for pH measurements is described and the choice of electrodes and measurement techniques is discussed. The proper interpretation of pH numbers is set forth briefly, and procedures for pH measurement with indicators are described.

The revised version includes the addition of two new primary pH standards to tables 1 and 3, coefficients for calculating the temperature dependence of pH in table 2, and a collection of pH values for miscellaneous buffer solutions.

Beatty, R. W., **Coaxial power, impedance and attenuation calibration at the National Bureau of Standards,** *Microwave J.* **11,** *No. 5, 65–75 (May 1968).*

Key words: Attenuation; calibration; coaxial; impedance; microwave; power; standards.

NBS calibration methods are described for coaxial power, impedance, and attenuation at microwave frequencies. Present and future NBS capabilities in these areas are discussed. An indication is given of the state of the art, how NBS arrives at its quoted limits of error, and how it develops confidence in its reference standards. Details of some measurement procedures are given and a list of references is given for those who wish more information.

403-833 O - 70 - 6

Birmingham, B. W., Flynn, T. W., **Cryogenics in United States National Programs,** *Cryogenics* **9,** *No. 1, 3–10 (Feb. 1969).*

Key words: Agriculture; compressed gases; conservation; cryogenics; education; health; national goals; space; transportation.

The object is to discuss a segment of the compressed gas industry, namely the cryogenic industry, and its relation to selected national programs, such as space, health, agriculture, transportation, conservation, and education.

Bullis, W. M., **Measurement methods for the semiconductor device industry—a summary of NBS activity,** *Nat. Bur. Stand. (U.S.), Tech. Note 511, 24 pages (Dec. 1969), 30 cents, SD Catalog No. C13.46: 511.*

Key words: Carrier lifetime; germanium; lithium-drifted gamma-ray detectors; resistivity; resistivity inhomogeneities; second breakdown; silicon.

Work at NBS which led to the development of a broad program on Methods of Measurement for Semiconductor Materials, Process Control, and Devices is described. Initial work was concentrated on resistivity of silicon wafers and second breakdown in transistors. In the first case, the basis for a significant improvement in the method for measuring resistivity of silicon wafers was established, and in the second, concepts were developed which formed the basis of a new type of specification for operating conditions free from second breakdown. Work was extended to include other projects, including studies of germanium for gamma-ray detectors, carrier lifetime, and resistivity inhomogeneities which are still in progress. Formation of the broad program in response to increased interest in improved measurement methods is described.

Bullis, W. M., Editor, **Methods of measurement for semiconductor materials, process control, and devices,** *Quarterly Report April 1 to June 30, 1969, Nat. Bur. Stand. (U.S.), Tech. Note 495, 45 pages (Sept. 1969), 50 cents.*

Key words: Carrier lifetime; die attachment; electrical properties; gamma detectors; germanium; gold-doped silicon; indium antimonide; metallization; methods of measurement; microelectronics; nuclear radiation detectors; resistivity; semiconductor devices; semiconductor materials; semiconductor process control; silicon; thermal resistance; thermographic measurements; wire bonds.

This quarterly progress report, fourth of a series, describes NBS activities directed toward the development of methods of measurement for semiconductor materials, process control, and devices. Principal emphasis is placed on measurement of resistivity, carrier lifetime, and electrical inhomogeneities in semiconductor crystals; evaluation of wire bonds; and measurement of thermal properties of semiconductor devices. Other tasks involve study of infrared measurement methods, deep-lying impurities in InSb, gold in silicon, and high field effects; establishment of a processing facility; evaluation of aluminum metallization and wafer die attachment; review of NASA measurement methods; and measurement of Hall effect in semiconductor crystals, second breakdown in transistors, and noise in microwave diodes. Related projects on silicon nuclear radiation detectors and specification of germanium are also described. Supplementary data concerning staff, committee activities, technical services, and publications are included as appendixes.

Bullis, W. M., Thurber, W. R., Pyke, T. N., Jr., Ulmer, F. H., Koenig, A. L., **Use of a time-shared computer system to control a Hall effect experiment,** *Nat. Bur. Stand. (U.S.), Tech. Note 510, 46 pages (Oct. 1969), 50 cents.*

Key words: Computer-controlled experiment; data acquisition system; digital scanner; experiment-computer interface; Hall effect; system control module; teletypewriter interface; time-shared computer.

An experimental time-shared computer system has been used to control and collect data from a Hall effect experiment. In addition to selection of the voltage sequence and control of specimen current and magnetic flux directions, the computer exerts positive control over the specimen temperature in accordance with a series of thermocouple voltages entered by the operator at the beginning of the run. The interface circuitry is constructed from four general purpose modules and a single special purpose unit. Details of the interface system and the programs used to control the experiment and to perform intermediate calculations are given. It was found that the time-shared system was well-suited to control an experiment of this type. The demands on the computer were essentially similar to those required by a human user interacting in a conversational mode. Substantial savings in time over manual data collection and reduction were realized; a temperature run with 38 to 40 data points between 10 and 320 K could be completed in less than 4 hours.

Carpenter, B. S., Cheek, C. H., **Trace determination of uranium in biological material by fission track counting,** *Anal. Chem.* **42,** *No. 1, 121–123 (Jan. 1970).*

Key words: Activation analysis; biological material; fission track; microanalysis; nuclear track; uranium.

The nuclear track technique for determining micro quantities of uranium in material, which consists of counting fission tarcks produced in solid-state detectors as a result of neutron irradiation, is employed to determine trace quantities of uranium in such biological materials as mammalian blood and plasma and oak leaves. Dry-ashed samples of the material are dissolved in dilute acid and make up to standard volumes. Aliquots of these solutions are placed on Lexan polycarbonate detectors, evaporated to dryness, and enclosed in a polyethylene bag. After irradiation in a thermal neutron flux, the bag is removed and the Lexan detectors are etched in a sodium hydroxide solution. The amount of uranium present in the biological matrices is determined by counting the etched fission tracts with an optical microscope and comparing the results with those obtained for simultaneously irradiated reference standards containing known amounts of uranium. Average results obtained from thermal neutron irradiations for the blood plasma samples were 86.1 ppb and 60.5 ppb, respectively, while the values for oak leaves ranged from 1.62 to 15.2 ppm.

Colwell, J. H., **The performance of a mechanical heat switch at low temperatures,** *Rev. Sci. Instr.* **40,** *No. 9, 1182–1186 (Sept. 1969).*

Key words: ^{3}He cryostat; low temperature; low temperature calorimetry; mechanical heat switch; pressed contacts; thermal conductance of contacts.

A mechanical heat switch used in calorimetry experiments down to 0.3 K is described and its performance analyzed in sufficient detail to be useful for design purposes. The thermal conductance of the indium-copper switch contacts was determined as a function of applied force and temperature over the range 0.3 to 2 K. These results are compared with other conductance measurements to evaluate choices of materials for heat switch contacts.

Crawford, M. L., **A new RF-DC substitution calorimeter with automatically controlled reference power,** *IEEE Trans. Instr. Meas.* **IM–17,** *No. 4, 378–384 (Dec. 1968).*

Key words: Coaxial dry-load calorimeter; feed-back control; radio-frequency power.

A new dual-dry-load calorimeter, incorporating automatically controlled reference dc input power, has been developed at the National Bureau of Standards. The calorimeter will be used as a reference standard at frequencies up to 4.0 GHz in the power range, 10 mW to 1 W. The maximum measurement uncertainty is 0.26 percent at frequencies below 1 GHz and 0.35 percent at frequencies above 1 GHz. The time required for the measurement system to reach equilibrium is less than two minutes. Construction details and design of the calorimetric and feedback control system are given along with an error analysis and results of intercomparisons with other standards.

Daney, D. E., Ludtke, P. E., Sindt, C. F., **Slush hydrogen pumping characteristics using a centrifugal-type pump** *(Proc. 1968 Cryogenic Engineering Conf., Case Western Reserve Univ., Cleveland, Ohio, Aug. 19–21, 1968), Chapter in, Advances in Cryogenic*

Engineering **14**, *Paper J–2, 438–445 (Plenum Press, Inc., New York, N.Y., 1969).*

Key words: Cavitation; centrifugal pumps; cryogenic pump; liquid-solid hydrogen mixtures; slush hydrogen.

The pumping characteristics of liquid-solid mixtures of para-hydrogen (slush hydrogen) were investigated using a centrifugal type liquid hydrogen pump with a design specific speed of approximately 2200. Performance tests from 8,000 to 19,000 rpm and cavitation tests at 11,000 and 14,000 rpm were made. The slush solid fraction varied from 0.19 to 0.55. As predicted by theory, the developed head for liquid and slush hydrogen are the same when the difference in density is considered. The pump efficiency, cavitation constant and NPSH requirements are also the same for slush hydrogen and triple-point liquid. After 34 minutes running time with slush hydrogen out of a total running time of 79 minutes, the pump components showed no wear over that expected from operation in liquid.

Davis, H. A., Jr., Hastings, J. R., Waxman, M., **An improved tool for refinishing the conical ends of high-pressure tubing,** *Rev. Sci. Instr.* **40**, *No. 9, 1238 (Sept. 1969).*

Key words: Coning tool; high-pressure tubing; pressure seal.

A simple tool has been developed for refinishing the conical ends of high-pressure tubing in order to obtain a satisfactory seal in a coned-and-threaded connection. The tool uses the threaded portion of the tubing as the reference for alignment and can be used to refinish tubing that has a bend very close to the end of the tubing.

Davis, J. C., **Radiation errors in air ducts under nonisothermal conditions using thermocouples, thermistors, and a resistance thermometer,** *Nat. Bur. Stand. (U.S.), Bldg. Sci. Ser.* **26**, *14 pages (Nov. 1969), 25 cents, SD Catalog No. C13.29/2:26.*

Key words: Conduction error; radiation error; resistance thermometer; temperature measurement; thermistor; thermocouple.

Studies were made to determine the radiation error in temperature measurements made with thermocouples, thermistors, and a resistance thermometer in moving air at velocities ranging from 300 to 1300 fpm when the temperature of the duct wall surrounding the air stream was from 0 to 50 deg F higher than that of the air in the center of the duct. To eliminate all but the variable under study, conduction errors were minimized to a point where they were almost nonexistent by using Chromel P–constantan thermocouple wire and by employing other techniques. Radiation effects were studied when the probe housing the three types of temperature sensors was unshielded and again when it was shielded. The studies showed that when the sensors were unshielded and the temperature difference between the duct wall and the air was 50 deg F (28 K, approximately), the error in the sensors was about 3.8 deg F (2.1 K) for an air velocity of 300 fpm (1.5 m/s) and 1.0 deg F (0.6 K) for an air velocity of 1300 fpm (6.6 m/s). When the sensors were shielded, the error was about 0.2 deg F (0.1 K) for 300 and 500 fpm velocities and the same duct wall air-temperature difference. Tests were not performed at 1300 fpm with the sensors shielded because theory indicated that radiation error would be negligible at this velocity. Under the test conditions that prevail in the testing of air conditioners and heat pumps in laboratories, it should be possible to reduce the error in temperature measurement of the moving air to about 0.2 deg F (0.1 K) by a suitable combination of air mixers, duct insulation, radiation shields, and calibration techniques.

Dean, J. W., Brennan, J. A., Mann, D. B., **Cryogenic flow research facility of the National Bureau of Standards** *(Proc. 1968 Cryogenic Engineering Conf., Case Western Reserve Univ., Cleveland, Ohio, Aug. 19–21, 1968), Chapter in Advances in Cryogenic Engineering* **14**, *Paper H–1, 299–305 (Plenum Press, Inc., New York, N.Y., 1969).*

Key words: Cryogenics; flow; fluid-metering.

The Cryogenics Division of the NBS-Institute for Basic Standards is currently involved in an extensive cryogenic fluid metering program. The objectives of this program are to study cryogenic fluid measuring practices, to develop recommended practices for the most effective transfer of cryogenic fluids of interest in commerce, and to allow testing of new concepts in measurement.

This paper describes the experimental facility built to implement this program. The facility consists of a cryogenic flow loop with a dynamic gravimetric mass flow calibration capability. A pump delivers from .00126 to .0126 m^3/s (20 to 200 GPM) of nitrogen or argon at pressures up to 1.9 MN/m^2 (275 psia). 15 kW of refrigeration is available at 63 K (113 R) to remove the pump and heat leak energy and thus controls the temperature environment in the test section. An analysis of the system errors is presented to provide an understanding of the system operation.

DeVoe, J. R., Editor, **Radiochemical Analysis Section: Mössbauer spectroscopy, nuclear chemistry, nuclear instrumentation, radioisotope techniques, Summary of activities, July 1968 to June 1969,** *Nat. Bur. Stand. (U.S.), Tech. Note 501, 149 pages (Feb. 1970), $1.25, SD Catalog No. C13.46:501.*

Key words: Calculations; conversion electrons; counting statistics; cross sections; cryostats; electric field gradient tensor; electronics; gas analysis; heterogeneity; interferometric; internal magnetic field; iron; molybdenum; Mössbauer spectrometer; Mössbauer spectrometry; nickel-61; proportional detector; radiochemistry; radioisotope dilution; rutile; self-consistent crystal field; Standard Reference Materials; structure analysis.

This is the sixth summary of progress of the Radiochemical Analysis Section of the Analytical Chemistry Division at the National Bureau of Standards.

The section's effort comprises five major areas: Mössbauer spectroscopy, nuclear chemistry, nuclear instrumentation, radioisotope tracer techniques and the application of statistics in nuclear and analytical chemistry.

Low temperature devices for Mössbauer spectroscopy are a subject of continuing interest, and this year's effort is centered around the design of variable temperature devices. A high temperature device is also described.

Preliminary data on the detection of conversion electrons show the potential for Mössbauer spectroscopy in the field of chemical bonding in surfaces.

Further exploration of the potential of Mössbauer spectroscopy for the measure of structural parameters of nickel compounds have been made.

Preliminary data are presented on the structure of iron doped rutile (TiO_2) which is of significance to the determination of mineral structures found on the moon. Theoretical predictions of Mössbauer spectra resulting from electric field gradients due to crystal field interactions are presented. Evaluation of the basic integrals using the self-consistent Hartree-Fock method is given for ions of the first row of transition elements.

Precautions to be taken in the analysis of gamma-ray spectra are presented when model errors exist and when a gain shift is detected.

A system for gas analysis which utilizes gas chromatography is described. Its application to nuclear cross section studies is also presented. A method for setting limits on sample heterogeneity using a specific analysis method provides a useful indicator for evaluation of the adequacy of standard reference materials.

An interesting presentation of detection and measurement in the femtogram region is given.

The complete circuitry for the optical interferometric Mössbauer spectrometer is presented in this report.

Quantitative analysis for molybdenum and iron using radioisotope dilution to a precision that rivals most other techniques is described.

Diamond, J. J., Editor, **Bibliography on the high temperature chemistry and physics of materials, July, August, Sept. 1969.** *Nat. Bur. Stand. (U.S.) Spec. Publ. 315-3, 90 pages (Oct. 1969), $1.00.*

Key words: Bibliography, high temperature; chemistry, high temperature; high temperature chemistry; materials properties; research at high temperatures; thermophysical properties.

The bibliography consists of references to research involving temperatures above 1000 °C, which were noted by the Contributors during the above three-month period. Since this is intended primarily as a current-awareness bibliography, there is no cross-referencing or indexing. This issue contains about 825 references roughly grouped under fifteen subject headings.

Durst, R. A., Editor, **Ion-selective electrodes. Proceedings of a symposium held at the National Bureau of Standards, Gaithersburg, Maryland, January 30–31, 1969,** *Nat. Bur. Stand. (U.S.), Spec. Publ. 314, 474 pages (Nov. 1969), $3.50, SD Catalog No. C13.10:314.*

Key words: Ion-selective electrodes; review of ion selective electrodes; specific-ion electrodes; symposium proceedings.

This volume contains a review of ion-selective electrodes, emphasizing the non-glass types, and provides a thorough and critical evaluation of the subject. It consists of eleven invited review papers and selected discussions from the Symposium on Ion-Selective Electrodes held at NBS on January 30–31, 1969. This publication provides a comprehensive survey of the field and should prove very valuable in advancing the state of the art. The chapters include discussions on the theory, characteristics, and methodology of all types of ion-selective electrodes; their use in thermodynamic, kinetic, and complex-ion studies; standards; pure and applied research in various biomedical areas of interest; industrial analysis and control systems; and applications to diverse analytical problems. Both the present status and future potential of these sensors are discussed in a wide range of scientific disciplines, from the physical sciences to biomedicine. Extensive bibliographies provide an excellent survey of the literature for anyone using or anticipating the use of these electrodes.

Edmonds, D. K., Hork, J., **Cavitation in liquid cryogens** (*Proc. 1968 Cryogenic Engineering Conf., Case Western Reserve Univ., Cleveland, Ohio, Aug. 19–21, 1968*), *Chapter in Advances in Cryogenic Engineering* **14,** *Paper G-4, 274–282 (Plenum Press, Inc., New York, N.Y., 1969).*

Key words: Cavitation; cavitation inception; cryogenic; cryogenic cavitation; developed cavitation; thermodynamic cavitation.

Cavitation characteristics of liquid hydrogen and liquid nitrogen flowing in a transparent plastic venturi have been determined and conventional cavitation inception parameter curves are given. Representative thermodynamic data, consisting of pressure and temperature measurements within fully-developed cavities, are also given; measured temperatures and pressures within the cavities were generally not in thermodynamic equilibrium. Existing theory was used to obtain equations which correlate the experimental data for developed cavities in liquid hydrogen or liquid nitrogen. The theory is extended to include the effect of cavity thickness and the experimental data are used to evaluate the results. Some recommendations for future work are given.

Eisele, J. W., **Technical Standard Coordinator, Uncored slab urethane foam for bedding and furniture cushioning,** *Nat. Bur. Stand. (U.S.), Prod. Stand. 13-69, 6 pages (Dec. 1969), 10 cents, SD Catalog No. C13.20/2:13-69.*

Key words: Cellular; flexible; slab; uncored; urethane foam.

The foam covered by this Product Standard is intended for uses such as inserts for mattresses and cushions for indoor and outdoor furniture. This Standard provides material and dimensional requirements for uncored slab urethane foam and requirements and methods of test for the specific properties of load bearing capacity, permanent set, moisture resistance, fatigue resistance, and resiliency. The fatigue requirements will be revised to incorporate dynamic fatigue specifications when adequate data are available. Methods for marking and labeling to indicate compliance with this Standard are also provided.

Engen, G. F., **An introduction to the description and evaluation of microwave systems using terminal invariant parameters,** *Nat. Bur. Stand. (U.S.), Monogr. 112, 27 pages (Oct. 1969), 35 cents.*

Key words: Attenuation; impedance; microwave power; precision connector; terminal invariant.

The description and evaluation of microwave systems is usually by means of microwave circuit analysis, which may be regarded as an extension of the practice at lower frequencies. In order to insure its validity, it is necessary to postulate that the different components, which comprise the microwave system, are interconnected via uniform and lossless waveguide, and which is usually (but not necessarily) restricted to single mode operation. As a consequence, precision (uniform) waveguide and connectors are usually considered necessary elements for an accurate experimental evaluation of a microwave system.

It is possible to avoid this requirement in an alternative formulation where the description is based upon net power, instead of the complex traveling wave amplitudes. In this reformulation the basic parameters include available power, maximum efficiency (or intrinsic attenuation), and several different "mismatch factors." The important feature of these parameters is their "terminal invariant" property, i.e., their invariance to an arbitrary shift in the terminal reference surface (in an assumed lossless region).

In this way the precision waveguide and connector requirement is avoided for an important class of measurement problems. In addition the physical model, upon which the description is based, is a simple one which provides improved insight into mismatch errors and corrections.

Fenstermaker, C. A., McCrackin, F. L., **Errors arising from surface roughness in ellipsometric measurement of the refractive index of a surface,** *Surface Sci.* **16,** *85–96 (1969).*

Key words: Ellipsometry; index of refraction; light reflection; optical properties; rough surfaces.

The roughness of a surface is generally neglected when the refractive index of a material is calculated from ellipsometer measurements. Errors produced by neglecting the roughness of the surface are evaluated for three models of the topography of the surface (square ridges, triangular ridges, and pyramids). A range of roughness from 0 to 500 Å and six substrate materials (glass, silicon, chrome, mercury, gold, and silver) are considered. Large errors in determination of indices, even for small values of roughness (50 Å), were found.

Frederick, N. V., **A low loss sliding short of limited travel for precision coaxial transmission lines,** *Proc. IEEE* **56,** *No. 12, 2188 (Dec. 1968).*

Key words: Coaxial cavity tuning; coaxial short; precision transmission line; reflection coefficient; sliding short.

A precisely adjustable sliding short with high reflection coefficient is described. The reflection coefficient is approximately 0.996 at 4 GHz. Instructions are given for fabrication. The device is especially useful for measuring electrical lengths and for tuning of coaxial cavities and for coaxial line bridge work.

Furukawa, G. T., **Automation problems in thermometry and calorimetry** (*Proc. 2d & 3d Japanese Calorimetry Conf., Osaka, Japan, Nov. 27–28, 1967*), *Chapter 1 in Calorimetry, Thermometry, and Calorimetry, Y. Otsubo, H. Kanbe, and S. Seki, Ed.,* **2,** *1–35 (Kagaku Gijitsu-Sha, Tokyo, Japan, 1969).*

Key words: Autometic calorimetry; calorimetry; heat capacity; Mueller bridge; thermometry.

For high-precision low-temperature calorimetry, the techniques used in measurement periods of temperature and of power are discussed separately. The application of electronic preset counters to automatic control of the calorimetric process is proposed. The thermometer resistances are measured by means of an automated Mueller bridge and the measurements are analyzed on a high-speed digital computer to obtain temperature-time observations. The electrical power introduced is automatically determined using a commercially available integrating digital voltmeter (IDVM) to measure a small fraction of the total calorimeter heater voltage biased by a stable reference voltage. A modification of the IDVM to integrate over the heating interval to obtain the total electrical energy input is described.

Gatterer, L. E., **Clock synchronization experiments at VHF utilizing the ATS–1 and ATS–3 transponders,** *Natl. Aeronaut. Space Admin. Report ATS Tech. Summary (National Aeronautics and Space Administration, Greenbelt, Md., Feb. 16, 1968).*

Key words: Clock; synchronization; transponder; VHF.

Experiments are described which repeat demonstrations of the effectiveness of a technique for synchronizing widely separated clocks to better than 10 μsec, and which investigate extensions of this technique, preliminary results are described. These experiments utilized the VHF transponder on ATS–1.

Geller, S. B., Mantek, P. A., Cleveland, N. G., **Standard reference materials: Calibration of NBS secondary standard magnetic tape (computer amplitude reference) using the reference tape amplitude measurement "Process A",** *Nat. Bur. Stand. (U.S.), Spec. Publ. 260–18, 41 pages (Nov. 1969), 50 cents.*

Key words: Average peak signal level; computer amplitude reference; magnetic tape; master standard; saturation curves; secondary standard; signal level calibration; standard reference materials; unrecorded reference.

This publication describes the design and operation of the NBS signal amplitude measuring system (Process A) that is used for calibrating unrecorded Secondary Standard Magnetic Tapes (Computer Amplitude Reference). The signal level calibration is made with respect to a reference signal level derived from the NBS Master Standard Magnetic Tape (Computer Amplitude Reference) that is kept in repository at NBS. The techniques for measuring and recording the data that accompany each Secondary Standard Magnetic Tape in the form of strip chart recordings and saturation curves are described.

Gorden, R., Jr., Rebert, R. E., Ausloos, P., **Rare gas resonance lamps,** *Nat. Bur. Stand. (U.S.), Tech. Note 496, 55 pages (Oct. 1969), 60 cents.*

Key words: Aluminum window; extinction coefficients; ionization quantum yield; photochemistry; photoionization; rare gases; resonance lamps; saturation ion current.

Rare gas resonance lamps having high spectral purity, high intensity, and long lifetimes have successfully been manufactured. The design and filling procedure for these lamps is described in detail. Particular operational characteristics of the xenon, krypton, argon, neon, and helium resonance lamps are also given. Windows suitable for use with each of these lamps are described, with particular emphasis given to the procedure for fabricating thin aluminum windows for use with neon and helium lamps. In addition, a method for determining extinction coefficients and ionization quantum yields based on the measurement of saturation ion currents is described.

Greenfeld, S. H., **Natural weathering of mineral stabilized asphalt coatings on organic felt,** *Nat. Bur. Stand. (U.S.), Bldg. Sci. Ser. 24, 17 pages (Oct. 1969), 30 cents.*

Key words: Additive; asphalt; durability; felt; stabilizer; weathering.

Sixteen years of outdoor weathering of laboratory-prepared smooth-surface and mineral-surfaced, felt-base roofing specimens has provided information on the effects of mineral additives on the durability of coating-grade roofing asphalts. Six finely divided mineral additives (blue black slate, clay, dolomite, fly ash, mica, and silica) were evaluated at concentrations up to 60 percent in California, Mid Continent and Venezuela asphalts. The mineral-surfaced specimens are all performing satisfactorily, and show only minor degrees of degradation. Of the smooth-surfaced specimens, the Mid-Continent asphalt performed the best and the California asphalt the poorest. The mica and blue black slate increased the durabilities of all three asphalts at all concentrations and two coating thicknesses. Fly ash, clay, dolomite, and silica were beneficial in some combinations, but had little effect in others. In general, these early results from outdoor exposure tend to corroborate the results obtained on these coatings exposed in weatherometers.

Gugeler, A. L., Ballard, D. B., **The aluminum-porcelain enamel interface as observed by electron microscopy,** *Am. Cerm. Soc. Bull.* **48,** *No. 9, 842–845 (Sept. 1969).*

Key words: Adherence; aluminum; electron microscope; interface; porcelain enamel; spall resistance.

The electron microscope was used in a study of the adherence of porcelain enamel to aluminum. Various combinations of aluminum alloys and metal pretreatments were studied. Shadowed plastic surface replicas of the porcelain enamel-aluminum interface were taken from polished and etched cross sections. Those combinations which had poor adherence, as indicated by low resistance to spalling, had a layered structure at the interface. This thin layer was not observed in those specimens which were considered to have good adherence. The susceptibility of the layered structure at the interface to corrosive attack appears to have a direct relationship to spall resistance.

Hall, L. A., **A bibliography of thermophysical properties of air from 0 to 300 K,** *Nat. Bur. Stand. (U.S.), Tech. Note 383, 121 pages (Oct. 1969), $1.25, SD Catalog No. C13.46:383.*

Key words: Air; bibliography; equation of state; low temperature; mechanical properties; thermodynamic properties; transport properties.

References together with an abbreviated abstract are presented for mechanical, thermodynamic, and transport properties of air from 0 to 300 K published up to December 1968. A total of 610 articles have been indexed. Each article has been reviewed and coded with regard to properties studied, type of article (i.e., experimental, theoretical, etc.), and method of presentation of data. The temperature and pressure ranges for each property under consideration are also given. An index has been prepared according to property with four sub-categories: solid, liquid, gas up to 200 K, and gas above 200 K.

Heaton, H. T., II, **Use of an on-line computer in neutron time-of-flight measurements,** *Nat. Bur. Stand. (U.S.), Tech. Note 515, 31 pages (Jan. 1970), 35 cents, SD Catalog No. C13.46:515.*

Key words: Data handling system; interruptable computer; neutron time-of-flight; neutron total cross sections; on-line computer; program selector board.

This paper describes the on-line data handling system at the NBS Electron Linear Accelerator facility as it is used for measuring neutron total cross sections by time-of-flight techniques.

Hendricks, R. C., Simoneau, R., Smith, R. V., **Heat transfer with a near-critical fluid,** *Nat. Aeronaut. Space Admin. Report TNX 52612 (National Aeronautics and Space Administration, Greenbelt, Maryland, June 16, 1969).*

Key words: Choking, critical; fluid; fluid flow; heat transfer; oscillations.

The three authors have reviewed the field and added some new material. The intent of the paper is to bring the literature together, to provide information for designers, and to suggest needed research.

Hudson, G. E., Allan, D. W., Barnes, J. A., Hall, R. G., Lavanceau, J. D., Winkler, G. M. R., **A coordinate frequency and time system,** *Proc. 23d Frequency Control Symp., Atlantic City, N.J., May 6–8, 1969, p. 249 (1969).*

Key words: Coordinate time; local atomic standards; metric time; national unified atomic standards; proper time; universal coordinated time.

A coordinate frequency and time system, suitable for extension to worldwide coverage, is described in relation to the form evolving in the United States. It consists of a network of component primary and associated stations, at fixed locations and altitudes, and a reference coordinating component at a reference location and altitude. A unified local atomic standard for the system serves as the coordinating component.

The system could be extended internationally, by regarding the national unified standards as components of an international one whose assigned frequency would equal $f(Cs)$.

Hudson, G. E., Barnes, J. A., **Clock error statistics as a renewal process,** *Proc. 22d Frequency Control Annual Symp., Atlantic City, N.J., Apr. 22–24, 1968, pp. 384–413 (1968).*

Key words: Clock errors; dispersion of clock reading; flicker noise; random-walk noise; renewal equation; renewal processes; statistics of clock ensembles; white noise; zero crossings.

A model ensemble specifying the distribution of its clock readings about their average obeys an integral equation of renewal type. Renewal processes ordinarily describe when mechanical or electrical components need to be replaced. In this case, clocks in the ensemble may repeatedly read correctly and "renew" themselves. Solutions of the equation are discussed and are related to other error statistics.

Jefferson, C. F., Baker, C. K., **Mechanism of electrical conductivity in nickel-iron ferrite,** *IEEE Trans. Magnetics* **MAG-4,** *No. 3, 460–464 (Sept. 1968).*

Key words: Conductivity; ferrites; Hall mobility; thermal emf; transition metal oxides.

Measurements of the frequency dependence of the dielectric-conductivity, Hall mobility and thermal emf as a function of temperature on polycrystalline $Ni_{0.6}Fe_{0.4}Fe_2O_4$ indicate that this data can be interpreted in terms of the band model. Previous analyses of the semiconductor properties of ferrites according to the hopping model assume that the number of carriers, n, is identical with the concentration of divalent iron ions. Hall measurements indicate that this is not the case here and that n is best described by the equation

$$n^2 = (N_D - n) N_0 \frac{m^{*\,3/2}}{m} g^{-1} \exp - \frac{E_D}{kT}.$$

Assigning a value of 2 to g, m^*/m is 9.3 and E_D *is* 0.034 eV.

The temperature dependence of the dc conductivity is considerable different from that of the ac conductivity. This difference is found for polycrystalline $Ni_{0.6}Fe_{0.4}Fe_2O_4$ and $LiFe_5O_8$ as well as for single crystal $LiFe_5O_8$. A Wagner type relaxation associated with interfacial polarization is present in all materials, indicating that precautions must be taken in the interpretation of dc conductivity data even when single crystals are used.

The thermal emf, calculated from Hall data, shows that the measured value considerably larger than the calculated value. This implies that the measured values might contain a contribution from the phonon drag effect.

Jellison, J. C., Collier, R. S., **Fluid phase and temperature measurement with a single sensor** *(Proc. 1968 Cryogenic Engineering Conf., Case Western Reserve Univ., Cleveland, Ohio, Aug. 19–21, 1968), Chapter in Advances in Cryogenic Engineering* **14,** *Paper H–5, 322–330 (Plenum Press, Inc., New York, N.Y., 1969).*

Key words: Carbon; cryogenic; fluid phase; hydrogen; low-gravity; resistance thermometry; thin film; temperature.

A technique is described, which permits a single sensor to measure temperature and the presence of liquid or vapor at a specific point in cryogenic containers. This technique compensates for disturbances such as cryogen temperature variations, and it offers indication of a gas to liquid transition in a fraction of a second. Although designed and used for LH_2 instrumentation, the basic principle has been applied to LN_2 with slight modification. The system is able to dicriminate liquid presence under normal and low-gravity conditions.

Optimum use of the system under low-gravity requires the development of a sensor having a fast thermal time constant, a geometry capable of repelling cryogen films from its surface, and which can be used as a resistance thermometer. Vacuum deposited thin films of carbon are discussed as a possibility for satisfying these requirements. The resistance-temperature curve for these carbon films is nearly log-log linear over a wide temperature range, providing easy calibration of the sensor, and they have good stability on aging and thermal cycling.

Jennings, D. A., West, E. D., Evenson, K. M., Rasmussen, A. L., Simmons, W. R., **Laser power and energy measurements,** *Nat. Bur. Stand. (U.S.), Tech. Note 382, 64 pages (Oct. 1969), 65 cents.*

Key words: Calorimetry; laser; laser calorimetry; laser energy; laser power.

Most laser calorimeters operate in a constant temperature environment. The calorimeters can be used as deflection devices or the data can be analyzed by extrapolation or integration. Consideration of the heat flow problem common to all of these methods points up the underlying assumptions and the possible errors involved.

Calorimeters for measuring the output energy of pulsed ruby and neodymium glass lasers have been built and calibrated. The absorbing medium is an aqueous solution of $CuSO_4$. Calibration of laser energy detectors has an estimated uncertainty of $\pm 2\%$ for input energies of 0.1 J to 100 J. Comparisons of absorption cell calorimeters with metal plate calorimeters agree within 1%.

Instrumentation is described that is used for the calibration of CW laser power meters. The calibration unit employs an absorption cell calorimeter to calibrate the output of a photovoltaic cell transfer detector. The power meter to be calibrated is then compared to the calibrated output of the transfer detector. The calibrations are within an accuracy of 4%.

A discussion and description is also given of several types of calorimeters that have been used to measure the output of a 100 watt CO_2 laser. The most recent design provides for measurement from 1 watt to 5 kilowatts with a measured accuracy of better than 3%.

Joiner, B. L., **The median significance level and other small sample measures of test efficacy,** *J. Am. Statist. Assoc.* **64,** *971–985 (Sept. 1969).*

Key words: Efficiency of tests; median significance level; significance level; statistical tests.

The concepts of the "median significance level" (MSL) and the "significance level of the average" (SLA) are introduced and some relationships among these measures and the recently introduced "expected significance level" (ESL), "average critical value" (ACV), and "median critical value" (MCV) are considered. The median significance level is defined as the median of the distribution of the observed significance level for a given alternative, and for one-sided tests is shown to be the significance level attained by the median of the test statistic. The "significance level of the average" is analogously defined for one-sided tests to be the significance level attained by the average (expectation) of the test statistic. For one-sided tests the MSL and SLA are inverse functions of Geary's MCV and ACV. Some relations between these small sample measures of test efficacy, and Pitman's and Bahadur's asymptotic measures are described. The MCV is shown to be formally related to Hamaker's "indifference quality" method of classifying acceptance sampling plans. Several simple examples are given illustrating some relationships among the several criteria.

Kamper, R. A., Mullen, L. O., Sullivan, D. B., **Some applications of the Josephson effect,** *Nat. Bur. Stand. (U.S.), Tech. Note 381, 63 pages (Oct. 1969), 65 cents.*

Key words: Josephson effect; superconductivity; thermometry; tunnel junctions.

We describe techniques for fabricating permanent Josephson junctions between thin films of niobium and lead, and for absolute noise thermometry at very low temperatures using the Josephson effect. We discuss the possible benefits of applying superconductivity to nuclear magnetic resonance detection, and review other applications of the Josephson effect.

Koeser, R. L., Report Editor, **Report of the 54th National Conference on Weights and Measures 1969,** *Nat. Bur. Stand. (U.S.), Spec. Publ. 318, 270 Pages (Nov. 1969), $1.50, SD Catalog No. C13.6/3:318.*

Key words: Conference; weights and measures; weights and measures—history; weights and measures—laws; weights and measures—regulations; weights and measures—technical requirements.

This is a report of the proceedings (edited) of the Fifty-fourth National Conference on Weights and Measures, sponsored by the National Bureau of Standards, held in Washington, D.C., June 9–13, 1969 and attended by State, county, and city weights and measures officials and representatives of the Federal Government, business, industry, railroads, and associations.

Kropschot, R. H., **Thermal diffusivity of powder insulation** *(Proc. 1968 Cryogenic Engineering Conf., Case Western Reserve Univ., Cleveland, Ohio, Aug. 19–21, 1968), Chapter in Advances in Cryogenic Engineering* **14,** *Paper F-4, 224–229 (Plenum Press, Inc., New York, N.Y., 1969).*

Key words: Conductivity; cryogenics; diffusivity; powders; thermal insulation.

The thermal diffusivity of selected powder insulations (carbon, silica-magnesia and a silica-aluminum mix) has been experimentally determined over the temperature range 76–300 K. These results were used, along with the estimated specific heat, to calculate the thermal conductivity. Good agreement is obtained between these data and thermal conductivities obtained from steady state measurements. As expected, the diffusivity of highly evacuated 50–50 weight percent silica-aluminum powder varies by a factor of three over this temperature range. These data also enhance the justification for assuming the specific heat for bulk and powdered materials to be the same in this temperature range.

Experimentally, the diffusivities were determined from transient temperature response to a step input change in temperature. Mathematical solution of the problem for constant diffusivity is known, and it is shown here that the same basic mathematical approach is valid for the case of a temperature dependent diffusivity. The experimental apparatus is briefly described and details of the experimental results and the mathematical analysis are included.

Kushner, L. M., **The NBS contribution to technological measurements and standards,** *Mater. Res. Std.* **9,** *No. 10, 8–10 (Oct. 1969).*

Key words: Performance standards; technological measurements and standards.

Our national system of measurement incorporates physical, material and technolgocial measurements and standards. Whereas the first two are concerned largely with enabling us to describe the physical world, technological measurements and standards are userelated and are at the interface between science and its application in industry and Government. The NBS program in technological measurements and standards is an effort to extend the principles of good measurement to the engineering fields and to the complex needs of today's society. This goal is pursued mainly through projects designed to enable the government to use technology effectively in its role as a consumer and employer of innovative resources.

With government at all levels becoming more and more involved in developing and setting standards in a variety of fields related to public health and safety, it becomes increasingly important that the standards be of such a nature that they do not hamper the introduction of new technology for accomplishing program objectives. This leads to a need to develop more fully the concept of performance requirements as the basis for standards. This must include a concern with subjective factors which of necessity enter the measurement problems as soon as man becomes part of the system to be measured.

A related phenomenon is the "systems" nature of many of our national problems. These problems to which physical scientists and engineers are now being directed are not purely technical but have large and important social and economic components. Completely new measurement criteria are required to specify the problem and provide measures of progress toward its amelioration. The development of this new measurement methodology is being undertaken in a relatively new field of applied science, systems analysis. This is a new technology for the decision making process in business, industry and government.

The NBS technological measurements and standards program attempts to support and stimulate these activities as effective means for bringing our national scientific and engineering skills to bear on current problems.

LaFleur, P. D., **Determination of molybdenum in steels and biological materials by activation analysis,** *Radiochem. Radioanal. Letters* **1,** *No. 3, 225–229 (July 1969).*

Key words: Activation analysis; biological materials; hydrogen *bis*(2-ethylhexyl) phosphate; molybdenum; radiochemical separations; steels.

A procedure for determining molybdenum by activation analysis in steels and biological matrices is described. The procedure involves a chemical separation of molybdenum by solvent extraction using the reagent hydrogen *bis*(2-ethylhexyl) phosphate, and subsequent back extraction with $HNO_3 - H_2O_2$. Using the procedure as described precisions of 1–2% (at the 95% confidence level) are possible and 3–4% are routine.

LaVilla, R. E., Mendlowitz, H., **Optical properties of germanium,** *J. Appl. Phys.* **40,** *No. 8, 3297–3300 (July 1969).*

Key words: Electron energy losses; germanium; $M_{IV, V}$ edge; optical constants; oscillator; strengths; sum rules; vacuum ultraviolet.

The set of optical constants of germanium reported by Marton and Toots, from 8 to 25 eV, have been assessed. An extension of the n and k values up to photon energy of 100 eV using Hunter's k values also has been studied. The analysis consisted of an internal consistency check by applying the Kronig-Kramers dispersion relations to the optical constants and an evaluation and study of the optical and electron oscillator strength distributions. From an application of the general sum rules to the oscillator strength distribution, the computed effective number of electrons per germanium atoms suggests a redetermination of the k values in the spectral region covered by Hunter.

Logan, H. L., **Studies of hot salt cracking of the titanium 8%-Al-1% Mo-1% V alloy** *(Proc. Ohio State Stress Corrosion Symp., Ohio State Univ., Columbus, Ohio, September 11–15, 1967), pp. 662–672 (National Association of Corrosion Engineers, Houston, Texas, 1969).*

Key words: Hot salt cracking; LiCl-KCl eutectic; stress-corrosion; Ti-8-1-1 alloy; titanium oxides.

Two approaches to the problem of hot salt cracking of the titanium alloy are reported. In the first of these the susceptibility of the alloy to cracking in contact with a number of chlorides was studied. Only NaCl, LiCl and a molten eutectic mixture of LiCl and KCl were found to severely crack stressed specimens exposed in air at 800 °F.

In the second phase of the program the effects of environments on the alloy in contact with NaCl were investigated. Data indicate that

the oxide or series of oxides formed on the alloy surface were important in determining whether specimens developed stress-corrosion cracks.

Data also indicate that little or no chlorine was produced in the corrosion reaction.

McBee, C. L., Kruger, J., **Ellipsometric-spectroscopy of films formed on metals in solution,** *Surface Sci.* **16,** *340–352 (1969).*

Key words: Ellipsometry; iron; optical constants; passive films; spectra.

The computational problems involved in the analysis of "ellipsometric-spectroscopic" data are considered, including the existence of multiple values of the optical constants for a single wavelength.

Suggestions are made for eliminating the extra values. Examples of pertinent experiments to study corrosion processes are given for passive films grown on single crystals of iron in sodium borate-boric acid solution.

McCaa, W. D., Jr., Nahman, N. S., **Frequency and time domain analysis of a superconductive coaxial line using the BCS theory,** *J. Appl. Phys.* **40,** *No. 5, 2098–2100 (Apr. 1969).*

Key words: BCS theory; superconductive lines; time and frequency response; two-fluid model.

A miniature superconductive lead-teflon-niobium coaxial line has been analyzed in terms of the complete BCS theory of superconductivity. The surface impedance of both superconductors, the line attenuation and the picosecond step responses have been calculated for a temperature of 4.24 °K. The dielectric has been assumed lossless.

In addition, the frequency and time domain responses obtained with the BCS theory are compared with those predicted for the same line parameters by the two fluid model.

Maki, A. G., Jr., **Vibrational spectroscopy,** *Ann. Rev. Phys. Chem.* **20,** *273–292 (1969).*

Key words: Absorption spectra; infrared; instrumentation; potential functions; spectroscopy; vibration.

A review is given of the recent scientific literature on the subject of vibrational spectroscopy. Topics which are covered include instrumentation, gas phase spectra including band contour calculations, condensed phase spectra, and vibrational potential functions.

Mandel, J., **A method for fitting empirical surfaces to physical or chemical data,** *Technometrics* **11,** *No. 3, 411–429 (Aug. 1969).*

Key words: Curve fitting; data analysis; empirical fitting of curves and surfaces; model, mathematical; response surface; surface fitting; two-way tables.

This paper presents an illustration of a recently developed method of surface fitting. Data on the specific volume of two types of rubber, measured at various temperatures and pressures, are used to establish empirical relationships between specific volume, temperature, and pressure.

An important feature of the method is that, to a considerable extent, it evolves the model from the data. Another basic feature is that it reduces the problem of surface fitting to that of fitting a few functions of one variable each.

Margoshes, M., **Remarks on linearization of characteristic curves in photographic photometry,** *Appl. Opt.* **8,** *No. 4, 818 (Apr. 1969).*

Key words: Arrak transform; Baker transform; emulsion calibration; Kaiser transform; photographic emulsions; Sampson transform; Seidel transform; spectrochemical analysis.

A discussion is given of the transformation $\Delta = \log(10^D - 1)$, where $D = \log(1/T)$ and T is the transmittance of the photographic image, this function was recently rediscovered by de Vaucouleurs, who claimed that Δ is a linear function of the relative exposure, $\log(E)$, over the range of values of D which are of interest. It is pointed out that this transform has been independently discovered three or more times, and that it is well known in spectrochemical analysis as the Seidel transform. Previously published and new data are cited to illustrate that Δ is only rarely a linear function of $\log(E)$. Other transforms are noted which do appear to give a linear relation with $\log(E)$ in many cases.

Margoshes, M., Rasberry, S. D., **Application of digital computers in spectrochemical analysis—computational methods in photographic microphotometry,** *Spectrochim. Act.* **24B,** *497–513 (Jan. 14, 1969).*

Key words: Computers; microphotometry; photographic emulsion; photographic photometry; programs; spectrochemical analysis.

A new method is described for calibration of photographic emulsions and conversion of microphotometer readings to relative intensities on a digital computer with special application to spectrochemical analysis. The method for emulsion calibration replaces graphical procedures by a numerical method which is well suited for digital computations. The method of computation and its underlying assumptions are described, and results are given of test of the procedure. It is recognized that the entire experimental arrangement is being calibrated, not merely the photographic emulsion, and it is shown how malfunctions of the microphotometer which affect the calibration can be recognized from the output of the computer. The program for conversion of microphotometer readings to relative intensities provides for several alternate calculations, including selection of the proper calibration parameters according to the wavelength of the line when these data are supplied for more than one wavelength region, as well as correction for step and background where required. The program is written to provide for automatic selection of the required alternative calculation, based on preliminary analysis of the input data.

Marron, B. A., Tauber, S. J., **Evolution of a general computer-based information system from pharmacological requirements,** *Proc. Conf. 32d Annual Meeting of the American Society for Information Science, San Francisco, California, Oct. 1–4, 1969,* **6,** *223–230 (Greenwood Publ. Corp., Westport, Conn., 1969).*

Key words: Chemical data; computers; information storage and retrieval; information systems; parameter control; pharmacological data.

A general information storage and retrieval system capable of handling most kinds of information by parameter control is described. The system is characterized by user description of data processing requirements and the capability of attaching modules for handling special processing problems. A specific implementation of the system for representative data types taken from chemistry and pharmacology is detailed.

Melmed, A. J., **Surface characterization by ellipsometry low-energy electron diffraction, and field-electron microscopy** *(Proc. Conf. Third Battelle Memorial Institute Materials Science Colloquium, Kronberg, Germany, May 6–11, 1968), Chapter in Molecular Processes on Solid Surfaces, pp. 105–127 (McGraw-Hill Book Co., Inc., New York, N.Y., 1969).*

Key words: Ellipsometry; field-emission microscopy; low-energy-electron diffraction; optical constants; oxidation; surface characterization.

Two types of experiments are described. In the first ellipsometry and LEED are combined in a study of the room temperature interaction of oxygen with (011)-oriented tungsten. Based on published interpretations concerning the LEED aspects of this experiment, the ellipsometer is shown to be capable of detecting small fractions of a monolayer of adsorbed oxygen, and the average sticking probability for oxygen is estimated to be 0.2 or 0.4 for the first half monolayer of oxygen atoms. Inability to completely understand the ellipsometry

data is encountered and is attributed to inadequacy of existing theory to cope with phenomena occurring in the sub-monolayer coverage range. In the second type experiment a technique is introduced which enables FEM and LEED observations to be made on a single specimen with reasonable assurrance that the entire specimen undergoes the same thermal and environmental history. Oxidation of tungsten and the adsorption and removal of carbon on tungsten are used to demonstrate surface characterization with this FEM-LEED combination.

Nahman, N. S., **Superconducting transmission lines—communication and power,** *Proc. 1968 Summer Study on Superconducting Devices and Accelerators, Brookhaven National Laboratory, Upton, L. I., New York, June 10–July 19, 1968, BNL–50155, 622–627 (1968).*

Key words: Superconductive; transmission.

Reviews are given on (1) the experimental and theoretical work on S.C. signal transmission lines and (2) theoretical designs of S.C. power transmission lines. A brief exposition is presented on the constituents of a generalized data communication system. Elements of the above described topics are drawn together in a consideration of the idea of combining S.C. power and communication lines into one system.

Nemoto, T., Beatty, R. W., Fentress, G. H., **A two-channel off-null technique for measuring small changes of attenuation,** *IEEE Trans. Microwave Theory Tech.* **MTT–17,** *No. 7, 396–397 (July 1969).*

Key words: Attenuation; microwave, off-null technique; small attenuation changes; two-channel.

A technique is described for measuring small changes of attenuation which are not accompanied by significant changes in phase shift. It is a two-channel technique in which a small off-null output signal undergoes relatively large changes upon making small changes in a test attenuator in one of the channels.

The procedure is described and measurements from 0.01 to 0.1 decibel on a rotary vane attenuator are compared with similar measurements by a different method. Agreement is within 4 percent.

Pfrange, E. O., Yokel, F. Y., **Structural performance evaluation of a building system.** *Nat. Bur. Stand. (U.S.), Bldg. Sci. Ser. 25, 127 pages (Nov. 1969), $1.25.*

Key words: Building systems; low-income housing; performance criteria; performance testing.

A full-scale, first-story portion of a building system was tested in the laboratory in such a manner as to simulate the structural behavior of a three-story building under both service and potential ultimate loading conditions. Additional tests were performed on the system components to provide behavioral data needed for the evaluation of the system.

Performance criteria for the evaluation of the strucutural safety and adequacy of certain building systems were developed. This report presents the results of the physical tests performed in the evaluation of the safety and structural adequacy of one such system, and discusses their significance. The report also presents data concerning the complex interaction between components which takes place in the building system.

The primary conclusions reached were:

(1) The system, as erected in the laboratory, satisfied the performance criteria which were set for its evaluation with a substantial margin. As a system, it exhibited strength and stiffness in excess of service and ultimate load requirements.

(2) The walls of the system behaved as an integral part of the structure. They provided most of the stiffness of the system with respect to lateral loads, and provided a significant portion of the stiffness against vertical loads.

Post, M. A., **Determination of styrene-butadiene and styrene-acrylate resins in solvent type paint,** *J. Paint Technol.* **41,** *No. 537, 567–580 (Oct. 1969).*

Key words: Chlorinated paraffin; infrared spectroscopy; solvent type paint; styrene-acrylate resin; styrene-butadiene resin.

Styrene-butadiene and styrene-acrylate resins are determined quantitatively in solvent type paint by two methods. One, a short and convenient method, is useful in acceptance testing of Federal Specifications paints where the chlorinated paraffins 40 and 70 are used in 1:1 ratio. It involves determination of total benzene extractables and the styrene resin content therein. The latter is evaluated by measuring the 3.3 μm/3.5 μm absorbance ratio for styrene-butadiene and the 5.8 μm/3.5 μm absorbance ratio for styrene-acrylate, using the baseline method for both. The ratios are obtained from infrared spectrograms of cast films of benzene extracts. The styrene resin content then is determined from the appropriate standard curve. The second method separates the plasticizer (chlorinated paraffins) and styrene resin by Soxhlet extraction of the dried dispersed paint, first with *n*-pentane, which removes the plasticizers and 5–10% of the styrene resin, and then with benzene, which removes the remainder of the styrene resin. A combination of the two methods can be used for paints where the type and proportion of plasticizers are unknown. Methods are applicable to commercial materials.

Reader, J., **Optimizing Czerny-Turner spectrographs: A comparison between analytic theory and ray tracing,** *J. Opt. Soc. Am.* **59,** *No. 9, 1189–1196 (Sept. 1969).*

Key words: Aberrations; coma; Czerny-Turner; geometrical optics; plane grating; ray tracing; spectrograph.

The analytic theory of aberrations has been used to derive an expression for the magnitude of the comatic width of the image in the meridional plane in a Czerny-Turner spectrograph with unequal mirror radii. The calculated properties of a 4-m spectrograph with equal radii and a recently constructed 3.34-m spectrograph with unequal radii are compared with the results obtained by tracing individual rays. The agreement is excellent, in contrast to the results of Chandler, J. Opt. Soc. Am. **58,** 895 (1968). The lateral position of the grating for complete elimation of coma found experimentally with the 3.34-m instrument is also in good agreement with the theory. A correction to the $\sqrt{3}$ longitudinal grating position is given for a Czerny-Turner spectrograph which results in a flatter focal surface.

Reed, R. P., **Low-temperature mechanical properties of welded and brazed copper** *(Proc. 1968 Cryogenic Engineering Conf., Case Western Reserve Univ., Cleveland, Ohio, Aug. 19–21, 1968), Chapter in Advances in Cryogenic Engineering* **14,** *Paper C–3, 83–87 (Plenum Press, Inc., New York, N.Y., 1969).*

Key words: Brazed; copper; low temperature; notch-tensile; tensile; welded.

The tensile and notch-tensile properties of butt-welded and overlap brazed copper plate were examined at test temperatures 300, 195, 76, and 4 °K. The brazed strengths were determined for both 1/8 and 1/4 inch overlap widths. It was found that the strength and ductility of copper joints increase at lower temperatures. Also, the joint strength decreases and elongation increases as the brazed overlap width is increased.

Reed, R. P., Schramm, R. E., **Lattice parameters of martensite and austenite in Fe-Ni alloys,** *J. Appl. Phys.* **40,** *No. 9, 3453–3458 (Aug. 1969).*

Key words: Fe-Ni alloys; lattice parameters; martensite.

The lattice parameters of the martensitic, body-centered cubic phase and the face-centered cubic phase were determined for a series of Fe-Ni alloys. Compositions ranged from pure Fe to Fe-35 at. % Ni. Careful Debye-Scherer powder techniques and computerized calculations and error analyses were employed. The martensite lattice parameter has been precisely determined for the

first time as a function of composition in Fe-Ni alloys. Results indicate that the martensite lattice parameter reaches a maximum between 9 and 15 at. % Ni and the room temperature lattice parameter of the face-centered cubic phase has a maximum in alloys having greater than 35 at. % Ni. The face-centered cubic parameter was not measurable in alloys having less than 27 at. % Ni.

Roberts, D. E., **Recrystallization and melting of partially melted stark rubber,** *Rubber Chem. Technol.* **42,** *540–546 (Mar. 1969).*

Key words: Crystal size; crystallized rubber; heating rate; melting range; melting temperature; oriented; partial melting; recrystallization; rubber; slow melting; stark rubber.

Two specimens from a piece of stark rubber which had a melting temperature originally at 41 °C were partially melted at 38 °C and allowed to stand for 11 years, one at about 25 °C, the other at 38 °C. The first showed a continuous slow decrease in specific volume, while the second increased slowly in volume for 5 months and remained constant for about 5 months more before showing the continuous slow decrease. The melting temperature of the first increased to 45 °C and the melting range was broadened. The melting temperature of the second became 52 °C and the range was narrowed. Perfecting or enlarging of crystals and the effect of higher recrystallization temperatures have influenced the melting temperatures. The effect of heating rate is discussed in connection with slow increases in volume, attributed to relaxation of oriented regions, during melting.

Rockett, J. A., **Planned operation of the National Bureau of Standards Fire Research and Safety Office,** *Fire J.* **63,** *No. 6, 41–43 (Nov. 1969).*

Key words: Fire; research program.

The proposed program for the Fire Research and Safety Center is outlined. This consists of (1) Statistical studies on deaths and injuries in fires and on the effectiveness of fire protection measures; (2) A study of the way in which fire grows and spreads in a building; and (3) Three programs related to fire service operations: (a) The use of Operations Research; (b) Improvement of breathing masks; and (c) A study of fire service training and education.

Ruthberg, S., **Calibration to high precision in the medium vacuum range with stable environments and micromanometer,** *J. Vacuum Sci. Technol.* **6,** *No. 3, 401–412 (May/June 1969).*

Key words: Calibration; capacitance-diaphragm gauge; medium vacuum range; micromanometer; stable pressure generation; vacuum measurements.

Ultra stable vacuum environments are utilized with a micrometer point contact manometer as reference standard for measurement and calibration with an uncertainty of 1.2×10^{-4} torr $+6$ parts in 10^5 of the reading from least count to several torr. The stable pressures are generated by dynamic vacuum systems and a servo control loop with cascaded error signals from a capacitance-diaphragm gauge for stabilities of better than 1 part in 10^5 at 1 torr. Precise evaluation of systems and procedures is given. Operational factors affecting accuracy were studied, such as sorption in the manometer fluid, pressure distribution in the test chamber, time constants in the micromanometer, and thermal response of the control loop.

Rybicki, G. B., Hummer, D. G., **Non-coherent scattering—V. Thermalization distances and their distribution function,** *Monthly Notices Roy. Astron. Soc.* **144,** *313–323 (1969).*

Key words: Noncoherent scattering; radiative transfer; spectral line; thermalization length.

The distribution function for thermalization lengths is derived for an infinite atmosphere with a plane source. Precise definitions of the thermalization length are discussed from the point of view of representing the distribution by a single characteristic length; of these a definition in terms of the medium of the distribution seems to be most useful. The distribution of longest flights is derived and shown to provide a good approximation to the distribution of thermalization lengths at large distances from the source. Extensive numerical illustrations are provided.

Simson, B. G., Radlinski, R. W., **The accuracy of air tower pressure gages in suburban Washington, D.C.,** *Nat. Bur. Stand. (U.S.), Tech. Note 512, 10 pages (Dec. 1969), 25 cents, SD Catalog No. C13.46:512.*

Key words: Air towers; tire pressure.

A survey of 50 air tower pressure gages in service stations of suburban Washington, D.C., was performed. Results showed that a motorist using these towers has only a 20 percent chance of inflating his tires within ± 1 psi of the pressure indicated by the tower's gage. It is shown that a calibration of the tower gages would reduce the standard deviation of the obtained pressure to 0.5 psi.

Sparks, L. L., Powell, R. L., Hall, W. J., **Progress on cryogenic thermocouples** *(Proc. 1968 Cryogenic Engineering Conf., Case Western Reserve Univ., Cleveland, Ohio, Aug. 19–21, 1968), Chapter in Advances in Cryogenic Engineering* **14,** *Paper H–4, 316–321 (Plenum Press, Inc., New York, N.Y., 1969).*

Key words: Cryogenics; gold alloy; thermocouples.

Experimental tests between 4 and 280 K have been completed on the following thermocouple materials: Chromel; copper, "normal" silver, platinum, *silver*-28 at. % gold, constantan, Alumel, and *gold*-(0.02, 0.03, 0.07) at. % Fe. Many thermocouple combinations can be made from the above materials; the four most important being Chromel vs. constantan, copper vs. constantan, Chromel vs. Alumel, and Chromel vs. gold-0.07 at. % iron. Results on the last combination are of particular interest for measurements near liquid hydrogen temperatures and will be presented in some detail. The calibration cryostat is described briefly. Special methods of measurement and data analysis have been designed to study and minimize systematic errors. Simple illustrations of these measurement schemes are given.

Standard Reference Materials, Catalog and price list of standard materials issued by the National Bureau of Standards, *Nat. Bur. Stand. (U.S.), Spec. Publ. 260, 1969 Edition, 44 pages (July 1969) (Supersedes NBS Misc. Publ. 260—1968 edition), 50 cents.*

Key words: Analysis; catalog; certificate; characterization; composition; price list; property of material; purity of material; standard reference materials; standards.

This catalog describes the various Standard Reference Materials issued by the National Bureau of Standards. These materials are used to calibrate measurement systems and provide scientific information that can be referred to a common base. A schedule of prices and quantities is included for each material, as well as directions for ordering. Listed are the types and compositions of those chemical standards that are presently available. Announcements of new standard reference materials are made in the Federal Register, in scientific and trade journals, and in the Technical News Bulletin of the National Bureau of Standards. Changes affecting the current status of the various standards will be indicated by an insert sheet available quarterly from the Bureau.

Taggart, H. E., **Field strength and RFI standards at the National Bureau of Standards,** *Proc. IEEE Electromagnetic Compatibility Conf., Seattle, Wash., July 23–25, 1968, pp. 149–158 (1968).*

Key words: Antenna electromagnetic interference standards; calibration; measurement techniques.

Some of the calibration services offered to industry and other governmental agencies by the National Bureau of Standard's Radio Standards Laboratory are discussed. The emphasis is placed on field strength measurements and related calibration services at frequencies from 30 Hz to 12 GHz. These include the calibration of 3 basic types of antennas: (1) Loop antennas, (2) Half-wave dipole antennas and (3) Horn antennas. Methods of calibrating these antennas are described and illustrated.

A discussion of calibration problems at microwave frequencies emphasizing the measurement errors as related to the antenna and receiver voltage standing wave ratios (VSWR). Antenna and receiver VSWR's are exemplified, and corresponding measurement errors are shown. Methods of estimating errors are given.

The National Bureau of Standards recently designed and constructed some antenna standards for both the Air Force and the Navy. These standards were designed to calibrate loop and half-wave dipole antennas. The frequency range is 10 kHz to 1000 MHz. These antenna standards are briefly described and illustrated.

The future plans for the development of antenna standards and broadband EMC standards at the National Bureau of Standards are discussed. Work is in progress in areas of impulse generators, random noise generators, and other instruments.

Thompson, B. A., LaFleur, P. D., **Activation analysis for molybdenum in samples containing large amount of tungsten,** *Anal. Chem.* **41,** *No. 13, 1888–1889 (Nov. 1969).*

Key words: Activation analysis; molybdenum; radiochemistry; solvent extraction; technetium; tungsten.

Molybdenum has been determined by neutron activation analysis in the presence of large amounts of tungsten using a double extraction with *bis*(2-ethylhexyl) orthophosphoric acid (HDEHP). In the first estraction W and Mo are separated from the matrix elements. In the second extraction, made after equilibration of ^{99m}Tc with ^{99}Mo, the ^{99m}Tc daughter of ^{99}Mo is separated from W and Mo and used as a measure of the Mo present. The method is very rapid and has good precision and accuracy.

Wiederhorn, S. M., **Fracture of sapphire,** *J. Am. Ceram. Soc.* **52,** *No. 9, 485–491 (Sept. 21, 1969).*

Key words: Crack propagation; cracks; double-cantilever-cleavage technique; fracture; fracture surface energy; sapphire.

The fracture of sapphire was studied using the double-cantilever-cleavage technique. Fracture surface energies of 7.3 and 6.0 J/m^2 were found for the (10$\bar{1}$0) and (10$\bar{1}$2) planes respectively. Attempts to measure the fracture surface energy on the (0001) plane proved unsuccessful. The failure of sapphire to fracture along the basal plane was attributed to the fact that these planes lack charge neutrality. The possibility of fracture induced dislocation motion in sapphire at room temperature was investigated. No evidence for dislocation motion was found and it was estimated that dislocations do not move in sapphire at room temperature at stresses less than approximately 7×10^9 N/m^2 (10^6 psi). Fracture behavior on (10$\bar{1}$2) planes was found to be erratic, varying from boule to boule. The topology of surfaces formed by crack propagation along this plane is described, but no explanation for the erratic behavior or the observed fracture features is given.

Weir, C. E., Piermarini, G. J., Block, S., **Instrumentation for single crystal x-ray diffraction at high pressures,** *Rev. Sci. Instr.* **40,** *No. 9, 1133–1136 (Sept. 1969).*

Key words: High pressure; single crystal; x-ray diffraction.

A diamond-anvil high pressure cell made of beryllium, a special goniometer head and a Buerger-type camera designed for X-ray diffraction by single crystals at high pressures are described in some detail. The most important problems still to be solved are discussed.

West, E. D., Ishihara, S., **Experimental evaluations of heater lead error in calorimetry,** *Rev. Sci. Instr.* **40,** *No. 10, 1356–1359 (Oct. 1969).*

Key words: Calorimeter; energy measurement; errors in calorimetry.

Improper location of the potential leads for calorimeter heaters can cause an appreciable systematic error. Calculations to estimate limits on this error are usually based on greatly simplified heat flow problems. An easily understood experimental test not involving such simplifications provides a more convincing demonstration of a limit on the magnitude of the systematic error. Such a test is provided by measurements with the same or equivalent heater leads and heaters of very different resistances.

Williams, R., **The effects of extended high-temperature storage on the performance characteristics of several strain gage pressure transducers,** *Nat. Bur. Stand. (U.S.), Tech. Note 497, 22 pages (Oct. 1969), 30 cents.*

Key words: Life testing; pressure transducer; sensitivity shift; strain gage; temperature cycling; temperature storage; zero shift.

This publication reports the results of a test program to evaluate the effects of high-temperature storage on the performance characteristics of several types of commercial strain gage pressure transducers. The results obtained indicate shifts in the zero pressure output and the sensitivity, some of which are permanent. The equipment used and the procedure followed are described.

Wilson, W. K., Hebert, R. L., **Evaluation of the stability of record papers,** *Tappi* **52,** *No. 8, 1523–1529 (Aug. 1969).*

Key words: Accelerated aging; aging; deterioration; laboratory aging; preservation; records; stability.

Information has been developed on the relative stabilities of papers made from a variety of pulps including groundwood, neutral sulfite semichemical, bleached chemical wood and rag. After laboratory aging at 90° C and 50% relative humidity for various time periods, changes in reflectance, pH, folding endurance, tear, burst, and tensile properties were determined. Alkaline papers as a group were more resistant to laboratory aging than any of the others. The papers made from groundwood also showed good resistance to aging. Papers containing large percentages of neutral sulfite semichemical pulp covered a wide range of stability depending on the pH. The pH was an important factor in laboratory aging, but the correlation between pH and the rate of deterioration of physical properties was not high.

Other NBS Publications

J. Res. Nat. Bur. Stand.(U.S.), 73A (Phys. and Chem.), No. 2 (Mar.–Apr. 1969), SD Catalog No. C13.22/sec.A:73/2. $2.00.

Color representation of electron micorprobe area-scan images by a color separation process. H. Yakowitz and K. F. J. Heinrich.

Configurations $3d^n4p$ in singly ionized atoms of the iron group. C. Roth.

Configurations $3d^n4p + 3d^{n-1}4s4p$ in Sc II, Ti II, and V II. C. Roth.

Effective interactions in the even configurations of the third spectra of the iron group. Y. Shadmi, E. Caspi, and J. Oreg.

Test of a kinetics scheme: Emission in H(^{2}S) + NO($^2\Pi$). M. Krauss.

A nuclear magnetic resonance and relaxation study of dimethoxyborane. T. C. Farrar and T. Tsang.

The effects of low energy irradiation on organometallics. Organometal halides of group IVA. F. E. Brinckman, Gerald F. Kokoszka, and Norman K. Adams, Jr.

Measurements of gaseous diffusion coefficients by a gas chromatographic technique. S. P. Wasik and K. E. McCulloh.

Phase relations in the Ru-Ir-O_2 system in air. C. L. McDaniel and S. J. Schneider.

Heats of reaction of natural rubber with sulfur. N. Bekkedahl and J. J. Weeks.

A table of rotational constants of symmetric top molecules giving rise to microwave spectra. M. S. Lojko and Y. Beers.

Energy levels, wave functions, dipole and quadrupole transitions of Fe^{+++} ions in sapphire. J. Lewiner and P. H. E. Meijer.

J. Res. Nat. Bur. Stand. (U.S.), 73A (Phys. and Chem.), No. 3 (May–June 1969), SD Catalog No. C13.22/sec.A:73/3. $1.50.

New even levels and classified lines in the first spectrum of tungsten (W I). C. H. Corliss.

The heat of combustion of beryllium in fluorine. K. L. Churney, and G. T. Armstrong.

Deuterium isotope effect on the dissociation of weak acids in water and deuterium oxide. R. A. Robinson, M. Paabo, and R. G. Bates.

Vortex motions in ideal Bose superfluid. M. J. Cooper.
Franck-Condon factors for the ionization of H_2O and D_2O. R. Botter and H. M. Rosenstock.
Topological features of hot carrier induced anisotropic breakdown on silicon diode surfaces. G. G. Harman.
The third spectrum of praseodymium (Pr III) in the vacuum ultraviolet. J. Sugar.

J. Res. Nat. Bur. Stand. (U.S.), 73A (Phys. and Chem.), No. 4 (July–Aug. 1969), SD Catalog No. C13.22/sec.A:73/4. $1.25.
Classical path methods in line broadening. I. The classical path approximation. E. W. Smith, C. R. Vidal, and J. Cooper.
Classical path methods in line broadening. II. Application to the Lyman series of hydrogen. E. W. Smith, C. R. Vidal, and J. Cooper.
The second virial coefficient for the realistic pair potential. H. W. Woolley.
Synthesis of barium ferrates in oxygen. T. Negas and R. S. Roth.
The system SrO—"chromium oxide" in air and oxygen. T. Negas and R. S. Roth.

J. Res. Nat. Bur. Stand. (U.S.), 73A (Phys. and Chem.), No. 5 (Sept.–Oct. 1969), SD Catalog No. C13.22/sec.A:73/5. $1.50.
Conversion of existing calorimetrically determined thermodynamic properties to the basis of the International Practical Temperature Scale of 1968. T. B. Douglas.
Measured enthalpy and derived thermodynamic properties of alpha beryllium nitride, Be_3N_2, from 273 to 1200 K. T. B. Douglas and W. H. Payne.
Measured enthalpy and derived thermodynamic properties of solid and liquid lithium tetrafluoroberyllate, Li_2BeF_4, from 273 to 900 K. T. B. Douglas and W. H. Payne.
Nonanalytic vapor pressure equation with data for nitrogen and oxygen. R. D. Goodwin.
Some precise measurements of the vapor pressure of water in the range from 25 to 100 °C. H. F. Stimson.
The configurations $(3d+4s)^n 4p$ in neutral atoms of calcium, scandium, and titanium. C. Roth.
Absolute isotopic abundance ratio and atomic weight of terrestrial rubidium. E. J. Catanzaro, T. J. Murphy, E. L. Garner, and W. R. Shields.

J. Res. Nat. Bur. Stand. (U.S.), 73A (Phys. and Chem.), No. 6 (Nov.–Dec. 1969), SD Catalog No. C13.22/sec.A:73/6. $
Scaling analysis of thermodynamic properties in the critical region of fluids. M. Vicentini-Missoni, J. M. H. L. Sengers, and M. S. Green.
Formulation of a nonanalytic equation of state for parahydrogen. R. D. Goodwin.
Dynamical model for Brillouin scattering near the critical point of a fluid. R. D. Mountain.
Odd configurations in singly-ionized copper. C. Roth.
Capillary depressions for nearly planar menisci. M. C. I. Siu.
Phase transformation in barium tetraborate. C. R. Robbins and E. M. Levin.
Crystallography and preparation of some $ABCl_3$ compounds. H. F. McMurdie, J. de Groot, M. Morris, and H. E. Swanson.

J. Res. Nat. Bur. Stand. (U.S.), 74B (Math. Sci.), No. 1 (Jan.–Mar. 1970), SD Catalog No. C13.22/sec.B:74/1. $1.25.
Partitions—a survey. H. Gupta.
A relation between the coefficients and roots of two equations and its application to diophantine problems. T. N. Sinha.
An enumeration problem for a congruence equation. R. A. Brualdi and M. Newman.
Orthogonal decompositions of tensor spaces. S. Pierce.
Partitioned hermitian matrices. R. Merris.
Bounds on a polynomial. T. J. Rivlin.
Entire functions of exponential type. F. Gross.

Angeles, R., Aldridge, M., Freeman, D., Wall, L., Cryodegradation of polyelectrolyte networks, Polymer Letters **7**, No. 8, 609–611 (1969).

Armstrong, G. T., King, R. C., The heats of formation of some fluorine-containing oxidizers, Proc. Conf. Interagency Chemical Rocket Propulsion Group, Thermochemistry Working Group, Cleveland, Ohio, Apr. 9–11, 1969, 7th Meeting Bulletin 1, 19–40, (Chemical Propulsion Information Agency, Johns Hopkins University, Applied Physics Laboratory, Silver Spring, Maryland, Aug. 1969).

Armstrong, G. T., Hydrogen fluoride and the thermochemistry of fluorine, Proc. Conf. Interagency Chemical Rocket Propulsion Group, Thermochemistry Working Group, Cleveland, Ohio, Apr. 9–11, 1969, 7th Meeting Bulletin 1, 119–135 (Chemical Propulsion Information Agency, Johns Hopkins University, Applied Physics Laboratory, Silver Spring, Maryland, Aug. 1969).

Bennett, L. H., "Charge transfer" in intermetallic compounds: Example—the sodium thallide structure, Chapter in Structural Developments in Alloy Phases, B. C. Giessen, ed., Discussion I, 41–44 (Plenum Press, Inc., New York, N.Y., 1969).

Braun, W., Bass, A. M., Davis, D. D., Simmons, J. D., Flash photolysis of carbon suboxide: absolute rate constants for reactions of $C(^3P)$ and $C(^1D)$ with H_2, N_2, CO, NO, O_2 and CH_4, Proc. Roy. Soc. **A312**, 417–434 (1969).

Brennan, J. A., Edmonds, D. K., Smith, R. V., Two-phase (liquid-vapor), mass-limiting flow with hydrogen and nitrogen (Proc. 1968 Cryogenic Engineering Conf., Case Western Reserve Univ., Cleveland, Ohio, Aug. 19–21, 1968), Chapter in Advances in Cryogenic Engineering **14**, Paper G–6, 294–298 (Plenum Press, Inc., New York, N.Y., 1969).

Brown, J. E., Tryon, M., Horowitz, E., Thermal decomposition of Cu(II)-*bis*(8-hydroxy-5-quinolyl) methane coordination polymer, J. Appl. Poly. Sci. **13**, 1937–1947 (1969).

Burke, P. G., Cooper, J. W., Ormonde, S., Low energy scattering of electrons by helium, Phys. Rev. **183**, No. 1, 245–264 (July 5, 1969).

Carroll, J. J., Melmed, A. J., Ellipsometry-LEED study of the adsorption of oxygen on (011) tungsten, Surface Sci. **16**, 251–264 (Aug. 1969).

Colwell, J. H., Molecular reorientation and nuclear spin conversion in the solid deuteromethanes at low temperature, J. Chem. Phys. **51**, No. 9, 3820–3832 (Nov. 1, 1969).

Cooper, M. J., Vicentini-Missoni, M., Joseph, R. I., Linear parametrization of the equation of state near the critical point, Phys. Rev. Letters **23**, No. 2, 70–73 (July 14, 1969).

Coxon, B., Studies of ^{15}N-labeled amino sugars. Synthesis and spectroscopy of derivatives of 6-amino-6-deoxy-D-glucose-6-^{15}N, Carbohydrate Res. **11**, 153–155 (1969).

Darwent, B. deB., Bond dissociation energies in simple molecules, Nat. Bur. Stand. (U.S.), Nat. Stand. Ref. Data Ser. 31, 52 pages (Jan. 1970), SD Catalog No. C13.48:31, 55 cents.

DeLancey, G. B., Analysis of multicomponent diaphragm cell data, J. Phys. Chem. **73**, No. 5, 1591–1593 (May 1969).

Dickens, B., Brown, W. E., The crystal structures of $CaNa_2(CO_3)_2 \cdot 5H_2O$, synthetic gaylussite and $CaNa_2(CO_3)_2 \cdot 2H_2O$, synthetic pirssonite, Inorg. Chem. **8**, No. 10, 2093–2103 (Oct. 1969).

Donovan, R. J., Husain, D., Bass, A. M., Braun, W., Davis, D. D., Kinetic spectroscopic studies of $Cl(3p^{52}p3/2, 1/2)$ in the vacuum ultraviolet, J. Chem. Phys. **50**, No. 9, 4115–4116 (May 1, 1969).

Drechsel, D., Maximon, L. C., Warner, R. E., Noncoplanar *p-p* Bremsstrahlung calculations at 48 and 30 MeV, Phys. Rev. **181**, No. 4, 1720–1722 (May 20, 1969).

Duerst, R. W., Kokoszka, G. F., Hyperfine fields in dimeric metal ion complexes, J. Chem. Phys. **51**, No. 4, 1673–1674 (Aug. 15, 1969).

Evenson, K. M., Microwave magnetic-dipole transitions between excited electronic state of CN, Phys. Rev. **178**, No. 1, 1–4 (Feb. 5, 1969).

Fatiadi, A. J., Acylation of tetrahydroxy-*p*-benzoquinone, J. Chem. Eng. Data **13**, No. 4, 591–593 (Oct. 1969).

Fatiadi, A. J., Novel iodination of the γ-methylene group in 1,3-diphenylpropane-1, 3-dione and related β-diketones with periodic acid, Chem. Commun., p. 11 (1970).

Flynn, T. M., Birmingham, B. W., Cryogenics and national goals (Proc. 1968 Cryogenic Engineering Conf., Case Western Reserve Univ., Cleveland, Ohio, Aug. 19–21, 1968), Chapter in Advances in Cryogenic Engineering **14**, Paper A–1, 1–12 (Plenum Press, Inc., New York, N.Y., 1969).

Gadzuk, J. W., Band-structure effects in the field-induced tunneling of electrons from metals, Phys. Rev. **182**, No. 2, 416–426 (June 10, 1969).

Gadzuk, J. W., Many-body tunneling-theory approach to field emission of electrons from solids, Surface Sci. **15,** 466–482 (1969).

Garvin, D., Suggestion: the minireview, Phys. Today **22,** No. 10, 13–15 (Oct. 1969).

Halldane, J. F., Visual responses of travelers in urban environments (Proc. Symp. Man-Machine Systems, Cambridge, England, Sept. 8–12, 1969), Chapter in Transport Systems Vehicle Control 2, Paper No. 8, 17 pages (1969).

Hardy, S. C., Coriell, S. R., Morphological stability of cylindrical ice crystals, J. Crystal Growth **5,** 329–337 (1969).

Herron, J. T., Huie, R. E., Rates of reaction of atomic oxygen. II. Some C_2 to C_8 alkanes, J. Phys. Chem. **73,** No. 10, 3327–3337 (Oct. 1969).

Hiza, M. J., Duncan, A. G., Equilibrium gas-phase compositions of ethane and ethylene in binary mixtures with helium and neon below 150 K and a correlation for deviations from the geometric mean combining rule (Proc. 1968 Cryogenic Engineering Conf., Case Western Reserve Univ., Cleveland, Ohio, Aug. 19–21, 1968), Chapter in Advances in Cryogenic Engineering **14,** Paper B–1. 30–40 (Plenum Press, Inc., New York, N.Y., 1969).

Hummer, D. G., Non-coherent scattering—VI. Solutions of the transfer problem with a frequency-dependent source function, Mon. Notices Roy Astron. Soc. **145,** 95–120 (1969).

Isbell, H. S., Fatiadi, A. J., Phenylhydrazone-phenylazo tautomerism. Part III. Reactions of phenylformazans and certain *bis*(phenylhydrazones) with strong acids, Carbohydrate Res. **11,** 303–311 (1969).

Isbell, H. S., Frush, H. L., Wade, C. W. R., Hunter, C. E., Transformations of sugars in alkaline solution, Carbohydrate Res. **9,** 163–175 (1969).

Iacox, M. E., Milligan, D. E., Matrix-isolation study of the infrared and ultraviolet spectra of several first-series transition-metal dichlorides, J. Chem. Phys. **51,** No. 9, 4143–4155 (Nov. 1, 1969).

Johnson, V. J., A memoir of Russell B. Scott (Proc. CRYO/68 Conf., Chicago, Illinois, June 9–12, 1968), Chapter in Applications of Cryogenic Technology, R. W. Vance and H. Weinstock, ed., Introduction, pp. 1–11 (Tinnon-Brown, Inc., Los Angeles, California, 1969).

Kamper, R. A., Possible contribution of superconducting devices to nuclear magnetic resonance detection, J. Appl. Phys. **40,** No. 5, 2163 (Apr. 1969).

Kieffer, L. J., The reliability of property data, or, whose guess shall we use? J. Chem. Doc. **9,** No. 3, 167–168 (Aug. 1969).

Kidnay, A. J., Hiza, M. J., Dickson, P. F., The kinetics of adsorption of methane and nitrogen from hydrogen gas (Proc. 1968 Cryogenic Engineering Conf., Case Western Reserve Univ., Cleveland, Ohio, Aug. 19–21, 1968), Chapter in Advances in Cryogenic Engineering **14,** Paper B–2, 41–48 (Plenum Press, Inc., New York, N.Y., 1969).

Knoeck, J., Vibrational spectrometric and electrochemical evidence for lanthanum(III)-nitrate complexes aqueous solution, Anal. Chem. **41,** No. 14, 2069–2071 (Dec. 1969).

Knoeck, J., Taylor, J. K., Aqueous boric acid-borate-mannitol equilibria, Anal. Chem. **41,** No. 13, 1730–1734 (Nov. 1969).

Kuriyama, M., X-ray diffraction from a crystal containing isolated imperfections, Acta Cryst. **A,** No. 25, 682–693 (Nov. 1969).

Lehner, J., Lectures on modular forms, Nat. Bur. Stand. (U.S.), Appl. Math. Ser. **61,** 77 pages (Dec. 1969), 70 cents, SD Catalog No. C13.32:61.

Lutz, G. J., LaFleur, P. D., Determination of yttrium in rare earths by photon activation analysis, Talanta **16,** 1457–1460 (1969).

Madey, T. E., Yates, J. T., Jr., Temperature effects in desorption by electron impact: molecular vibrations in the chemisorbed layer, J. Chem. Phys. **51,** No. 3, 1264–1265 (Aug. 1, 1969).

Mahler, R. J., Interaction of Gunn domains with the Ga^{71} nuclei in GaAs, Appl. Phys. Letters **14,** No. 9, 277–279 (May 1, 1969).

Marinenko, G., On the atomic weight of potassium, Talanta **16,** 1339–1340 (1969).

Martin, W. C., Sugar, J., Perturbations and coupling in the d^9sp configurations of Cu I, Zn II, Ag I, Cd II, and Tl III, J. Opt. Soc. Am. **59,** No. 10, 1266–1280 (Oct. 1969).

Mason, S. T., Dependence of the phase shift on energy and atomic number for electron scattering by atomic fields, Phys. Rev. **182,** No. 1, 97–101 (June 5, 1969).

Maximon, L. C., Comments on radiative corrections, Rev. Mod. Phys. **41,** No. 1, 193–204 (Jan. 1969).

Mendlowitz, H., Calculated transition array for the configurations $3d^2$-$3d4p$ in Ti III, Astrophys. J. **158,** 385–388 (Oct. 1969).

Menis, O., Analytical Coordination Chemistry Section: Summary of activities July 1968 to June 1969, Nat. Bur. Stand. (U.S.), Tech. Note 504, 120 pages (Oct. 1969), SD Catalog No. C13.46:504, $1.00.

Mies, F. H., Resonant scattering theory of association reactions and unimolecular decomposition. I. A united theory of radiative and collisional recombination, J. Chem. Phys. **51,** No. 2, 787–797 (July 1969).

Miller, R. C., Prausnitz, J. M., Statistical thermodynamics of simple liquid mixtures. Henry's constants, Ind. Eng. Chem. Fundamentals **8,** No. 3, 449–452 (Aug. 1969).

Milligan, D. E., Jacox, M. E., Matrix-isolation study of the infrared and ultraviolet spectra of the free radical HCO. The hydrocarbon flame bands, J. Chem. Phys. **51,** No. 1, 277–288 (July 1, 1969).

Milligan, D. E., Jacox, M. E., Studies of the photoproduction of electrons in inert solid matrices. The electronic spectrum of the species C_2^-, J. Chem. Phys. **51,** No. 5, 1952–1955 (Sept. 1, 1969).

Moore, C. E., Bibliography on the analyses of optical atomic spectra, Section 4. ^{57}La-^{71}Lu and ^{89}Ac-^{99}Es, Nat. Bur. Stand. (U.S.), Spec. Publ. 306, Section 4, 55 pages (Aug. 1969), SD Catalog No. C13.10:306, 55 cents.

Motz, J. W., Olsen, H. A., Koch, H. W., Pair production by photons, Rev. Mod. Phys. **41,** No. 4, Part I, 581–639 (Oct. 1969).

O'Connell, J. S., Prats, F., Isospin sum rules and the photodisintegration of the $A=3$ nuclei, Phys. Rev. **184,** No. 4, 1007–1012 (Aug. 20, 1969).

Paabo, M., Bates, R. G., Dissociation of deuteriocarbonate ion in deuterium oxide from 5 to 50°, J. Phys. Chem. **73,** No. 9, 3014–3017 (Sept. 1969).

Peiser, H. S., Wachtman, J. B., Jr., Jump rates for point defects in special positions held by a trapping centre of cubic symmetry, Chapter 12 in Physics of the Solid State, S. Balakrishna, M. Krishnamurty, and Rao B. Ramachandra, ed., pp. 207–222 (Academic Press, Inc., New York, N.Y., 1969).

Piermarini, G. J., Mighell, A. D., Weir, C. E., Block, S., Crystal structure of benzene II at 25 kilobars, Science **165,** 1250–1255 (Sept. 19, 1969).

Richardson, A. C. B., Multiple scattering corrections for the associated-particle neutron time-of-flight technique, Nat. Bur. Stand. (U.S.), Tech. Note 499, 68 pages (Oct. 1969), SD Catalog No. C13.46:499, 65 cents.

Robinson, R. A., An osopiestic vapor pressure study of the system potassium chloride-sodium chloride in deuterium oxide solution at 25°, J. Phys. Chem. **73,** No. 9, 3165–3166 (Sept. 1969).

Rush, J. J., Melveger, A. J., Lippincott, E. R., Laser-Raman spectra of PH_4I, PH_4Br, and PH_4Cl, J. Chem. Phys. **51,** No. 7, 2947–2955 (Oct. 1, 1969).

Qureshi, I. H., McClendon, L. T., LaFleur, P. D., Extraction studies of the group IIIB–VIIB elements and the lanthanides utilizing *bis*(2-ethylhexyl) orthophosphoric acid, Radiochim. Acta **12,** No. 2, 107–111 (Aug. 1969).

Schaffer, R., Editor, Organic Chemistry Section: Summary of activities July 1968 to June 1969, Nat. Bur. Stand. (U.S.), Tech. Note 507, 145 pages (Oct. 1969), SD Catalog No. C13.46:507, $1.25.

Schwartz, R. B., Schrack, R. A., Heaton, H. T., A search for structure in the *n-p* scattering cross section, Phys. Letters **30B,** No. 1, 36–38 (Sept. 1, 1969).

Scribner, B. F., Editor, Activities of the NBS Spectrochemical Analysis Section, July 1968 to June 1969, Nat. Bur. Stand. (U.S.), Tech. Note 502, 108 pages (Dec. 1969), SD Catalog No. C13.46:502, $1.00.

Shumaker, J. B., Jr., Popenoe, C. H., Arc measurement of some Ar II optical transition probabilities, J. Opt. Soc. Am. **59,** No. 8, 980–985 (Aug. 1969).

Snyder, N. S., Thermal conductance at the interface of a solid and helium II (Kapitza conductance), Nat. Bur. Stand. (U.S.), Tech. Note 385, 90 pages (Dec. 1969), SD Catalog No. C13.46:385, $1.00.

Stair, R., Measurement of natural ultraviolet radiation; historical and general introduction (Proc. Conf. Fourth International Biometeorological Congress, Rutgers University, New Brunswick, N.J., 1966), Chapter in The Biologic Effects of Ultraviolet Radiation, Frederick Urbach, ed., pp. 377–390 (Pergamon Press Inc., New York, N.Y., August 1969).

Stern, K. H., Weise, E. L., High temperature properties and decomposition of inorganic salts. Part 2. Carbonates, Nat. Bur. Stand. (U.S.), Nat. Stand. Ref. Data Ser. 30, 32 pages (Nov. 1969), SD Catalog No. C13.48:30, 45 cents.

Sukle, D. J., Wells, J. S., Fine structure in EPR of Mn^{2+} in zinc sulfate, Phys. Rev. **180,** No. 2, 445–450 (Apr. 10, 1969).

Taylor, J. K., Editor, Microchemical Analysis Section: Summary of activities July 1968 to June 1969, Nat. Bur. Stand. (U.S.), Tech. Note 505, 140 pages (Oct. 1969), SD Catalog No. C13.46:505, $1.25.

Tipson, R. S., Brady, R. F., Jr., Synthesis of the two D-2-pentuloses. New derivatives of D-*erythro*-pentulose, Carbohydrate Res. **10,** 549–563 (Aug. 1969).

Toots, J., Marton, L., Optical properties of antimony and bismuth in the far ultraviolet, J. Opt. Soc. Am. **59,** No. 10, 1305–1308 (Oct. 1969).

Venable, W. H., Jr., Shumaker, J. B., Jr., Observations of departures from equilibrium in a nitrogen arc, J. Quant. Spectr. Radiative Transfer **9,** 1215–1226 (Sept. 1969).

Viezbicke, P. P., Why WWV moved to Colorado, Mark **5,** 13, No. 3, 14–16 (June 1968).

Waclawski, B. J., Hughey, L. R., Effect of heating on the photoelectron yield of polycrystalline tungsten in the vacuum ultraviolet, J. Opt. Soc. Am. **59,** 1494 (Nov. 1969).

White, H. S., Jr., Editor Congressional districts of the United States. Federal general data standard representations and codes, Nat. Bur. Stand. (U.S.), Fed. Info. Process. Stand. Publ. (FIPS Pub.) 9, 4 pages (Nov. 14, 1969), SD Catalog No. C13.52:9, 10 cents.

Wiese, W. L., Bridges, J. M., Kornblith, R. L., Kelleher, D. E., Transition probabilities for prominent Ar I lines in the near infrared, J. Opt. Soc. Am. **59,** No. 9, 1206–1212 (Sept. 1969).

Wiese, W. L., Smith, M. W., Miles, B. M., Atomic transition probabilities. Volume II. Sodium through calcium, a critical data compilation, Nat. Stand. Ref. Data Ser., Nat. Bur. Stand. (U.S.), 22, 306 pages (Oct. 1969), SD Catalog No. C13.48:22, $4.50.

Yates, J. T., Jr., Madey, T. E., Chemisorption on rhenium: N_2 and CO, J. Chem. Phys. **51,** No. 1, 334–337 (July 1, 1969).

Yates, J. T., Jr., Madey, T. E., Electron impact study of the γ–N_2 state chemisorbed on tungsten (Proc. Fourth International Materials Symp., Berkeley, Calif., June 1968), Chapter in The Structure and Chemistry of Solid Surfaces, Gabor A. Somorjai, ed., pp. 59–1, 59–27 (John Wiley & Sons, Inc., New York, N.Y., 1969).

**Publications for which a price is indicated are available by purchase from the Superintendent of Documents, U.S. Government Printing Office, Washington, D.C. 20402 (foreign postage, one-fourth additional). The NBS non-periodical series are also available from the National Technical Information Service, Springfield, Va. 22151. Reprints from outside journals and the NBS Journal of Research may often be obtained directly from the authors.*

JOURNAL OF RESEARCH of the National Bureau of Standards — C. Engineering and Instrumentation
Vol. 74C, Nos. 3 and 4, July–December 1970

INDEX TO VOLUME 74C

January to December 1970

A

Page

AC direct reading ratio set 63
AC measurements 63
A–C resistance thermometer bridge 15
Alperin, H. A., Prince, E., A time-shared computer system for diffractometer control 89
Antoine Equation 117
Automatic control 89
Automatic phase balance 15

B

Bolometric power standards 123
Bolovac application for HF microwave power measurement and standardization 123
Bolovac power measurements 123
Bridge 15, 63

C

Calibration of power meters 123
Capacitance measurement 111
Cezairliyan, A., A pulse heating method for the measurement of melting point of electrical conductors (thin wires) above 2000 K 87
Coaxial adaptor 111
Coaxial chokes 63
Coaxial connector 111
Compliance 21
Composites 97
Computer control 89
"Connector-Pair" techniques for the accurate measurement of two-terminal low-value capacitances 111
Copper 97
Crack-toughness 21
Creep 29
Cutkosky, R. D., An a-c resistance thermometer bridge 15
–, Techniques for comparing four-terminal-pair admittance standards 63

D

Defining transformers 63
Dew point 117
Dichroic polarizers 9
Diffractometer 89

E

Effect of notch geometry and temperature on the creep-rupture behavior of titanium alloy 29
Electrical conductivity 97
Elevated temperature 29
Engineering design 29
Equal power bridge 63

F

FORTRAN 89
Four-pair standards 63
Fracture 21, 97
Frequency-dependent bridge 63
Fringe capacitance 111
Frisch, R. C., VanderHart, D. L., Locked nuclear quadrupole resonance spectrometer for pressure measurements 3

H

Harne, D. A., Jenkins, W. D., Willard, W. A., Tensile deformation of vapor-deposited copper reinforced with tungsten wires 97
High-speed measurement 87
High temperatures 87
Humidity 117
Huntley, L. E., Some applications for series impedance elements in radio frequency immittance measurements 79
Hygrometry 117

I

Page

Immittance measurement 79
Interference fringes 1
Interferograms 1

J

Jenkins, W. D., Willard, W. A., Effect of notch geometry and temperature on the creep-rupture behavior of titanium alloy 29
–, –, *Harne, D. A.*, Tensile deformation of vapor-deposited copper reinforced with tungsten wires 97

K

$KClO_3$ 3
Kearsley, E. A., On the flow induced by a Maxwell-Chartoff rheometer 19

L

Law of mixtures 97
Locked nuclear quadrupole resonance spectrometer for pressure measurements 3

M

Maxwell-Chartoff rheometer 19
Mechanical compliance measurements of single-edge-notch tension specimens 21
Metallic bonding 97
Melting point 87
Millea, A., "Connector-pair" techniques for the accurate measurement of two-terminal low-value capacitances 111
Multistage transformers 15

N

Neutron diffractiometer 89
Normal stresses 19
Notch geometry 29
Nuclear quadrupole resonance 3

O

On the flow induced by a Maxwell-Chartoff rheometer 19
Operational amplifiers 15
Optics 9
Orloski, M. J., Mechanical compliance measurements of single-edge-notch tension specimens 21

P

Platinum 87
Precise continuous optical attenuator 9
Pressure transducer 3
Prince, E., Alperin, H. A., A time-shared computer system for diffractometer control 89
Production of near perfect inteferograms of variable visibility 1
Psychrometric chart 117
Pulse heating method for the measurement of melting point of electrical conductors (thin wires) above 2000 K 87
Pyrometry 9

Q

Quadrature bridge 63

R

Radio frequency 79
Radiometry 9

Page

Real time data processing 89
Relative humidity 117
Relative transmittance factor 9
Resistance bridge 15
Resistance thermometry 15
RF and microwave power measurements 123
Rheology 19
Rheometer 19
Ruffino, G., Precise continuous optical attenuator 9

S

Saunders, J. B., Production of near perfect interferograms of variable visibility 1
Selby, M. C., Bolovac application for HF and microwave power measurement and standardization 123
Series elements 79
Single-edge-notch specimen 21
Some applications for series impedance elements in radio frequency immittance measurements 79
Spectrometer 3
Standard capacitor 111
Standard of power through 18 GHz 123
Stress concentration 29
Stress-rupture 29

T

Techniques for comparing four-terminal-pair admittance standards 63
Temperature measurement 15
Tensile deformation of vapor-deposited copper reinforced with tungsten wires 97
Tensile properties 97
Time-shared computer system for diffractometer control 89
Time, sharing 89

Page

Titanium alloy 29
Two-port standards 79
Two-terminal capacitor 111
Tungsten 97

U

Use of dew-point temperature in humidity calculations 117

V

VanderHart, D. L., Frisch, R. C., Locked nuclear quadrople resonance spectrometer for pressure measurements 3
Vapor-deposited 97
Vapor pressure of water 117
Viscoelasticity 19

W

Wet-bulb temperature 117
Willard, W. A., Jenkins, W. D., Effect of notch geometry and temperature on the creep-rupture behavior of atitanium alloy 29
—, —, *Harne, D. A.*, Tensile deformation of vapor-deposited copper reinforced with tungsten wires 97
Wires 97
Wood, L. A., The use of dew-point temperature in humidity calculations 117

X

X-ray diffractometer 89

U.S. GOVERNMENT PRINTING OFFICE : 1970 O—403-833

UNITED STATES
GOVERNMENT PRINTING OFFICE
DIVISION OF PUBLIC DOCUMENTS
WASHINGTON, D.C. 20402

OFFICIAL BUSINESS
PENALTY FOR PRIVATE USE, $300

POSTAGE AND FEES PAID
U.S. GOVERNMENT PRINTING OFFICE

JOURNAL OF RESEARCH of the National Bureau of Standards Vol. 74C, Nos. 3 and 4 July–December 1970
C. Engineering and Instrumentation

Contents

	Page
Techniques for comparing four-terminal-pair admittance standards. R. D. Cutkosky.	63
Some applications for series impedance elements in radio frequency immittance measurements. Leslie E. Huntley.	79
A pulse heating method for the measurement of melting point of electrical conductors (thin wires) above 2000 K. A. Cezairliyan.	87
A time-shared computer system for diffractometer control. H. A. Alperin and E. Prince.	89
Tensile deformation of vapor-deposited copper reinforced with tungsten wires. William D. Jenkins, William A. Willard, and Donald A. Harne.	97
"Connector-pair" techniques for the accurate measurement of two-terminal low-value capacitances. Aurel Millea.	111
The use of dew-point temperature in humidity calculations. Lawrence A. Wood.	117
Bolovac application for HF and microwave power measurement and standardization. M. C. Selby.	123
Publications of the National Bureau of Standards.	135
Index to volume 74C, January–December 1970.	149

Library of Congress Catalog Card Number: 62-3900

For sale by the Superintendent of Documents, U.S. Government Printing Office, Washington, D.C. 20402. (Order by SD Catalog No. C 13.22/sec. C: 74/3 & 4). Price $1.25 (single copy). Subscription price: $5.00 a year; $1.25 additional for foreign mailing.
UNITED STATES GOVERNMENT PRINTING OFFICE, WASHINGTON : 1970